Strål
säkerhets
myndigheten
Swedish Radiation Safety Authority

Authors:
Weilin Zang
Jens Gunnars
Jonathan Mullins
Pingsha Dong
Jeong K. Hong

Research

2009:17

Effect of Welding Residual Stresses on Crack Opening Displacement and Crack-Tip Parameters

Report number: 2009:17 **ISSN:** 2000-0456
Available at www.stralsakerhetsmyndigheten.se

Title: Effect of Welding Residual Stresses on Crack Opening Displacement and Crack-Tip Parameters.
Report number: 2009:17
Authors: Weilin Zang [1], Jens Gunnars [1], Jonathan Mullins [1], Pingsha Dong[2] and Jeong K. Hong[2]
[1]Inspecta Technology AB, Stockholm, Sweden. [2]Center for Welded Structures Research, Battelle, Columbus, Ohio
Date: June 2009

Background

Weld residual stresses have a large influence on the behavior of cracks growing under normal operation loads and on the leakage-flow from a through-wall crack. Accurate prediction of these events is important in order to arrive at proper conclusions when assessing detected flaws, for inspection planning and for assessment of leak-before-break margins. The fracture mechanical treatment of weld residual stresses in commonly used engineering assessment methods generally use the crack face pressure method and account neither for the displacement controlled nature of weld residual stresses, nor for multi-axial residual stresses. In this report, these effects are studied.

Objectives of the project

The principal objective of the project is to investigate the accuracy of the commonly used Crack Face Pressure (CFP) method, such as in the computer code ProSACC, for evaluating the stress intensity factor K for cracks located in multi-dimensional weld residual stress fields in piping geometries. Another aim is to investigate the accuracy of existing methods to evaluate the Crack Opening Displacement (COD) for through-wall cracks in pipes.

Results

The following conclusions can be made for cracks located in the vicinity of welds in piping geometries subjected to a combination of primary loads (during normal operation) and weld residual stresses:

- The CFP method gives a relatively good estimation of K for surface cracks.
- The CFP method cannot in general be demonstrated to give good accuracy for evaluating K for through-wall cracks even if good approximations exist for certain cases. The results in the report should be carefully studied for more guidance.
- The CFP method gives a relatively good estimation of the COD except for very long through-wall cracks.
- In the estimation of COD through the CFP method, plasticity effects should be taken into account except for short through-wall cracks and low load levels.

Effects on SSM

The results of this project will be used by SSM in safety assessments of welded components with cracks and in assessments of Leak Before Break (LBB) applications.

Project information
Project leader at SSM: Björn Brickstad
Project number: 14.42-200542009, SSM 2008/77
Project Organisation: Inspecta Technology AB has managed the project with Dr Jens Gunnars as the project manager. Center for Welded Structures Research, Battelle in Columbus, Ohio has been used as subcontractor to Inspecta Technology AB for certain project tasks.

Contents

1 SUMMARY

Weld residual stresses have a large influence on the behavior of cracks growing under normal operation loads and on the leakage-flow from a through-wall crack. The fracture mechanical treatment of weld residual stresses in commonly used engineering assessment methods generally use the crack face pressure method and account neither for the displacement controlled nature of weld residual stresses nor for multi-axial residual stresses. This work investigates the approximation of the crack face pressure method in the presence of weld residual stresses under normal operating conditions. Comparisons are made with a control method where the deformation controlled characteristics of weld residual stresses are considered.

For **through wall cracks** the crack opening area results are of interest for performing leak before break assessments. The main conclusion is that good agreement is obtained between the elastic-plastic FE method (crack face pressure method), NURBIT (crack face pressure method) and the control method for typical minimum detectable crack sizes and load levels commonly seen in Swedish nuclear reactors (load level 1). The maximum observed variation between the methods was 26%, where COD was overestimated.

For full circumferential **internal surface cracks** *K* estimates are of interest for crack growth predictions. The main conclusions are:

- For the 8 mm thick pipe there is generally good agreement between *K* predictions for the elastic ProSACC (crack face pressure) method and the control method for crack depths up to a/t=0.6.
- For the 32 mm thick pipe there is generally good agreement between *K* predictions for the elastic ProSACC method and the control method. The largest variation of 15% was for the higher load level and deepest crack (a/t=0.8).
- For the 32 mm thick pipe, where the axial weld residual stress profile is sinusoidal, the surface COD due to 'residual stresses only' decreases rapidly, leading to the situation that it is more difficult to detect a deep crack than a shallow one. This may have implications for VT testing.
- For the 32 mm thick pipe, all methods predict crack arrest. For shallow cracks, *K* was overestimated by all crack face pressure methods where there was a tensile residual stress near the inner wall.

2 BACKGROUND

Weld residual stresses have a large influence on the behavior of cracks growing under normal operation loads and on the leakage-flow from a through-wall crack. Accurate prediction of these events is important in order to arrive at proper conclusions when assessing detected flaws, for inspection planning or for assessment of leak-before-break margin.

A first prerequisite for performing these predictions is reliable prediction of the magnitude and distribution of welding residual stresses. This issue was addressed in a first stage of this project reported in [1], which had the purpose to validate and improve the weld residual stress modeling procedure used in Sweden [2].

The fracture mechanical treatment of weld residual stresses in commonly used engineering assessment methods generally account for neither the displacement controlled nature of weld residual stresses nor for multi-axial residual stresses. These issues are considered in this stage of the project.

Stress corrosion crack growth under normal operation loads

An important crack growth mechanism that has to be accounted for in performing inspection planning and structural integrity assessments of stainless steel components is stress corrosion cracking (SCC). For stress corrosion cracking to take place tensile stresses and an unfavourable environment are required. The mechanism is generally active under normal operation conditions. Since weld residual stresses usually are very high, they can have a significant influence on initiation and the subsequent growth of stress corrosion cracks. Crack growth rates are commonly expressed using the stress intensity factor K which characterizes the mechanical state at the crack-tip. Thus, the fracture mechanical treatment of weld residual stresses is of a great importance when predicting cracking of welded components.

Leak-before-break assessments

The leak-before-break (LBB) concept is sometimes applied for nuclear piping, in order to demonstrate that crack growth will result in a leak that is detectable, long before the crack reaches a critical size resulting in fracture. For example demonstration of LBB is sometimes applied in order to show that building of pipe break restraints is not necessary. LBB analyses may show that the margin against guillotine pipe break is very high, for a given leak detection capability, and hence pipe break restraints are unnecessary for reaching an acceptably low level of risk for dynamic events. In LBB analyses the weld residual stresses influence the conclusions about the leak-before-break margin, especially with respect to the estimated crack opening area (or crack opening displacement COD) and the corresponding leak rate.

Testing by visual inspection technique

One non-destructive inspection method that is increasingly used is the visual inspection technique (VT). In order to use the method cracks must be detectable for sizes that are smaller than the maximum allowable. In practice inspection at each location requires that residual stresses are present that open the crack mouth. To demonstrate that the postulated crack is detectable it is important to have an accurate prediction of the crack opening displacement (COD) at room temperature.

Determination of K and COD in residual stress fields

The stress intensity factor and crack opening displacement for a crack in a weld residual stress field can be determined in more than one way. For engineering assessments it is common to utilize a calculation procedure sometimes called the crack-face pressure method. By this method the stress in an uncracked model is extracted along the plane were the crack is postulated. Only the stress resolved normal to the crack plane is considered. This stress is applied to the crack surface in a model where the crack exists. This method is used both for direct calculation of K by FEM, and for derivation of weight functions by FEM or analytical methods.

The crack-face pressure method involves an assumption of load-controlled conditions, but is also valid for situations where remote displacements are applied. As long as the response is essentially linear, for example a large elastic specimen containing a short crack, and the loading is dominated by the normal stress component, the crack-face pressure method holds. However, for a crack growing in a weld, the assumptions of remote loading and linearity do not apply in general:

In a weld, the residual stress field is created by thermal and plastic strains generated in and around the weld metal. If the crack size is comparable to the radius of this region then the loading conditions should be treated as local and the remote loading assumption is no longer appropriate.

Significant plastic deformation may occur as the crack grows. The residual stress field must satisfy equilibrium conditions within the component of concern. For a growing crack, the residual stresses nearby re-distribute as stress-free surfaces are generated, while for load-controlled conditions the far-field stresses can be assumed to be stationary.

Weld residual stress fields are triaxial so in these cases it cannot be assumed that loading is dominated by the normal stress component.

In spite of these limitations the crack-face pressure method is widely used. Thus it is important to investigate under which conditions the method remains conservative for calculation of the stress intensity factors and crack openings.

3 OBJECTIVE

This work investigates the treatment of weld residual stresses when performing fracture mechanical analysis of welded components. The objective is to determine if it is conservative to use the crack face pressure method for crack shapes and loading cases that might be found under normal operating conditions. The magnitude of the residual stress field and crack characterizing parameters affects crack growth and leak-before-break predictions in different ways, and accurate and conservative estimates are important.

Detailed simulations are made where a crack is created in full 3D weld residual stress fields by use of the node-relaxation technique. The crack-tip characterizing parameters and the crack opening displacement determined from this model are compared with results obtained from different implementations of the crack face pressure method. Of particular interest is comparison and validation of the prediction of the ProSACC stress corrosion crack growth module and NURBIT. Two pipe geometries with surface and through wall cracks are studied for normal operation cases where the weld residual stresses constitute a significant part of the loading. Also the alternating method is considered.

3.1 Basis for crack-tip characterizing parameters

In this investigation crack growth under normal operation is of interest. Relations that describe crack growth due to fatigue or stress corrosion normally use the elastic stress intensity factor K as the parameter describing the mechanical state at the crack tip. Values for K can be directly extracted from finite element models through nodal extrapolation from the near-tip finite element mesh. This method, however, requires a very fine mesh which makes analysis computationally expensive, especially in 3D models such as those considered in this study. Further, K is an elastic crack tip parameter and the test cases considered in this study involve ductile materials for which considerable plastic deformation may occur around the crack tip. For these reasons, the natural alternative crack tip parameter to consider is the J-integral. It can be shown to characterize the stresses and strains near the crack-tip in elastic-plastic materials and is also an energy conservation integral.

The standard J-integral is known to be unique for plastic materials provided unloading does not occur. However, it is path dependent for a growing crack in an elastic-plastic material (due to unloading in the wake) and also in the presence of a weld residual stress field. This has spawned considerable efforts in recent years to develop a path-independent form of J [3-6], where the influence of prior plastic deformation is decoupled from the standard surface integral and included as an additional term in the formulation. These efforts were successful and the modified J-integral formulation shows path-independence under combinations of residual stress and mechanical loading. Further, the modified J is also shown to be equivalent to the stress intensity factor K in cases of small scale yielding. The calculated J in this investigation will be converted to an equivalent stress intensity factor using the relation,

$$K = \sqrt{J\,E/(1-\nu^2)} \qquad (3.1)$$

where E is Young's modulus and ν is Poisson's ratio.

Studies on the modified J-integral [4-7] have also demonstrated that the standard J-integral can be used to provide an accurate estimate, provided that the evaluation path is suitably near to the crack tip. It has been found that in an area very close to the crack tip, J evaluated by the standard definition and by the modified definition both result in an almost identical value [4]. The reason for this is that the contribution from the additional 'prior plastic deformation' term vanishes to zero when the integral is evaluated very close to the crack tip [4]. One conclusion from this is that by using the modified J-integral a coarser mesh and a longer integration path can be used.

In [4-7] the difference between the standard and the modified *J*-integral tends to decrease as the primary load decreases. In this investigation we are focusing on growth and leakage under normal operation loads, and not on the prediction of fracture due to high primary loads. In order to conclude on the distance at which the two integrals become identical, it is necessary to calculate both the standard and the modified integral for the present loading situation. In the present investigation an implementation of the modified *J*-integral was not available for 3D cases so, alternatively, near-tip estimates of the standard *J*-integral are used. It is judged that the standard *J*-integral evaluated close enough to the crack-tip is sufficient to demonstrate the key trends for the present investigation. The standard *J*-integral evaluated between 0.01 and 0.1 mm from the crack tip is used.

An alternative measure for the near-tip state is CTOD [8]. The definition is illustrated in Figure 3.1. For an elastic-plastic material when no unloading occurs CTOD has a simple relation with the standard *J*-integral [8].

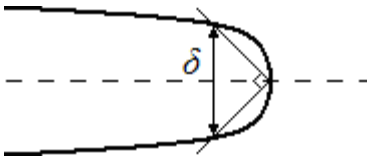

Figure 3.1 Definition of CTOD.

While CTOD could provide a valid measure of the mechanical state at the crack tip, the crack growth relations are usually based upon *K*, and it is more difficult to convert CTOD to *K*. It is typically more convenient to use the *J*-integral and equivalent *K*, although CTOD values are reported here.

3.2 Definition of leak before break parameters

The crack opening area COA is a key parameter for estimation of leakage rates in leak-before-break assessments. In the current investigation we will study the parameters defined below.

Figure 3.2 shows a through wall crack of length 2*a* approximated by an elliptical function. For such a geometry the crack opening displacement can be expressed as

$$u = \delta_e \sqrt{1-(l/a)^2}\,, \qquad (3.2)$$

where δ_e is the the crack opening displacement at the mid point of the crack. Integrating the displacement results in the (elastic) crack opening area

$$COA_e = \frac{\pi}{2}\delta_e\, a\,. \qquad (3.3)$$

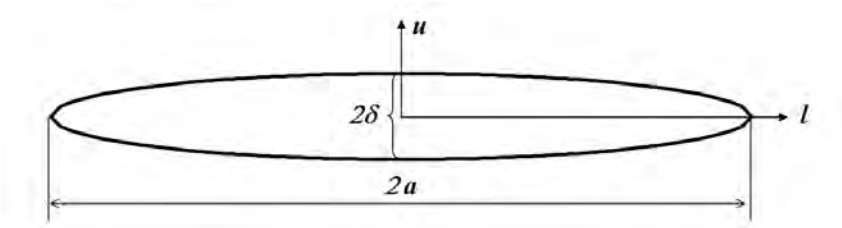

Figure 3.2 Elliptical model for crack opening displacement (through wall case).

The COA for each method can be compared directly. As seen above it is also possible to compare an equivalent maximum crack opening displacement, which will accentuate the difference in the crack opening area calculated by the different methods. We will present the results as an equivalent crack opening parameter defined by

$$\delta = \frac{2 * COA}{a * \pi} , \qquad (3.4)$$

where COA is evaluated by an integral of the crack opening displacement COD along the crack length.

4 DEFINITION OF EVALUATED CALCULATION METHODS

The different analysis methods evaluated for treatment of weld residual stresses are summarized in the table below.

Table 4.1. Notation and overview of the compared calculation methods.

Method denotation	Short description of calculation method	Parameters evaluated
Control	FEM, near tip J-integral calculation Node relaxation of crack Full 3D residual stress field Elastic-plastic model Considered as the most accurate simulation method.	*K*, CTOD COD, δ
$K_{Elastic}^{ProSACC}$	Weight functions, solutions determined for load controlled boundary conditions using the **crack face pressure method** Normal stresses taken from uncracked body Elastic model	*K*
EL_b	**FEM**, near tip J-integral calculation Crack face pressure Normal stresses taken from uncracked body Elastic model	*K*, CTOD COD, δ
NURBIT	Weight functions, solutions determined for load controlled boundary conditions using the **crack face pressure method** Normal stresses taken from uncracked body Elastic model using **plastic correction**	δ
EP_b	**FEM**, near tip J-integral calculation Crack face pressure Normal stresses taken from uncracked body Elastic **plastic** model	*K*, CTOD COD, δ
Alternating	FEM **alternating method** (coupled, iterative FE/analytical method) Infinite body K_I solution Elastic Full 3D residual stress field applied	*K* COD, δ

Below some more details are given for the different calculation methods.

4.1 Node relaxation in full 3D residual stress field (Control Method)

This simulation method is designed to best simulate the growth of a crack in a residual stress field. The procedure is as follows:

A 2D axi-symmetrical welding simulation is performed. The new welding simulation procedure according to [1] is applied.

Hydro-test pressure is applied and released at 20 °C.

The 2D solution is mapped into a 3D model with a crack. At this stage nodes along the crack are constrained.

The operating loads (membrane stress plus bending stress) are applied (load case 1).

Crack growth is activated by instantaneously releasing the constraints on the crack face nodes.

J-integrals, COD and CTOD are calculated.

Finally the primary loads are increased to a slightly higher level, called load case 2.
The *J*-integral, COD and CTOD are calculated for this load case.

The results generated in this manner are considered as the most accurate results.

4.2 Elastic *K* results using weight functions ($K_{Elastic}^{ProSACC}$)

This method uses the crack face pressure assumption. Elastic weight functions are used to calculate *K* values due to primary and secondary loads. These results are useful for assessment of crack growth calculations.

4.3 Elastic FEM method (EL_b)

This method uses the crack face pressure assumption where the stress in an uncracked model is extracted along the plane where the crack is postulated. Only the stress resolved normal to the crack plane is considered. This stress is applied to the crack surface in a model where the crack exists.
This method uses linear elastic finite element calculation and the residual stress obtained from the 2D welding simulation is applied as the crack face pressure.

The *J*-integral, COD and CTOD are calculated for two load cases. Results are denoted EL_b. Results for the residual stress only are denoted EL (Resi. only). This model is very similar to the $K_{Elastic}^{ProSACC}$ model

4.4 COD using weight functions with plastic correction (NURBIT)

The calculation procedures are similar to those used in ProSACC with the exception that some solutions are more detailed with regards to through wall crack geometries. In contrast to ProSACC, estimates of COD (and COA) can be extracted from NURBIT [10]. A plastic correction is also applied and details are available in [10].

4.5 Elastic-plastic FEM method (EP_b)

The calculation procedure is identical with the elastic FEM method, with the exception that the material response is elastic-plastic.

The *J*-integral, COD and CTOD are calculated for two load cases. Results are denoted by EP_b.

Elastic-plastic FEM analyses of cracks using the crack face pressure method are most relevant for COD assessment of fracture but not for crack growth assessments.

4.6 FEM alternating method using infinite body solution (Alternating)

The method involves an iterative procedure using a coupled finite element and infinite body (analytical) solution [11, 12]. This method uses an elastic constitutive model. A full 3D residual stress field is applied as an initial condition in an uncracked FE model. The FEM boundary conditions are successively updated until they display a (nearly) stress free state along the postulated crack surface. At the same time the crack face pressure in an infinite body crack model is successively updated until it converges. The alternating method is described in detail in chapter 10.

5 DEFINITION OF CASE STUDIES

The different analysis methods will be evaluated for four cases which represent loading scenarios that occur under normal operation of a nuclear power plant. The four cases were taken from a LBB study [13]. A thin and a medium thickness pipe are chosen, containing first a through wall crack and then an internal surface crack. Four crack sizes are considered for each crack geometry. As discussed in this chapter, two load levels are specified – in an effort to cover the range of conditions experienced under normal operation.

5.1 Pipe geometry, loading and material properties

A thin pipe and a medium pipe are selected for investigation. The geometries and mechanical loadings for the chosen cases are shown in Table 5.1 and 5.2. Note that in Table 5.2 the axial membrane stress is entirely due to internal pressure. The load case L2 deviates from [13] and is introduced to represent slightly higher loads than normal; in this case the bending load specified in load case L1 was doubled. The pipes are made of stainless steel TP304. The material properties used in the analysis are listed in Table 5.3. Bilinear isotropic hardening was specified.

Table 5.1 Geometry.

	Inner pipe radius (mm)	Thickness, *t* (mm)
Thin pipe	153.6	8.3
Medium pipe	146	31.8

Table 5.2 Applied mechanical loads for load levels 1 and 2.

	Temperature (°C)	Internal pressure (MPa)	**Load Level 1 (L1)**		**Load level 2 (L2)**	
			Axial membrane stress (MPa)	Bending stress (MPa)	Axial membrane stress (MPa)	Bending stress (MPa)
Thin pipe	145	4.6	41	32	41	64
Medium pipe	323	15.5	32.1	19	32.1	38

Table 5.3 Material properties

	Temperature (°C)	TP304	Weld material
E (GPa)	100	195	195
	200	185	185
	400	170	170
ν		0.3	0.3
σ_y (MPa)	100	173	419
	200	140	368
	400	116	264

5.2 Crack geometries

Cracks growing along the weld centerline are studied. Two crack geometries are considered:

A through wall circumferential crack. Four different crack lengths are evaluated, specified as shown in Table 5.4.

A complete circumferential internal crack. Four different crack depths a are considered, a/t = 0.2, 0.4, 0.6 and 0.8.

In the LBB study [13] the crack size was determined for a leakage rate of 10 gallons per minute. In reality this crack size is heavily dependent on the crack face morphology and for this reason different crack sizes were specified in Table 5.4, corresponding to typical observed morphologies.

The detectable through wall crack sizes considered are listed in Table 5.4. The maximum allowable crack size was also considered, although the shorter crack sizes are of greater interest because weld residual stresses make a larger contribution to the loading. A further reason why the shorter cracks are of more interest is that a crack spends most of its lifetime in stable growth, not at the maximum allowable size.

Table 5.4 Detectable through wall crack sizes chosen for evaluation [13].

Thin pipe (mm)	Medium pipe (mm)	Comments
137	175	Crack size resulting in detectable leakage (load level 1). Assumed crack morphology, 'fatigue 1.'
160	218	Crack size resulting in detectable leakage (load level 1). Assumed crack morphology, 'fatigue 2.'
185	246	Crack size resulting in detectable leakage (load level 1). Assumed crack morphology, 'PWSCC.'
350	330	Maximum allowable crack size, [13].

5.3 Weld geometry assumptions

Four weld passes are used for the thin walled pipe and twelve weld passes for the medium thickness pipe. The heat input is defined according to the phase 1 report from this project [1]. Welding is simulated using symmetry conditions at the weld centre line.

6 CASE ONE - THIN PIPE WITH A THROUGH WALL CRACK

6.1 Finite element models

The finite element mesh used for 2D welding simulation and the weld pass order is shown in Figure 6.1. The finite element mesh for the 3D fracture mechanics model with a through wall crack is shown in Figure 6.2. A small notch with a notch radius of 0.001 mm is introduced at the crack tip – this allows an accurate prediction of near-tip-*J* and CTOD.

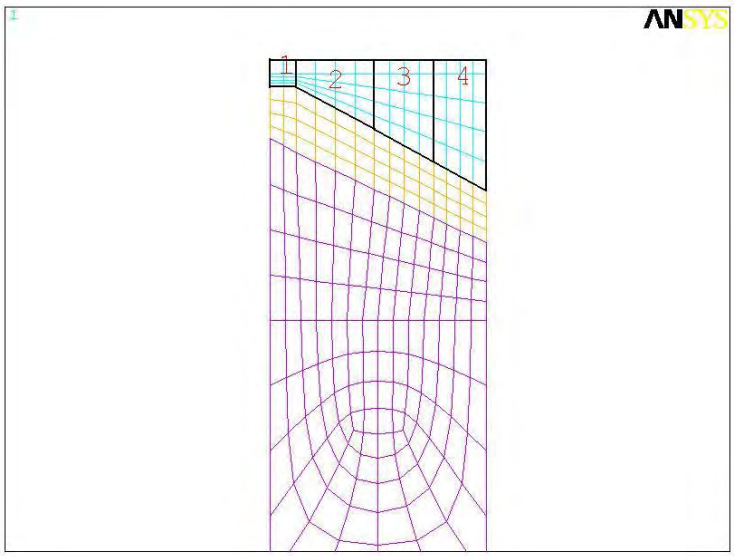

Figure 6.1 Finite element mesh for 2D welding simulation for case 1.

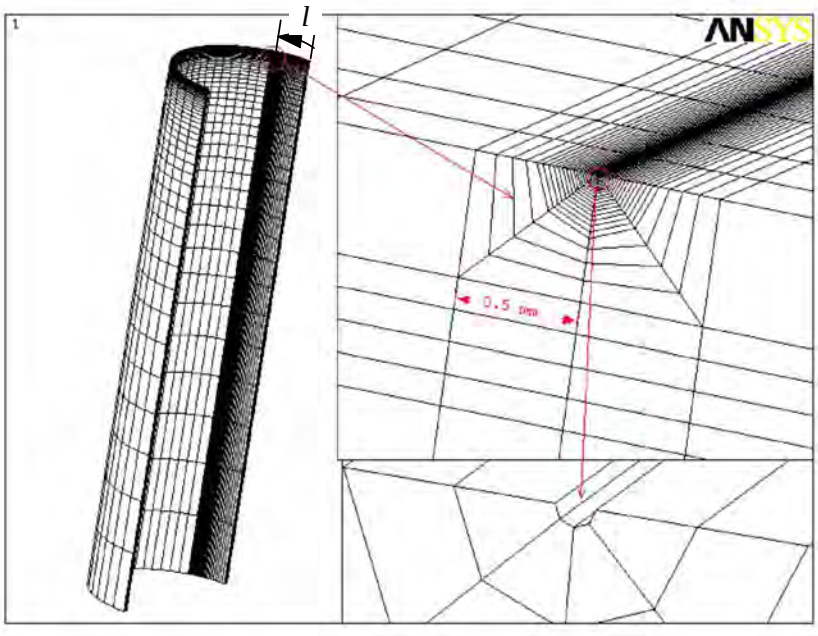

Figure 6.2 Case 1 - finite element mesh with a through thickness crack. The coordinate l = 0 corresponds to the center of the through wall crack, as previously defined in Figure 3.2.

6.2 2D welding simulation

The welding residual stress distribution at the operating temperature is shown in Figures 6.3 and 6.4. The axial residual stress along the weld centre is a bending stress, as illustrated in Figure 6.5

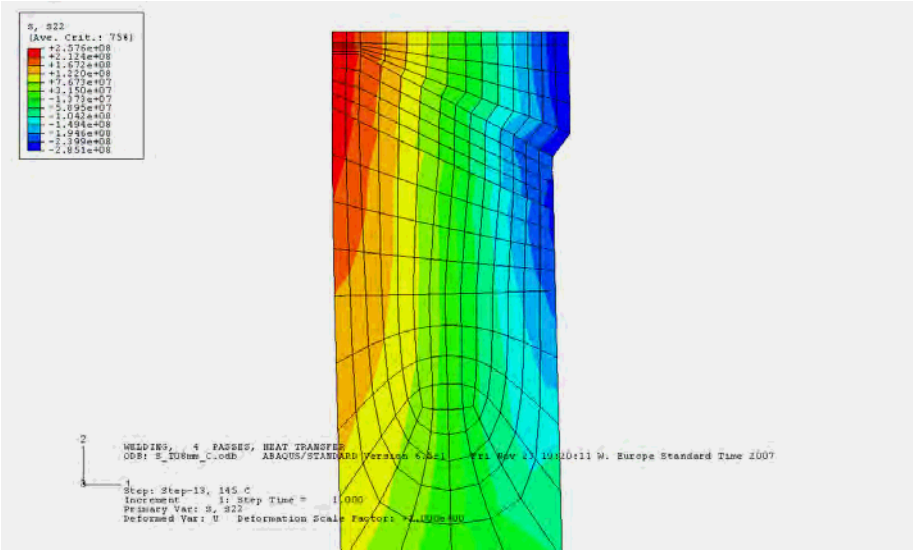

Figure 6.3 Welding residual stress in the axial direction at the operating temperature.

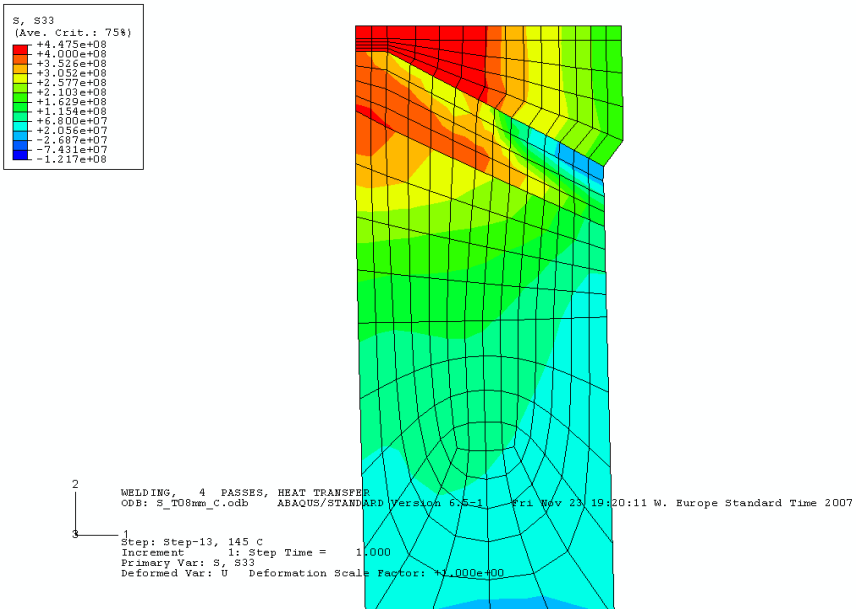

Figure 6.4 Welding residual stress in the circumferential direction at the operating temperature.

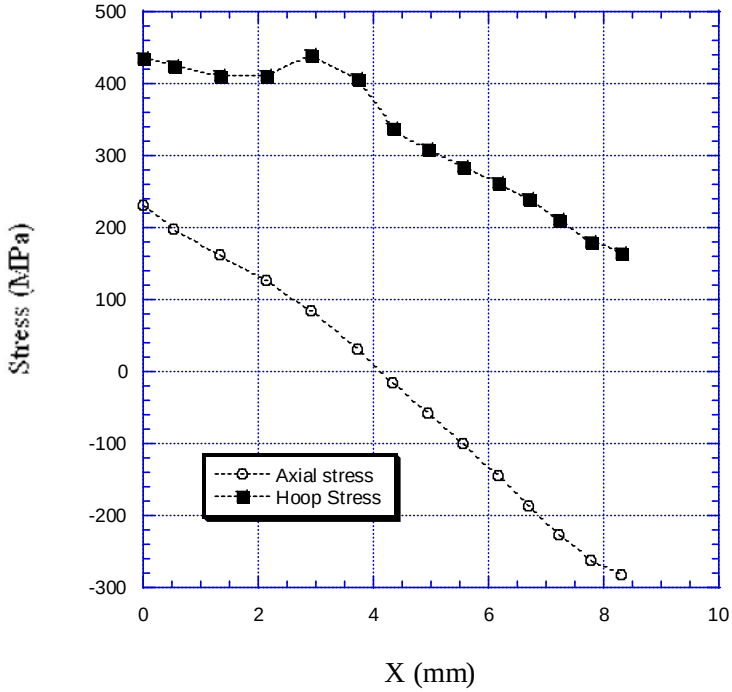

Figure 6.5 Welding residual stresses along the weld centre line. X is measured through the thickness from the pipe's inner surface.

6.3 Crack profiles

Crack profiles determined by the different evaluation methods are shown in Figures 6.6-6.9 for the four different through wall crack lengths. Results are shown for the two load levels L1 and L2. In the figures, open symbols indicate results at load level 1 and the solid symbols for load level 2. The figures are split into two parts: a) gives crack opening displacement COD results for the pipe inner surface and b) for the pipe outer surface. Results due to residual stress only calculated by the elastic FEM method are also included.

When compared with the control method, it is observed that the COD calculated by the elastic FEM method (EL_b) is underestimated, and the COD calculated by the elastic-plastic FEM method (EP_b) is overestimated. If the results are used for an LBB-analysis or assessment of detection by visual inspection technique, the results from the elastic FEM method are conservative in the sense that they under-predict the leak rate and the crack opening. The results from the elastic-plastic FEM method are non-conservative in the same sense.

Note that for one of the analysed cases the crack profile predicted by the elastic FEM method (EL_b) and the control method coincide, as indicated in Figure 6.6b. This could be explained by an essentially elastic behavior for this low load level and short crack. As the crack length is increased by 17%, we start to see a discrepancy, see Figure 6.7b.

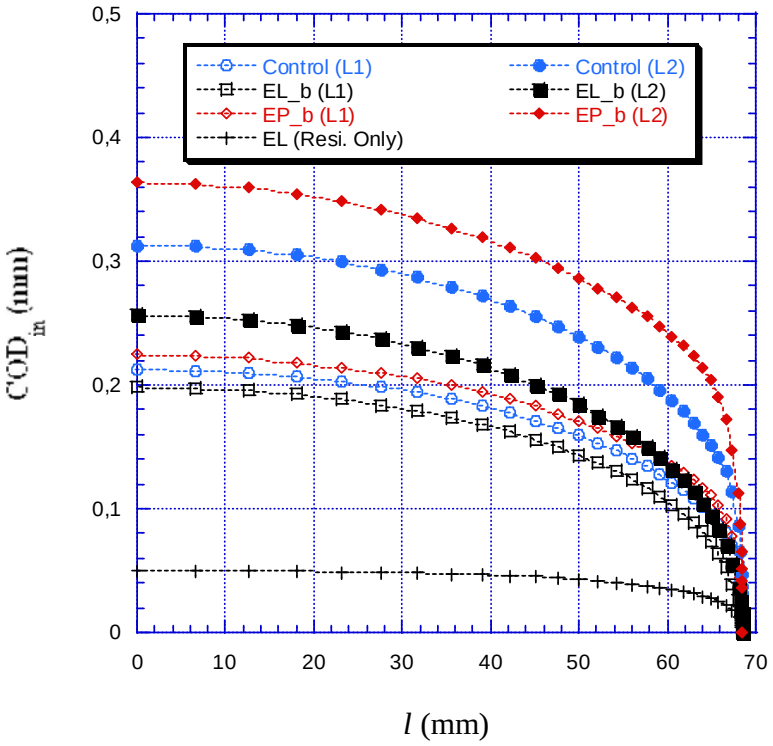

Figure 6.6a COD along pipe **inner surface** for crack length **137 mm**. L1 indicates the results at load level 1 and L2 at the higher load level 2. See Table 4.1 for the notation of the methods.

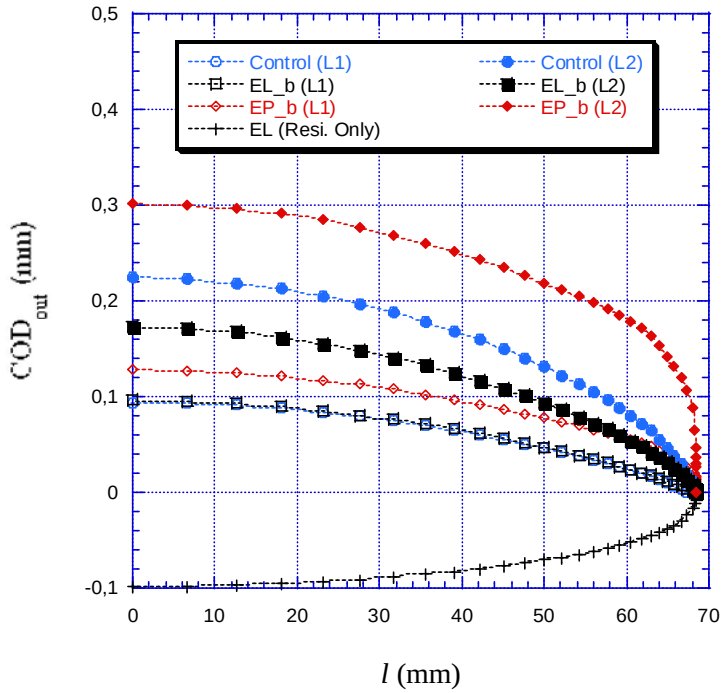

Figure 6.6b COD along pipe **outside surface** for crack length **137 mm**

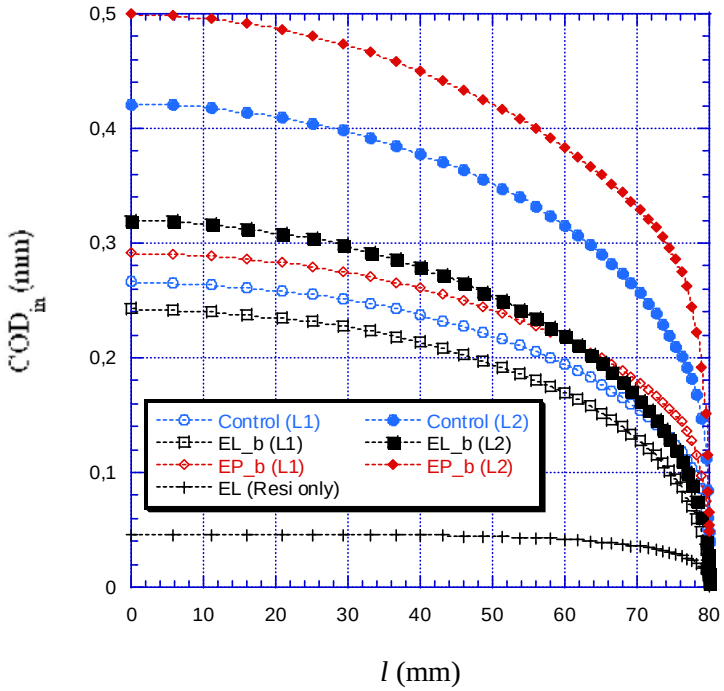

Figure 6.7a COD along pipe **inner surface** for crack length **160 mm**.

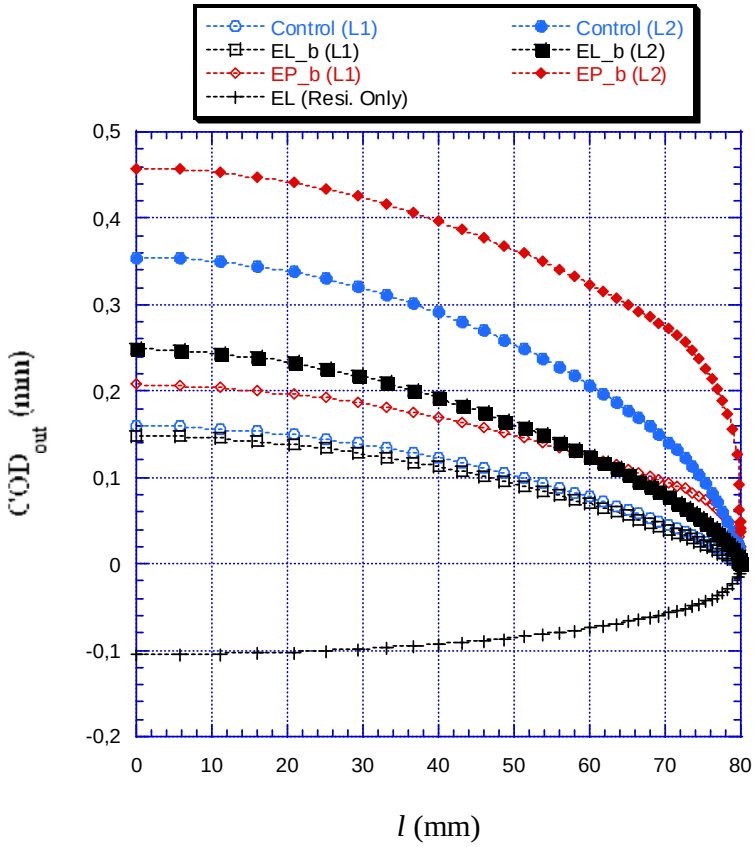

Figure 6.7b COD along pipe **outer surface** for crack length **160 mm**.

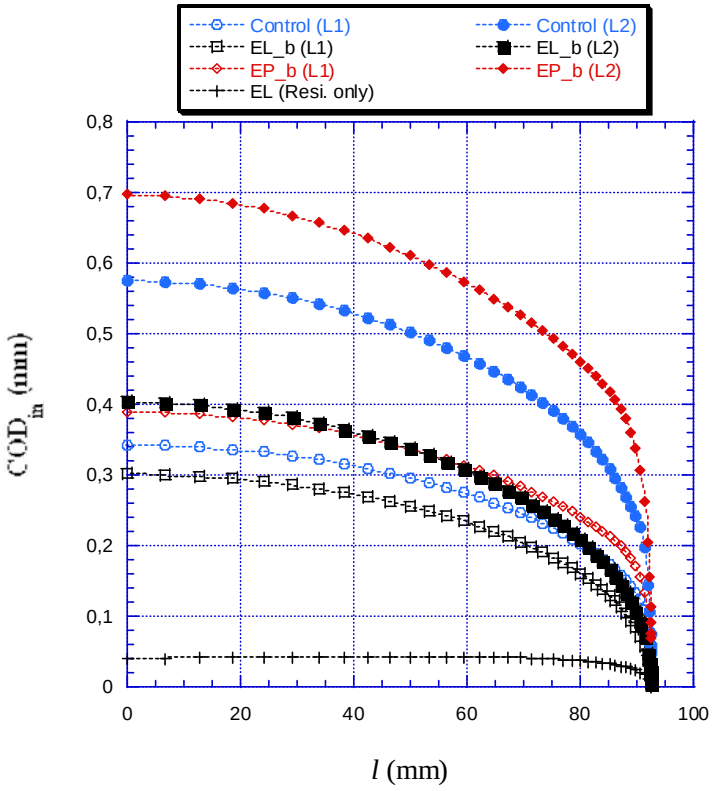

Figure 6.8a COD along pipe **inner surface** for crack length **185 mm**.

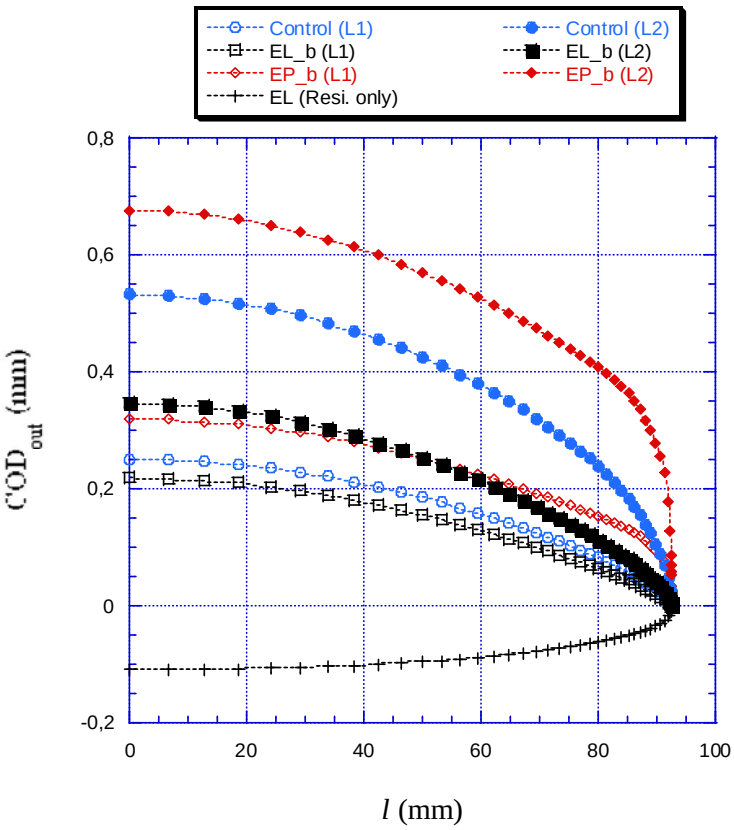

Figure 6.8b COD along pipe **outer surface** for crack length **185 mm**.

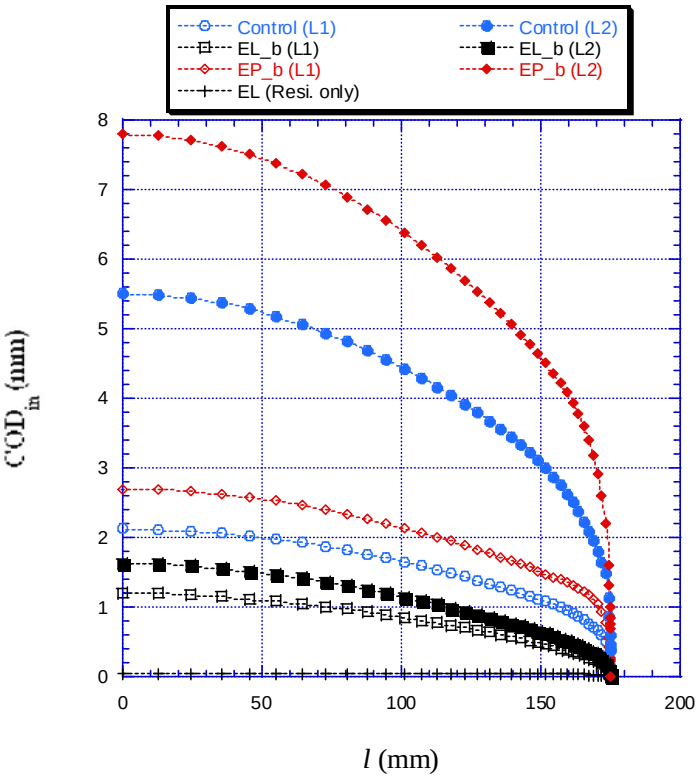

Figure 6.9a COD along pipe **inner surface** for crack length **350 mm**.

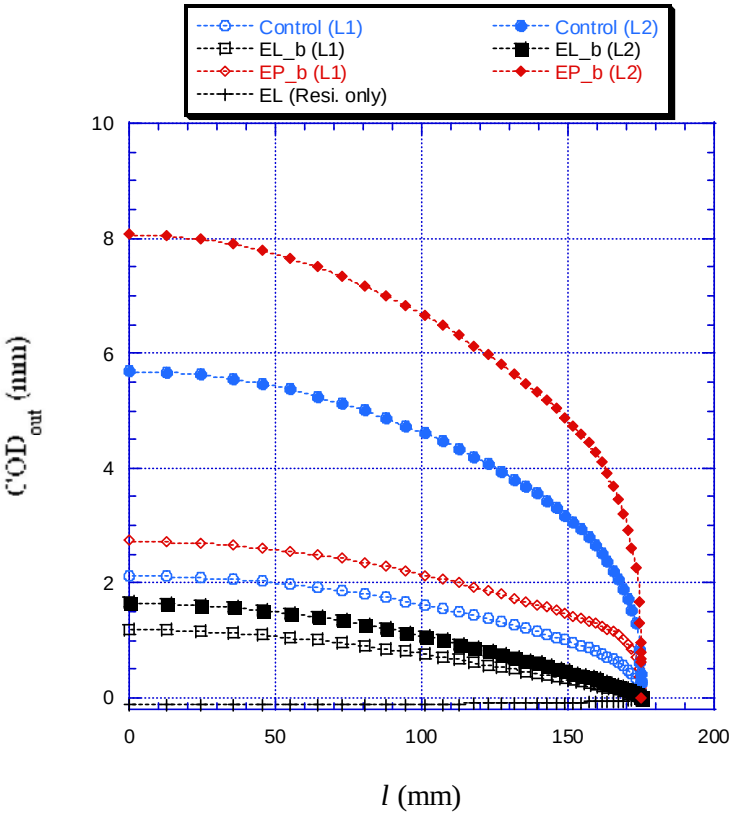

Figure 6.9b COD at pipe **outer surface** for crack length **350 mm**.

6.4 Maximum crack opening displacements

As discussed in section 3.2 the integrated crack opening area may be represented by an equivalent crack opening parameter, δ. Predictions from the FE analyses (from the previous section) are presented in Tables 6.1-6.2 and in Figure 6.10. Predictions from NURBIT are also shown.

When compared with the control method, it is observed that the δ calculated by the elastic-plastic FEM method (EP_b) is slightly overestimated for the shorter cracks (corresponding to the detectable sizes from Table 5.1). The δ calculated by NURBIT is similar to the results by EP_b. For the crack lengths up to 185 mm, the crack opening area is overestimated by 7-26% for the lower load case L1. Comparison to δ calculated by the elastic FEM method indicates that plastic effects are substantial even for the moderate crack lengths and low load level.

Table 6.1 Equivalent crack opening parameter δ at pipe inner surface.

Crack Length (mm)	Load Level	Control (mm)	Weight fcn Plastic corr^{n} NURBIT (mm)	Elastic FEM EL_b (mm)	Plastic FEM EP_b (mm)
137	L1	0.224	0.261	0.205	0.240
	L2	0.335	0.407	0.263	0.396
160	L1	0.280	0.313	0.248	0.310
	L2	0.448	0.536	0.324	0.541
185	L1	0.359	0.394	0.321	0.427
	L2	0.610	0.725	0.420	0.766
350	L1	2.10	-	1.10	2.74
	L2	5.60	-	1.48	8.07

Table 6.2 Equivalent crack opening parameter δ at pipe outer surface.

Crack Length (mm)	Load Level	Control (mm)	Weight fcn Plastic corr^{n} NURBIT (mm)	Elastic FEM EL_b (mm)	Plastic FEM EP_b (mm)
137	L1	0.081	0.070	0.083	0.123
	L2	0.209	0.268	0.156	0.316
160	L1	0.140	0.127	0.128	0.199
	L2	0.335	0.414	0.221	0.475
185	L1	0.223	0.218	0.207	0.328
	L2	0.511	0.633	0.325	0.720
350	L1	2.06	-	1.00	2.74
	L2	5.79	-	1.41	8.40

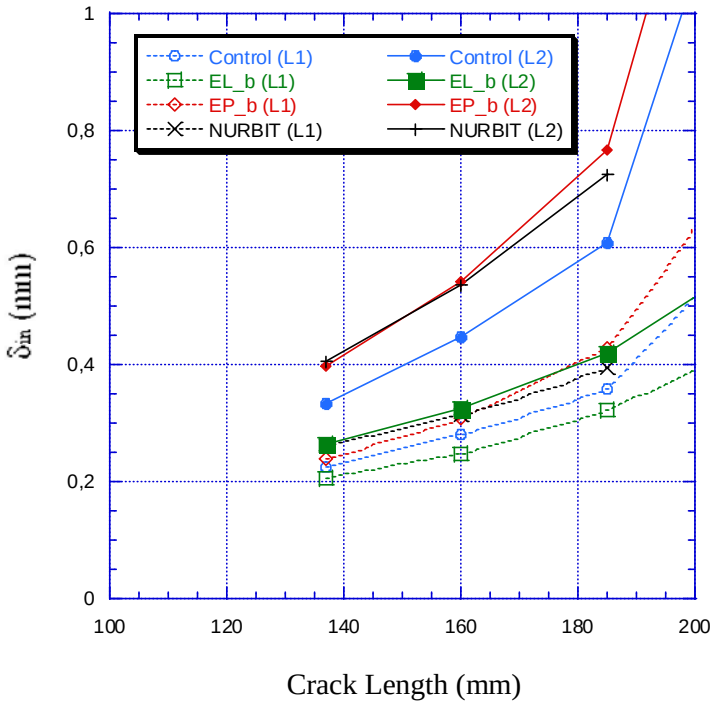

Figure 6.10a. Equivalent crack opening parameter δ at inside surface of pipe. In the figure L1 indicates the results at load level 1 and L2 at load level 2.

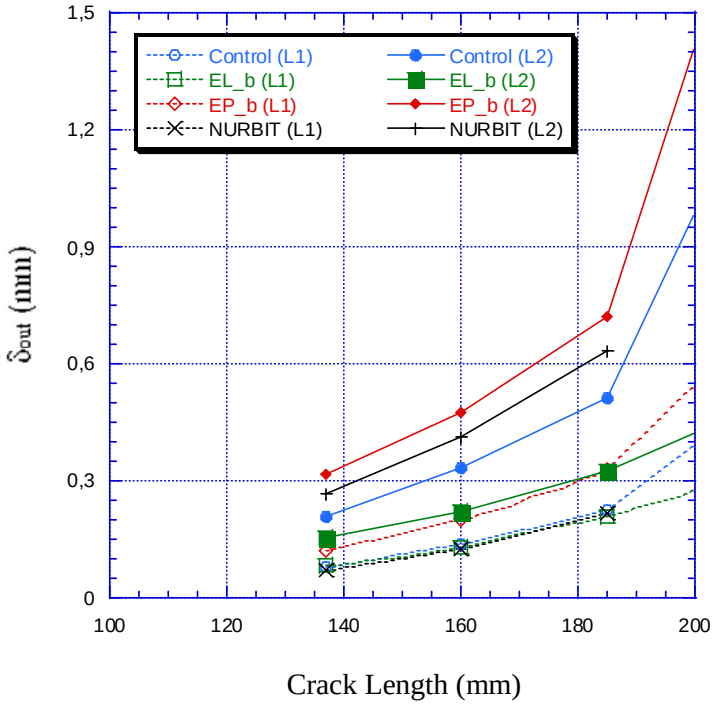

Figure 6.10b. Equivalent crack opening parameter δ at outside surface of pipe.

6.5 Stress intensity factor

The stress intensity factor calculated in this section is based on the near-tip *J*-integral. Eq. (3.1) is used to obtain *K*. The standard *J*-integral, when evaluated close enough to the crack-tip will provide an accurate estimate of the *J*-integral calculated using the integral modified to account for residual stresses, as discussed in Section 3.1.

The *J*-integral along different paths is shown in Figure 6.12 for the case of a 160 mm long crack. The crack is simulated using the control method. Figure 6.12a demonstrates that the standard integral is, in general, path dependent. However, close enough to the crack tip, path independence is displayed as proposed in [4]. In this case, within 1 mm from the crack tip the *J*-integrals are almost path independent. Figure 6.12b shows a detailed view of the paths very close to the crack-tip. The *J*-integral is evaluated for three different positions along the crack front as defined in Figure 6.11.

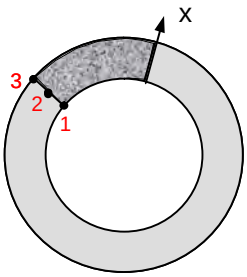

Figure 6.11. Definition of evaluation points along the crack front of the through wall crack. Crack locations 1, 2 and 3 are also refered to as Loc 1, Loc 2 and Loc 3.

For this case it was chosen to determine *K* based on *J*-integrals calculated at 0.1 mm from the crack-tip (path 10 from the tip).

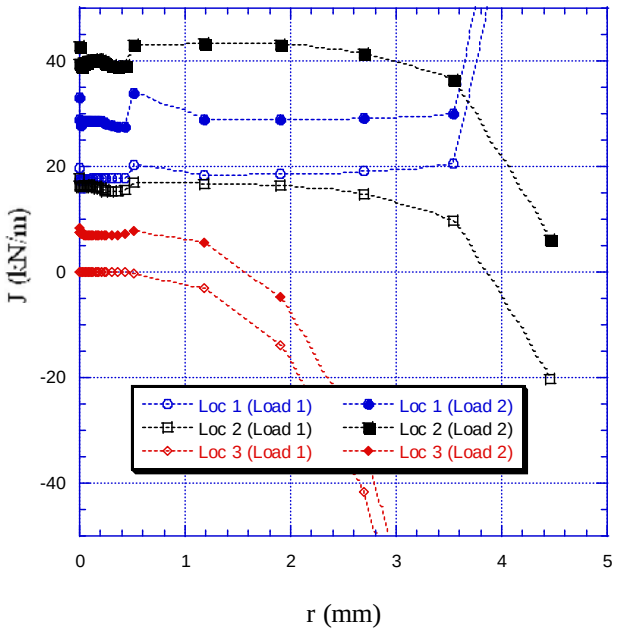

Figure 6.12a. *J*-integrals as function of distance *r* from the crack-tip for a crack simulated by the control method (crack length 160 mm).

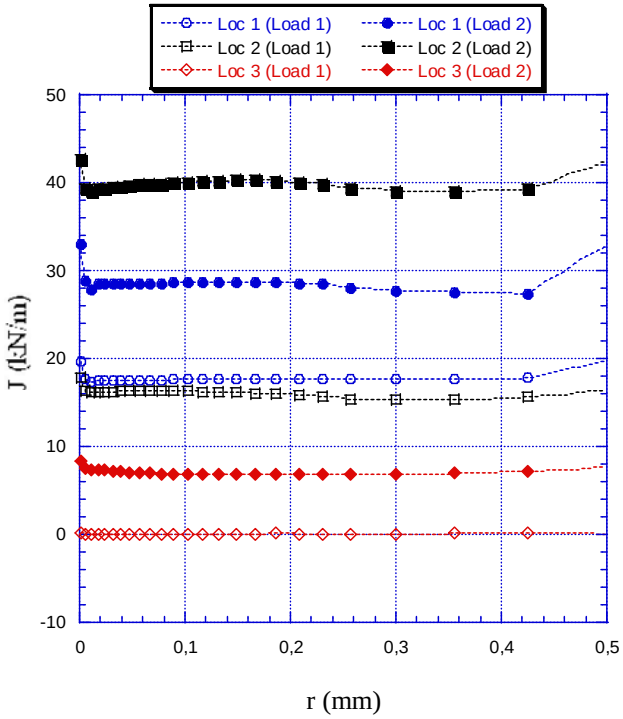

Figure 6.12b. *J*-integrals as function of distance *r* from the crack-tip for a crack simulated by the control method (crack length 160 mm). The 25 near-tip paths are shown.

The distributions of stress intensity factors along the crack front are shown in Figures 6.13-6.15. Results for three different methods are presented: control, elastic FEM and plastic FEM.

The most relevant comparison for crack growth assessments is the difference between the control method and the elastic FE method, because the growth calculations in ProSACC are made using linear elastic solutions. For the moderate cracks up to 185 mm the results for EL_b and control agree well, except at the pipe inside.

Below is a discussion about the deviation in K that is observed for the control method near the inner surface of the pipe. As discussed in the background, the different evaluation methods are based on different modeling assumptions. For example, the high out-of-plane residual stress is only included in the control method. Below some efforts are made to understand the important assumptions in the different models. Note that for the control method K actually decreases approaching the pipe inner surface. Such a results has not previously been observed by the authors and requires further investigation.

We first consider the results for the largest crack (a=350 mm) and the highest loading (L2). In this case the contribution from the residual stress is minimal as seen in Figure 6.15. This allows a comparison of the control method and the elastic-plastic FE method for a case dominated by primary loading. It is seen that the K-values predicted by the control method are consistently lower than those predicted by the elastic-plastic FE method. Since the contribution from the residual stresses to K is small, the major difference between these methods is that a high out-of-plane stress is only applied in the case of the control method (see the hoop stress from Figure 6.5). Addition of such an out-of-plane stress will increase the hydrostatic stress component and suppress near-tip plasticity which might explain the consistently lower reported K value, where K was converted from J using equation 3.1.

Considering then the other crack sizes and load levels, a somewhat different trend emerges. Towards the outer edge of the pipe the results for the elastic-plastic FE and control methods are in reasonably good agreement. The larger difference in predictions is seen towards the inner pipe surface. In this region the residual stresses are tensile and constitute a large proportion of the loading. At the outside the residual stress is compressive. It is hard to differentiate whether the difference towards the inner surface is due to the out-of-plane stress or due to the displacement controlled nature of the residual stress modelled by the control method.

Comparing the elastic FE and elastic-plastic FE models two observations can be made. For low loads the two methods are nearly identical. For high loads, and the largest crack size, higher K-predictions are obtained for the elastic-plastic FE method than for the elastic FE method. These trends may be explained by increased crack tip plasticity in the elastic-plastic FE model for increases in load and crack size. Increased crack tip plasticity effectively increases the crack size and therefore also increases the estimated value of K.

A final observation regarding the Figures 6.13 to 6.15 regards application of the different evaluation methods for crack growth calculations. Compared to the control method, the K-value calculated by the elastic-plastic FE method is conservative, whereas the elastic FE method is non-conservative.

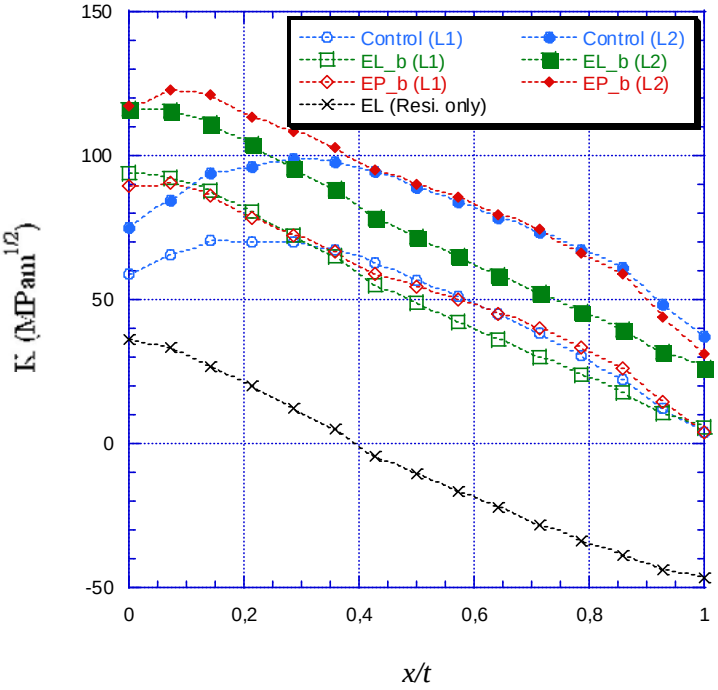

Figure 6.13 Stress intensity factors along the crack front for crack length 160 mm. In the figure, $x = 0$ at the pipe inner surface, L1 indicates the results at load level 1 and L2 at load level 2.

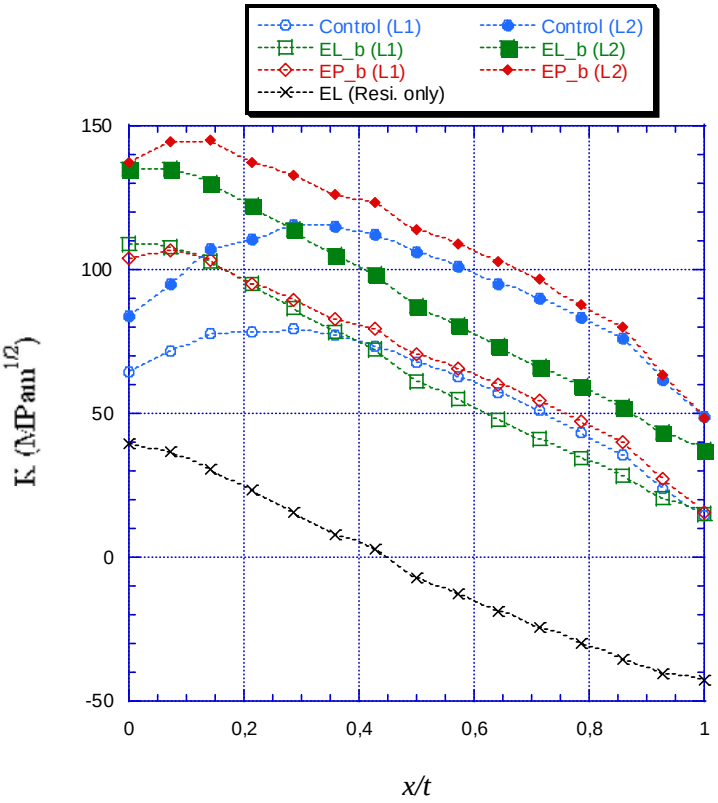

Figure 6.14 Stress intensity factors along the crack front for crack length 185 mm. In the figure, $x = 0$ at the pipe inner surface, L1 indicates the results at load level 1 and L2 at load level 2.

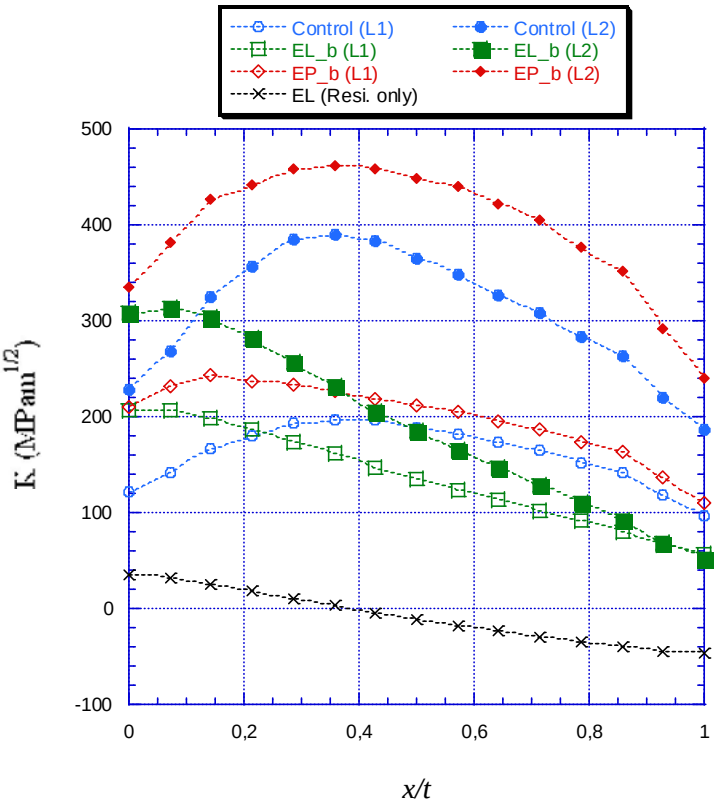

Figure 6.15 Stress intensity factors along the crack front for crack length 350 mm. In the figure, $x = 0$ at the pipe inner surface, L1 indicates the results at load level 1 and L2 at load level 2.

The results are also shown in Tables 6.5-6.6. Results from the software package ProSACC are included for comparison. For crack growth calculations it may be concluded that the elastic ProSACC predictions overestimate K near the inner surface of the pipe, in comparison to the control results.

Note that the maximum value of K is not always obtained at the inner or outer surfaces for the control method and EP_b, see Figure 6.15. This could have implications for predictions using ProSACC since only values at the surfaces are provided from ProSACC.

Table 6.5 Stress intensity factors estimated using different methods at load level 1.

Crack Length (mm)	Crack Location	Control (MPa√m)	$K^{ProSACC}_{Elastic}$ (MPa√m)	EL_b (MPa√m)	EP_b (MPa√m)
137	1	54.7	85.4	85.2	82.0
	2	46. 6	-	43.5	46.3
	3	4.1	-3.4	-0.19	-3.0
160	1	58.9	94.1	94.4	89.7
	2	56.9	-	48.5	56.6
	3	3.9	1.9	5.3	3.2
185	1	64.3	104.6	109.5	104.3
	2	67.8	-	61.5	71.1
	3	14.3	7.4	14.4	15.0
350	1	121.0	204.0	207. 5	209.2
	2	189.0	-	136.3	216.7
	3	97.4	50.2	56.3	108.9

Table 6.6 Stress intensity factors estimated using different methods at load level 2.

Crack Length (mm)	Crack Location	Control (MPa√m)	$K^{ProSACC}_{Elastic}$ (MPa√m)	EL_b (MPa√m)	EP_b (MPa√m)
137	1	67.4	105.2	103.8	106.4
	2	72.0	-	60. 7	76.1
	3	24.5	16.8	18.0	20.3
160	1	75.2	117.8	116.5	118.0
	2	88.8	-	72.0	92.0
	3	37.1	24.1	25.5	30. 5
185	1	84.0	132.9	135.9	137.9
	2	106.1	-	86.7	112.8
	3	48.8	31.8	36.5	47.5
350	1	228.3	270.5	308.0	333.7
	2	365.2	-	183.2	442.5
	3	187.5	88.2	51.7	237.5

Tables 6.7 and 6.8 are included to show the contribution from the residual stress to *K* for the load cases chosen for analysis in this investigation. The contribution at the inner surface is about 50% for the shortest crack and the low primary loading L1.

Table 6.7 Comparison showing the contribution of the residual stress to *K* calculated using the elastic-plastic FE method (load level L1).

Crack Length (mm)	Crack Location	Without residual stresses, (MPa√m)	With residual stresses, (MPa√m)
137	1	44.9	82.0
	2	54.7	65.0
	3	43.7	-3.0
160	1	53.0	89.7
	2	64.9	75.6
	3	50.3	3.18
185	1	64.1	104.3
	2	77.4	84.4
	3	58.6	15.0
350	1	173.7	209.1
	2	222.9	234.7
	3	156.9	108.9

Table 6.8 Comparison showing the contribution of the residual stress to *K* calculated using the elastic-plastic FE method (load level L2).

Crack Length (mm)	Crack Location	Without residual stresses, (MPa√m)	With residual stresses, (MPa√m)
137	1	69.4	106.4
	2	84.8	95.1
	3	67.0	20.3
160	1	81.3	118.0
	2	100.6	111.4
	3	77.5	30. 5
185	1	97.7	137.9
	2	120.7	127.8
	3	91.1	47.5
350	1	298.3	333.7
	2	460.7	472.5
	3	285.5	237.5

6.6 Crack tip opening displacements

Crack tip opening displacements were calculated at the three locations indicated in Figure 6.11. The results are listed in Tables 6.9-6.10 and are also plotted in Figure 6.17a and b to allow better visualization. These results show that the elastic FE method underestimates CTOD. For the three largest crack lengths the elastic-plastic FE method overestimates CTOD.

Table 6.9 Crack tip opening displacements estimated using different methods load level 1.

Crack Length (mm)	Crack Location	Control (mm)	Elastic FEM EL_b (mm)	Elastic-plastic FEM EP_b (mm)
137	1	0.0095	0.0018	0.0080
	2	0.0088	0.0009	0.0113
	3	-0.0004	0.0000	0.0053
160	1	0.0115	0.0017	0.0112
	2	0.0125	0.0018	0.0164
	3	-0.0001	0.0015	0.0074
185	1	0.0142	0.0023	0.0167
	2	0.0175	0.0014	0.0240
	3	0.0004	0.0003	0.0108
350	1	0.0924	0.0029	0.1053
	2	0.1332	0.0029	0.1857
	3	0.0361	0.0011	0.3488

Table 6.10 Crack tip opening displacements estimated using different methods load level 2.

Crack Length (mm)	Crack Location	Control (mm)	Elastic FEM EL_b (mm)	Elastic-plastic FEM EP_b (mm)
137	1	0.0156	0.0022	0.0201
	2	0.0200	0.0013	0.0296
	3	0.0015	0.0004	0.0149
160	1	0.0210	0.0024	0.0287
	2	0.0294	0.0016	0.0420
	3	0.0038	0.0005	0.0213
185	1	0.0281	0.0029	0.0456
	2	0.0425	0.0019	0.0600
	3	0.0068	0.0008	0.0326
350	1	0.1774	0.0042	0.3289
	2	0.4379	0.0025	0.7011
	3	0.1338	0.0019	0.2936

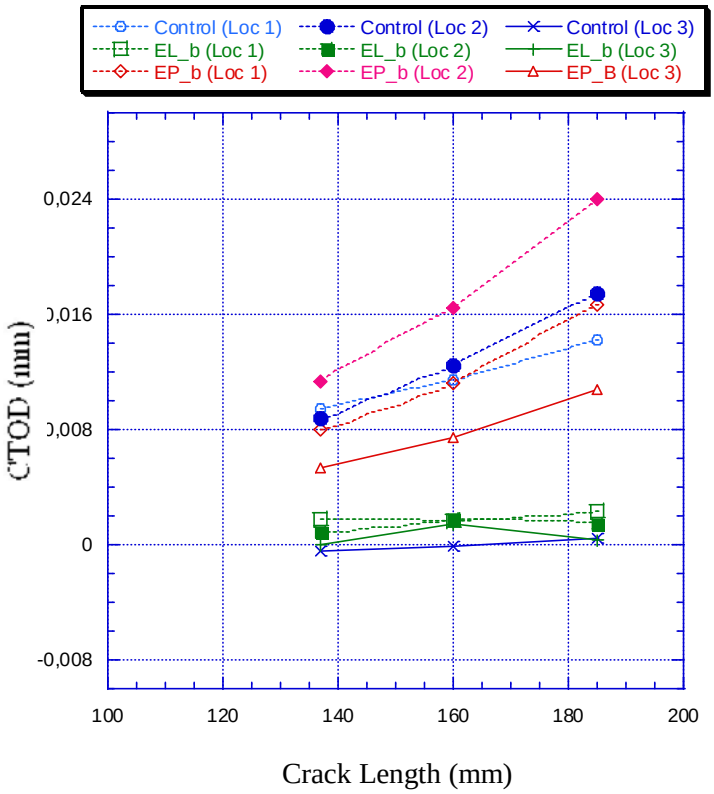

Figure 6.17a. Crack tip opening displacements for load level 1.

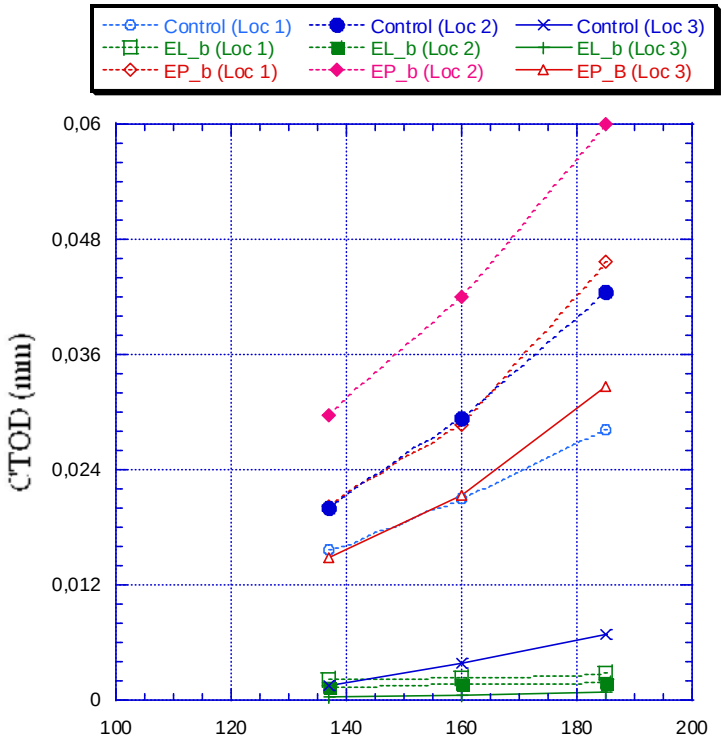

Figure 6.17b. Crack tip opening displacements for load level 2.

7 CASE TWO - THIN PIPE WITH A FULL CIRCUMFERENTIAL INTERNAL SURFACE CRACK

7.1 Finite element models

The pipe geometry considered in case two is the same as for case one with the difference that a full circumferential, internal surface crack is modeled, as opposed to a through-wall crack. The finite element mesh used for welding simulation is also the same, as shown in Figure 7.1. The finite element mesh for the fracture mechanics model is, however, different. A 2D, axisymmetric model was used and is illustrated in Figure 7.1. The notch radius is 0.001mm, allowing accurate prediction of near-tip-*J* and CTOD.

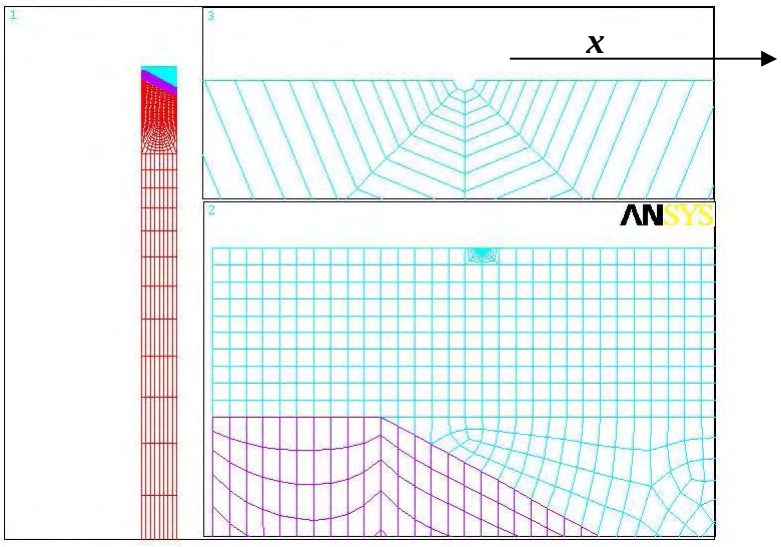

Figure 7.1 Case 2 – 2D axisymmetric finite element mesh for the full circumferential, internal surface crack.

7.2 Crack profiles

Crack profiles through the thickness are shown in Figures 7.2 to 7.5 for the different evaluation methods. Each figure represents a different crack depth, ranging from a/t=0.2 to 0.8. Results are shown for the two load levels L1 and L2. In the figures, open symbols indicate results at load level 1 and the solid symbols at load level 2. Results due to residual stresses only, calculated by the elastic FE method, are also included.

Note that the crack opening displacement due to welding residual stress contributes approximately 50% of the total COD for both the elastic and elastic-plastic FE methods. Inclusion of weld residual stresses is therefore very important in computation of COD for these cases.

It is observed that the crack opening displacement predicted by the elastic FE method and the elastic-plastic FE method are nearly identical when $a/t < 0.6$. This implies that the effect of plastic deformation in these cases is very limited. In comparison to the control method, both the elastic and elastic-plastic FE methods underestimate the crack opening displacement for a/t up to 0.6. For a/t equal to 0.8, the same trend is again observed for the lower load level L1, but for the higher load level L2, the COD for the elastic-plastic FE method is overestimated. The difference between the control method and EP_b could be due to the displacement controlled model and the high out-of-plane stress.

Note that for conclusions on VT inspection results for the control method and residual stresses only would be needed, since VT is performed in a state without pressure.

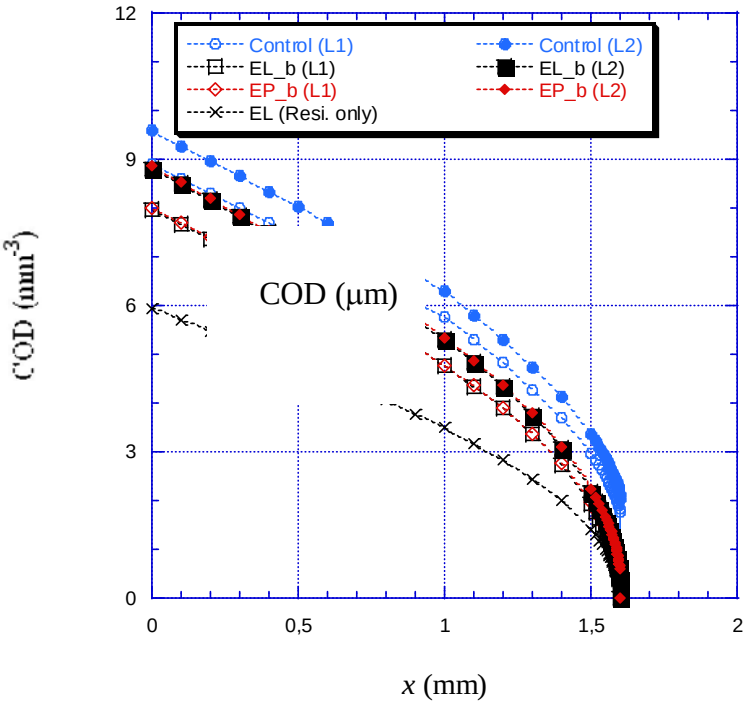

Figure 7.2 COD for crack depth a/t = 0.2. x = 0 at the pipe inner surface.

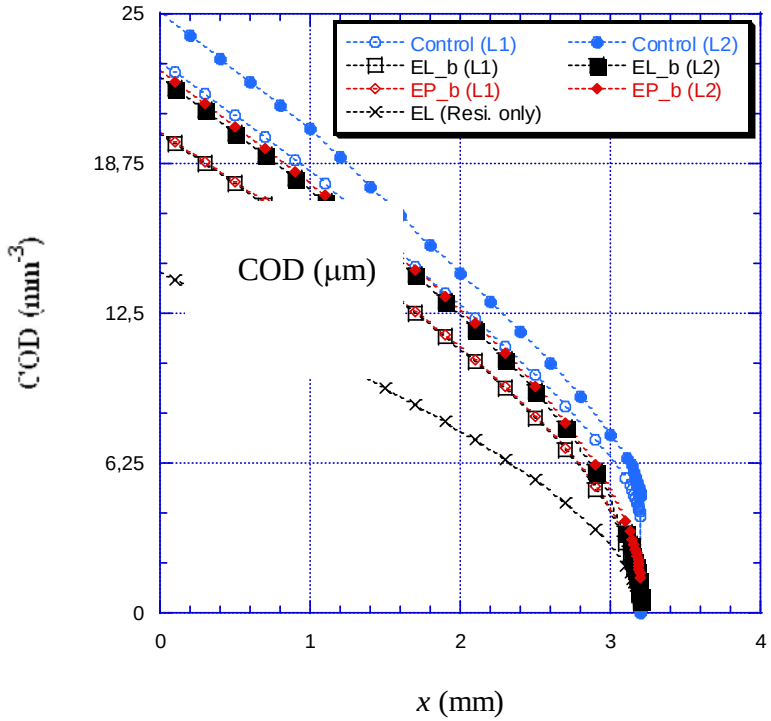

Figure 7.3 COD for crack depth a/t = 0.4. x = 0 at the pipe inner surface.

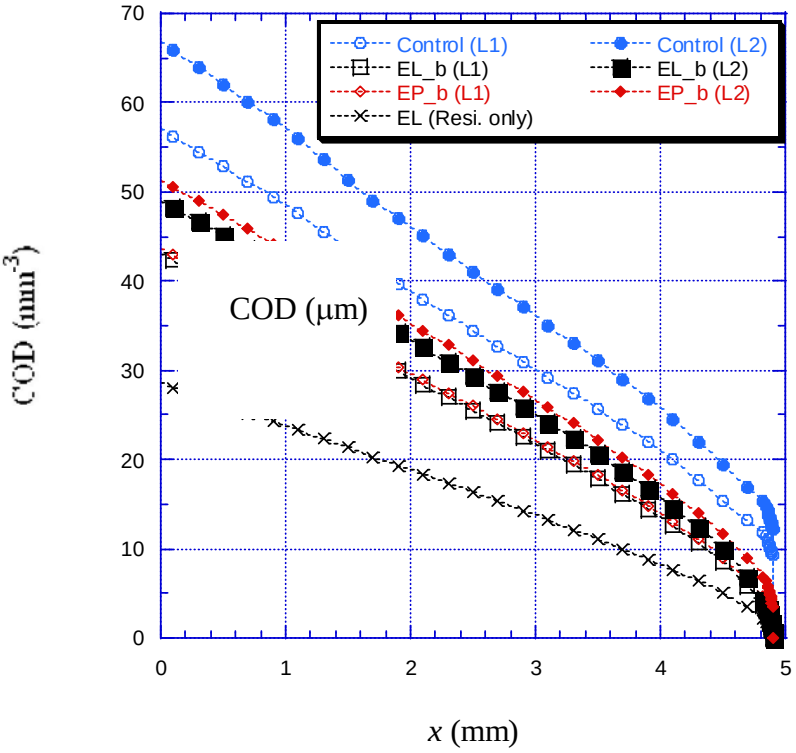

Figure 7.4 COD for crack depth a/t = 0.6. x = 0 at the pipe inner surface.

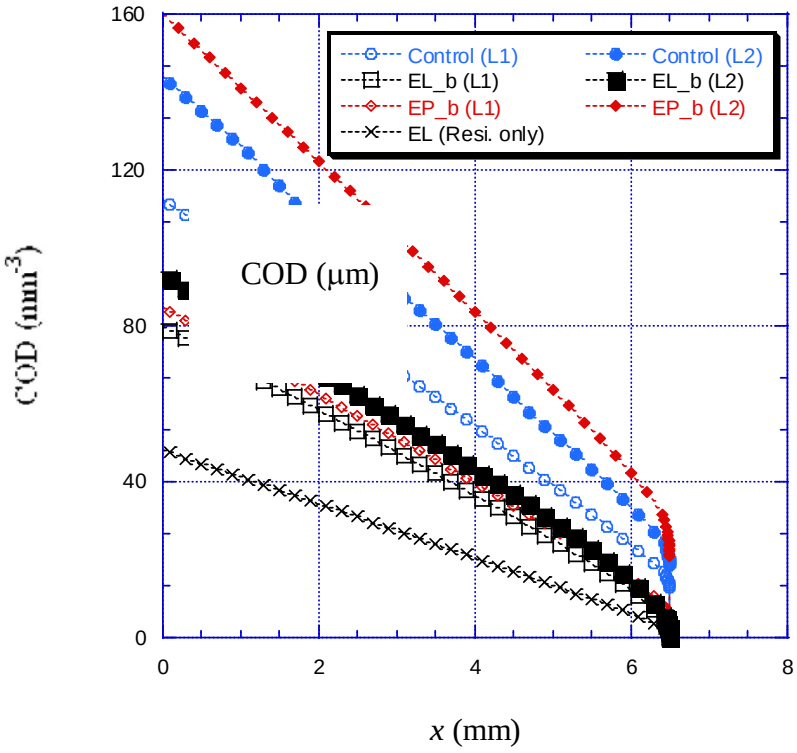

Figure 7.5 COD for crack depth a/t = 0.8. x = 0 at the pipe inner surface.

7.3 Stress intensity factor

As in Section 6.5 the stress intensity factor calculated in this section is based on the near-tip *J*-integral. Eq. (2.1) is used to obtain *K*. The *J*-integrals for crack depth *a/t* = 0.6 are shown in Figure 7.6. It is shown that the *J*-integrals are strongly path dependent about 0.05 mm away from crack tip. Within 0.05 mm from the crack tip, *J*-integrals are almost path independent.

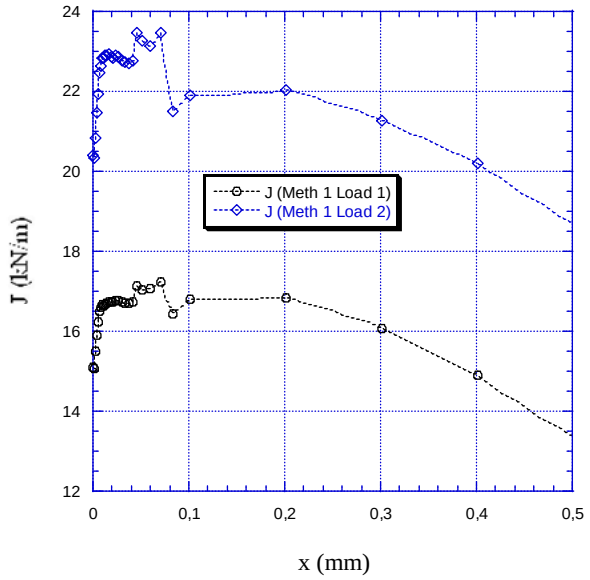

Figure 7.6a. *J*-integrals by Control Method for crack depth a/t = 0.6 (including remote paths).

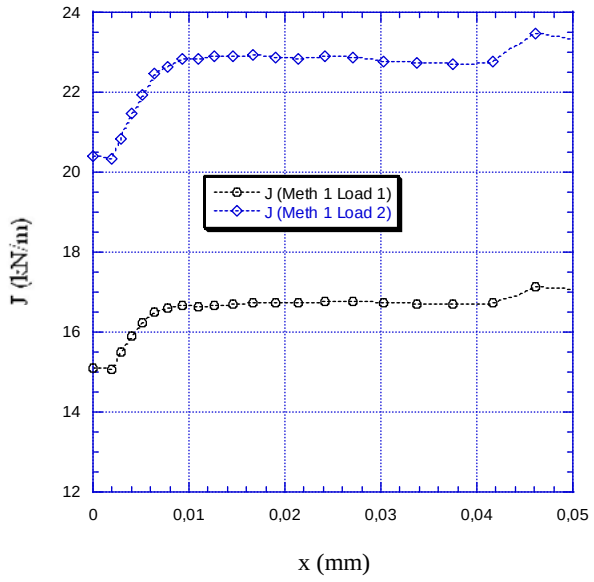

Figure 7.6b. *J*-integrals by Control Method for crack depth a/t = 0.6 (21 paths near the crack tip).

For this case it was chosen to determine *K* based on *J*-integrals at 0.015mm from the crack tip (path 10 from the crack tip).

Stress intensity factors for the different evaluation methods, including ProSACC, are shown in Table 7.1. The most relevant comparison for growth assessments is the difference between the control method, the elastic FE method and the elastic ProSACC method. It is observed that the elastic results from ProSACC provide slight overestimates of K except for the shallowest crack depth of a/t=0.2 where it is slightly underestimated. The relative difference is 7% for $a/t=0.6$ at the lower load level L1.

Table 7.1 Case 2 - stress intensity factors estimated using the different evaluation methods.

Load Level	Crack Depth (a/t)	Control Method (MPa√m)	$K_{Elasitc}^{ProSACC}$ (MPa√m)	EL_b (MPa√m)	EP_b (MPa√m)
1	0.2	27.0	26.3	25.0	25.2
	0.4	39.1	42.4	38.1	38.6
	0.6	57.4	61.6	52.7	53.0
	0.8	72.4	~	64.2	67. 6
2	0.2	29.3	29.3	27.9	28.3
	0.4	43.3	48.4	43.3	43.7
	0.6	67.2	72.1	61.7	62.8
	0.8	89.1	~	78.0	122.0

Table 7.2 is included to show that the contribution from the residual stress to K is significant. The elastic-plastic FE method was used for these calculations.

Table 7.2 Comparison showing the contribution of the residual stress to K, for the elastic-plastic FE method EP_b.

Load Level	Crack Depth (a/t)	Control Method (MPa√m)	Without residual stresses, (MPa√m)	With residual stresses, (MPa√m)
1	0.2	27.0	7.2	25.2
	0.4	39.1	13.3	38.6
	0.6	57.4	22.0	53.0
	0.8	72.4	36.8	67.6
2	0.2	29.3	10.3	28.3
	0.4	43.3	18.4	43.7
	0.6	67.2	31.8	62.8
	0.8	89.1	91.2	122.0

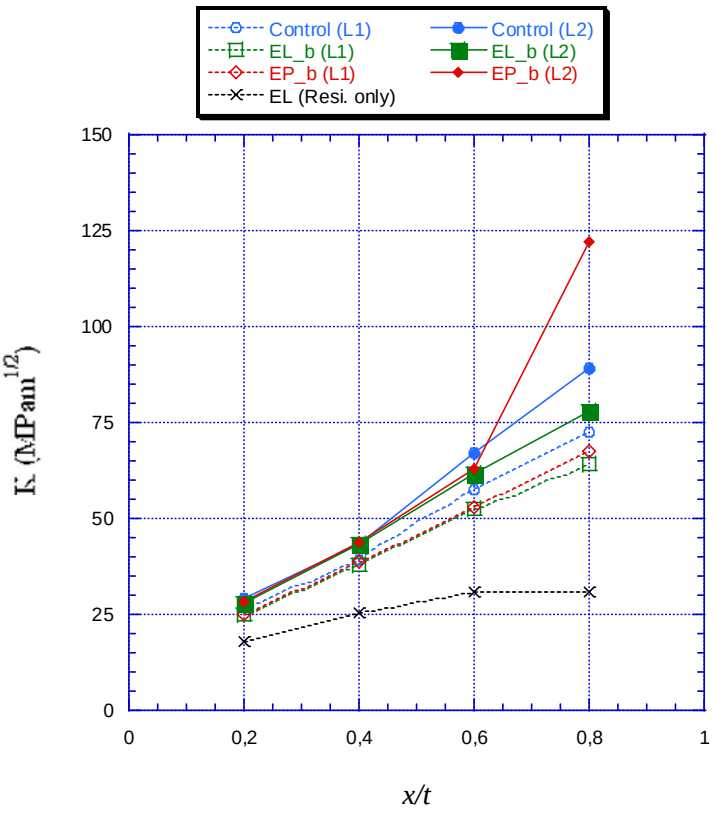

Figure 7.7 Case 2 - stress intensity factors for surface crack. In the figure, x = 0 at the pipe inner surface, L1 indicates the results at load level 1 and L2 at load level 2.

7.4 Crack tip opening displacements

The results for CTOD are listed in Tables 7.3-7.4 for load level 1 and load level 2, respectively. In comparison with the results by the control method, it is clear that the results for both elastic and elastic-plastic methods are underestimated.

Table 7.3 CTOD at load level 1.

Crack depth (*a/t*)	Control Method (mm)	Elastic FEM EL_b (mm)	Elastic-plastic FEM EP_b (mm)
0.2	0.00360	0.00058	0.00080
0.4	0.00440	0.00088	0.00188
0.6	0.02000	0.00121	0.00411
0.8	0.03400	0.00151	0.00931

Table 7.4 CTOD at load level 2.

Crack depth (*a/t*)	Control Method (mm)	Elastic FEM EL_b (mm)	Elastic-plastic FEM EP_b (mm)
0.2	0.00440	0.00070	0.00120
0.4	0.01000	0.00108	0.00288
0.6	0.03400	0.00143	0.00741
0.8	0.05400	0.00181	0.04171

8 CASE THREE - MEDIUM PIPE WITH A THROUGH WALL CRACK

8.1 Finite element model

The finite element mesh for 2D axial symmetrical welding simulation is shown in Figure 8.1. In the figure the weld pass order is also plotted. The 3D finite element mesh for the fracture mechanics model with a through wall crack is shown in Figure 8.2. Only a quarter of the model is considered due to symmetry. A small notch with a notch radius 0.001 mm is introduced at the crack tip – this allows an accurate estimation of near-tip-*J* and CTOD.

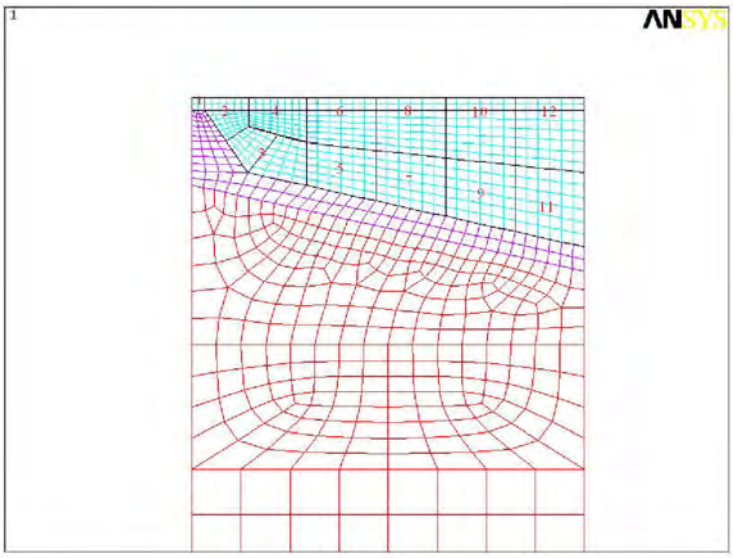

Figure 8.1 Finite element mesh for 2D welding simulation for case study 3.

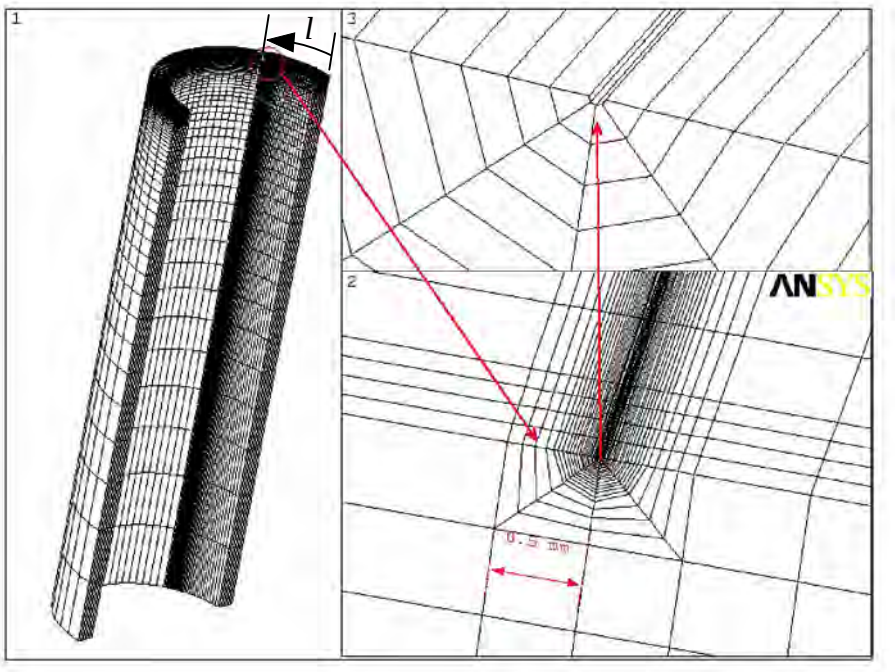

Figure 8.2 Case 3 - finite element mesh with a through thickness crack. The coordinate l = 0 corresponds to the center of the through wall crack, as previously defined in Figure 3.2.

8.2 Results from 2D welding simulation

The welding residual stress distribution at the operating temperature (323 °C) is shown in Figures 8.3 and 8.4. The welding residual stress in the hoop and axial directions along the weld centre line are graphed in Figure 8.5.

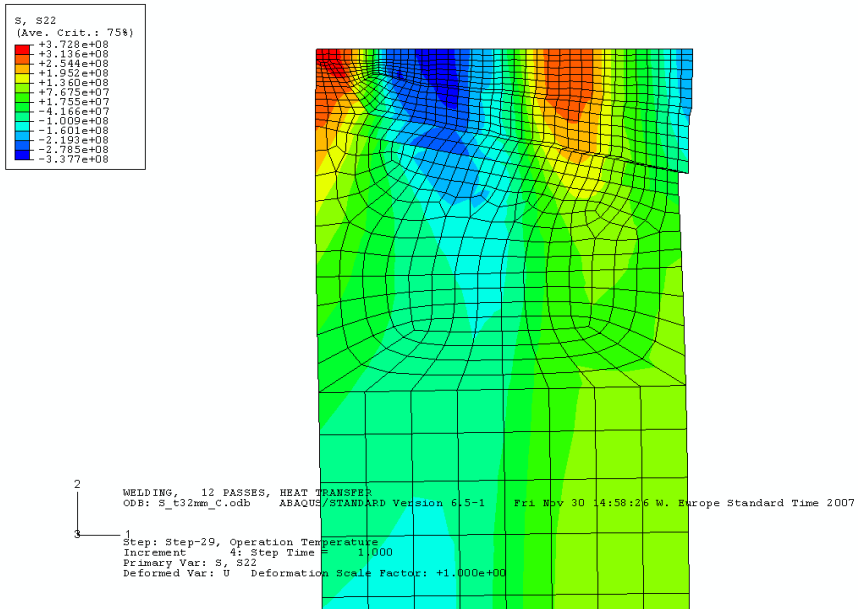

Figure 8.3 Welding residual stress along axial direction at 323 °C.

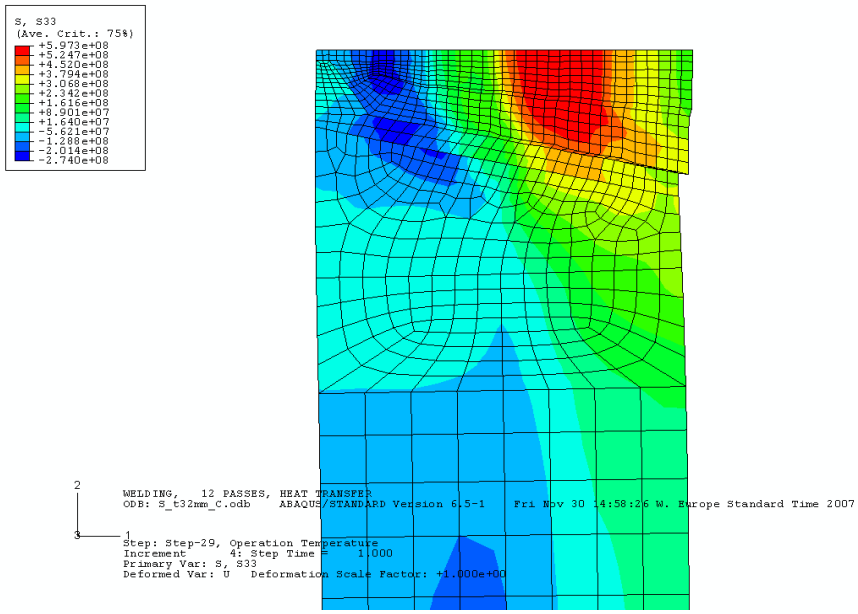

Figure 8.4 Welding residual stress along circumferential direction at 323 °C.

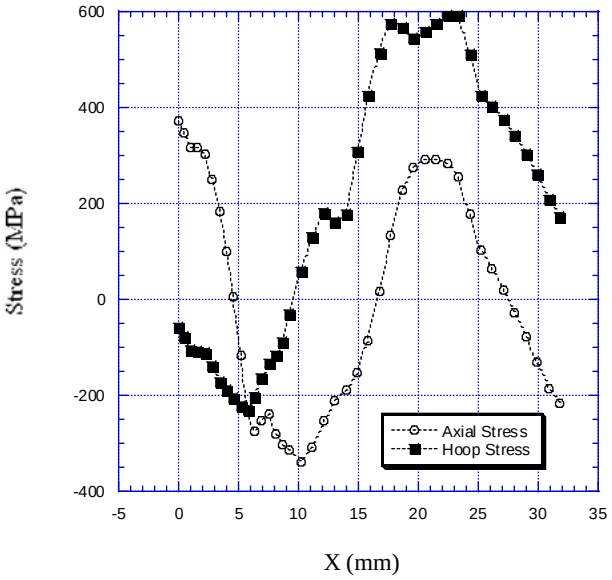

Figure 8.5 Case 3 - welding residual stresses along the weld centre line. X is measured through the thickness from the pipe's inner surface.

8.3 Crack profiles

Crack profiles determined by the different evaluation methods are shown in Figures 8.6-8.9 for the four different through wall crack lengths. Results are shown for the two load levels L1 and L2. In the figures, open symbols indicate results at load level 1 and the solid symbols for load level 2. The figures are split into two parts: a) gives crack opening displacement COD results for the pipe inner surface and b) for the pipe outer surface. Results due to residual stress only calculated by the elastic FEM method are also included. Note that for this case the contribution to COD from residual stresses only is small.

When compared with the control method, it is observed that the COD calculated by the elastic FEM method (EL_b) is underestimated. The COD calculated by the elastic-plastic FEM method (EP_b) is overestimated for all cases except the 175 mm crack on the outer surface. There the elastic-plastic COD is slightly underestimated.

If the results are used for an LBB-analysis or assessment of detection by visual inspection technique, the results from the elastic FEM method are conservative in the sense that they under-predict the leak rate and the crack opening. The results from the elastic-plastic FEM method are non-conservative in the same sense.

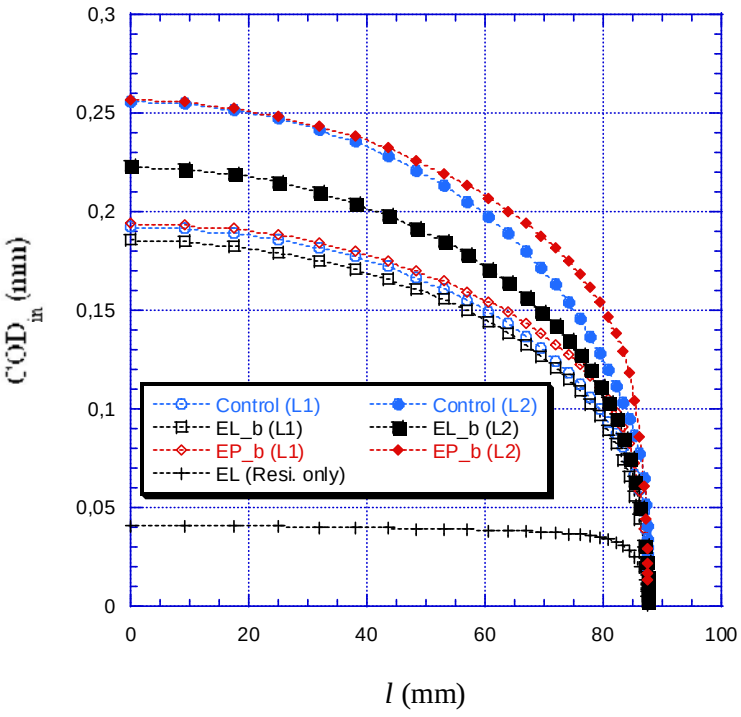

Figure 8.6a COD along pipe **inner surface** for crack length **175 mm**. l = 0 at the symmetry plane, L1 indicates the results at load level 1 and L2 at load level 2. .

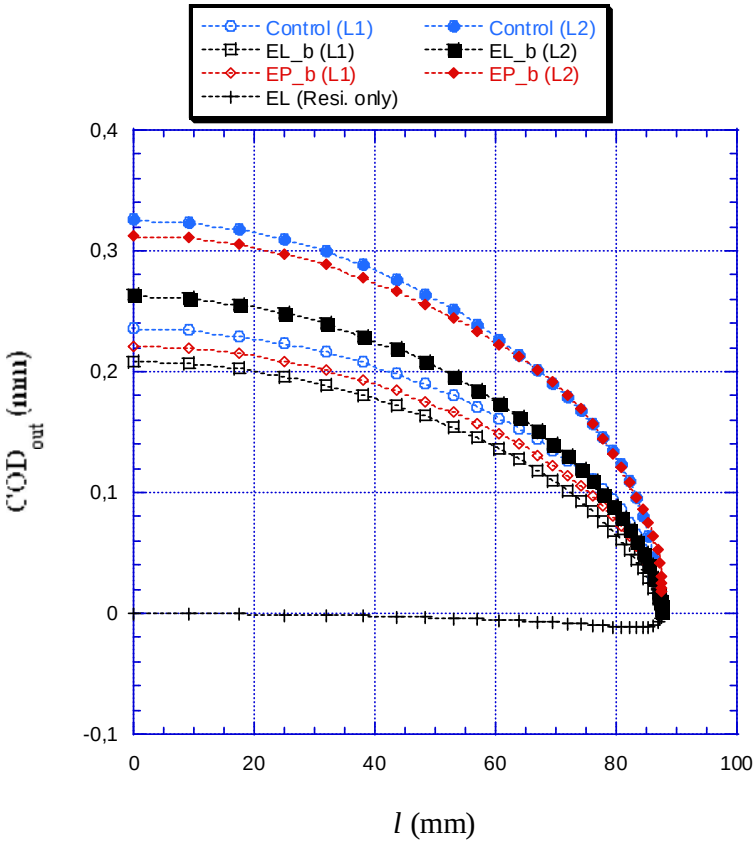

Figure 8.6b COD along pipe **outer surface** for crack length **175 mm**. l = 0 at the symmetry plane, L1 indicates the results at load level 1 and L2 at load level 2.

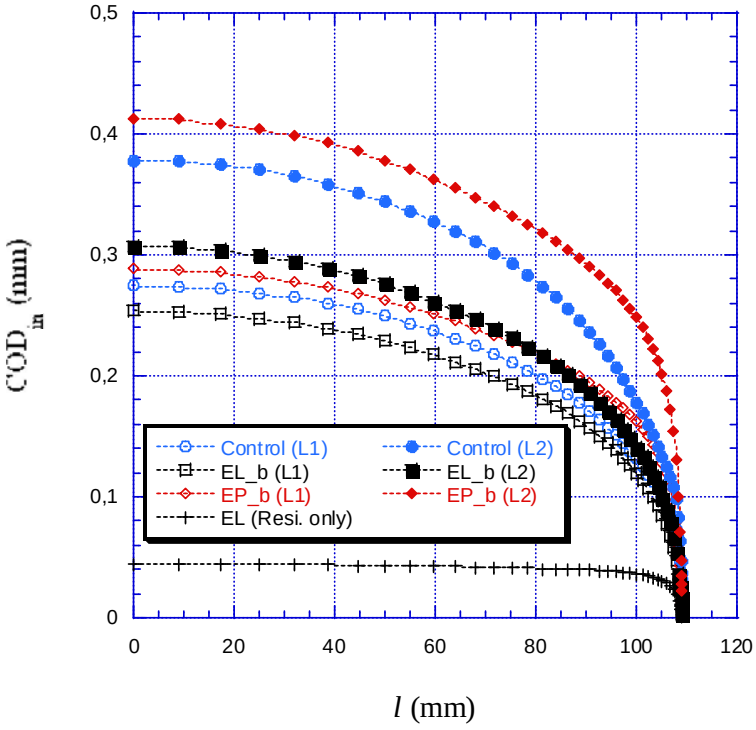

Figure 8.7a COD along pipe **inner surface** for crack length **218 mm**. l = 0 at the symmetry plane, L1 indicates the results at load level 1 and L2 at load level 2.

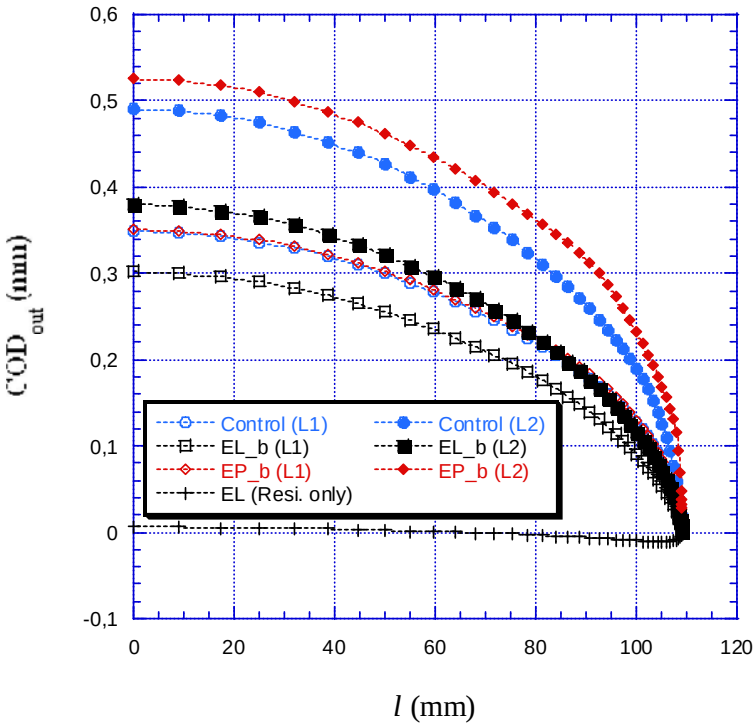

Figure 8.7b COD along pipe **outer surface** for crack length **218 mm**. l = 0 at the symmetry plane, L1 indicates the results at load level 1 and L2 at load level 2.

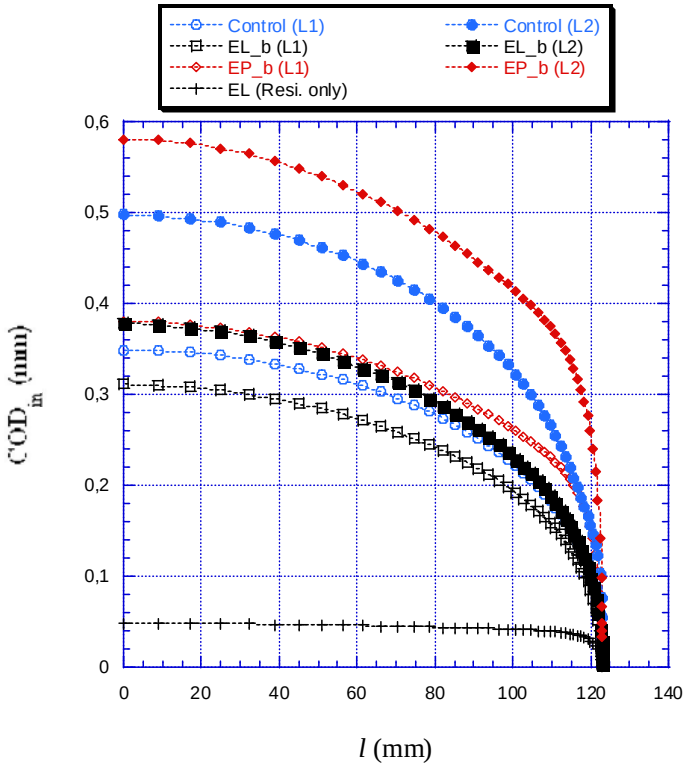

Figure 8.8a COD along pipe **inner surface** for crack length **246 mm**. l = 0 at the symmetry plane, L1 indicates the results at load level 1 and L2 at load level 2.

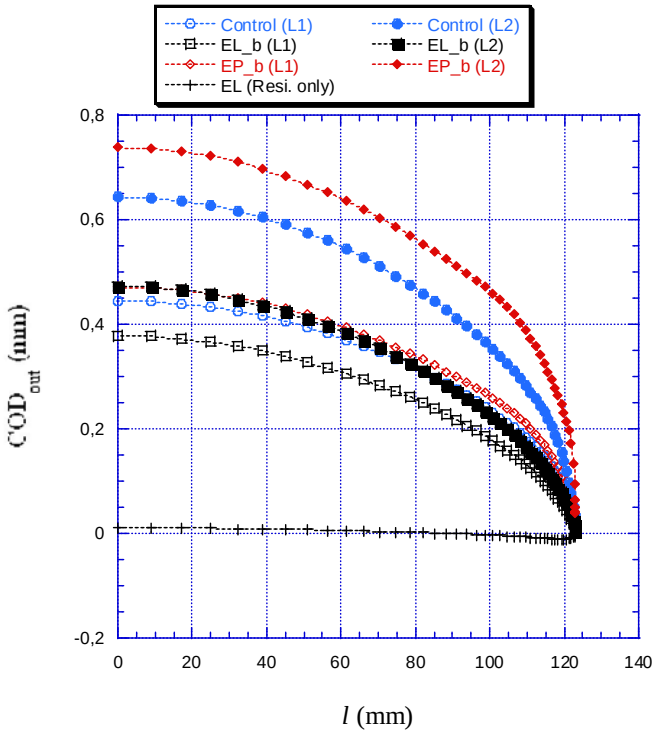

Figure 8.8b COD along pipe **outer surface** for crack length **246 mm**. *l* = 0 at the symmetry plane, L1 indicates the results at load level 1 and L2 at load level 2.

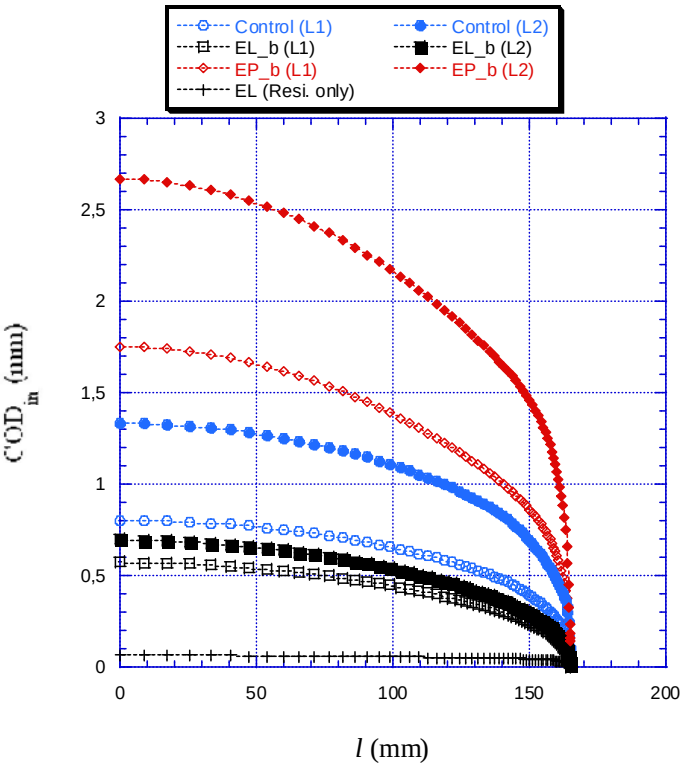

Figure 8.9a COD along pipe **inner surface** for crack length **330 mm**. *l* = 0 at the symmetry plane, L1 indicates the results at load level 1 and L2 at load level 2.

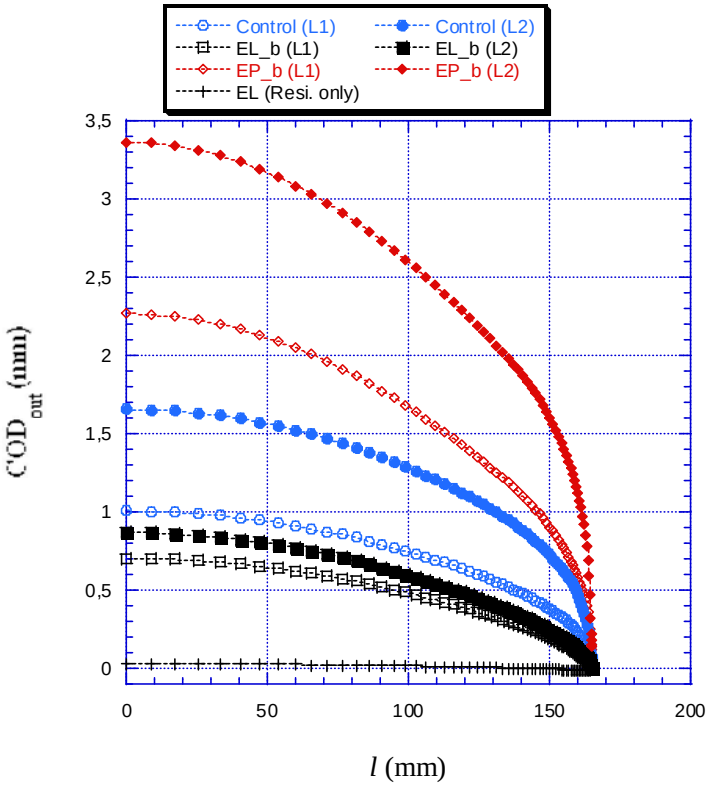

Figure 8.9b COD along pipe **outer surface** for crack length **330 mm**. l = 0 at the symmetry plane, L1 indicates the results at load level 1 and L2 at load level 2.

8.4 Maximum crack opening displacements

As discussed in section 2.2 the integrated crack opening area may be represented by an equivalent crack opening parameter, δ. Predictions from the FE analyses (from the previous section) are presented in Table 8.1 and in Figure 8.10.

When compared with the control method, it is observed that the δ calculated by the elastic-plastic FEM method (EP_b) is overestimated. For moderate crack lengths up to 246 mm and the lower load level L1, the crack opening area is overestimated by up to 12%.

Table 8.1a Equivalent δ at pipe inner surface.

Crack Length (mm)	Load Level	Control (mm)	EL_b (mm)	EP_b (mm)
175	1	0.202	0.194	0.207
	2	0.267	0.231	0.276
218	1	0.286	0.262	0.304
	2	0.394	0.315	0.446
246	1	0.361	0.318	0.403
	2	0.519	0.384	0.625
330	1	0.8263	0.566	1.106
	2	1.3933	0.686	2.103

Table 8.1b Equivalent δ at pipe outer surface.

Crack Length (mm)	Load Level	Control (mm)	EL_b (mm)	EP_b (mm)
175	1	0.230	0.202	0.217
	2	0.321	0.255	0.316
218	1	0.337	0.286	0.340
	2	0.480	0.360	0.533
246	1	0.428	0.353	0.461
	2	0.630	0.443	0.753
330	1	0.965	0.637	1.281
	2	1.646	0.788	2.466

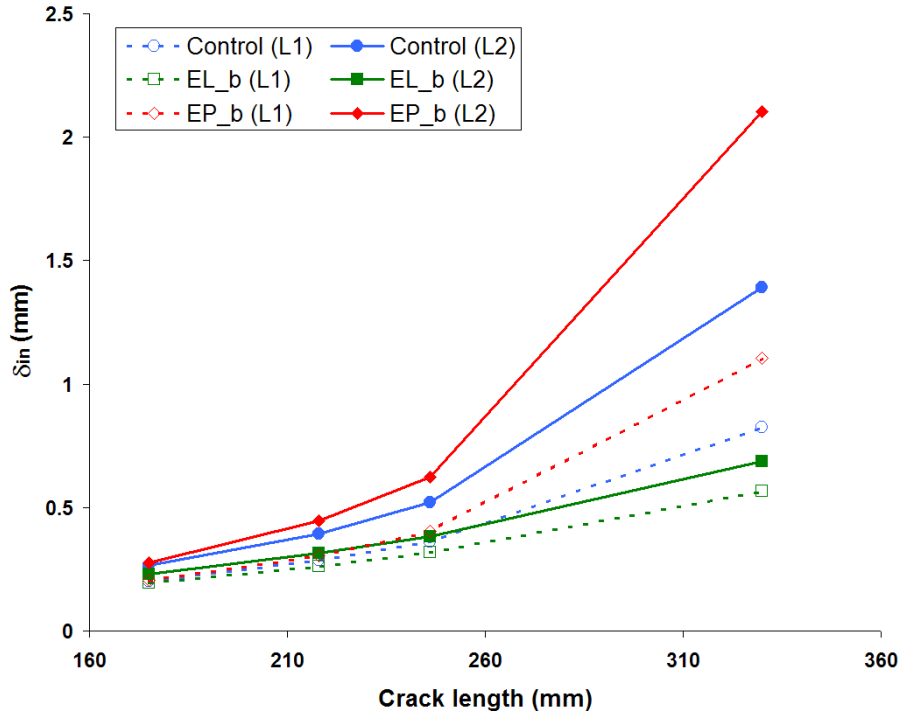

Figure 8.10a Equivalent crack opening parameter δ at the **inside surface** of the pipe. In the figure L1 indicates the results at load level 1 and L2 at load level 2.

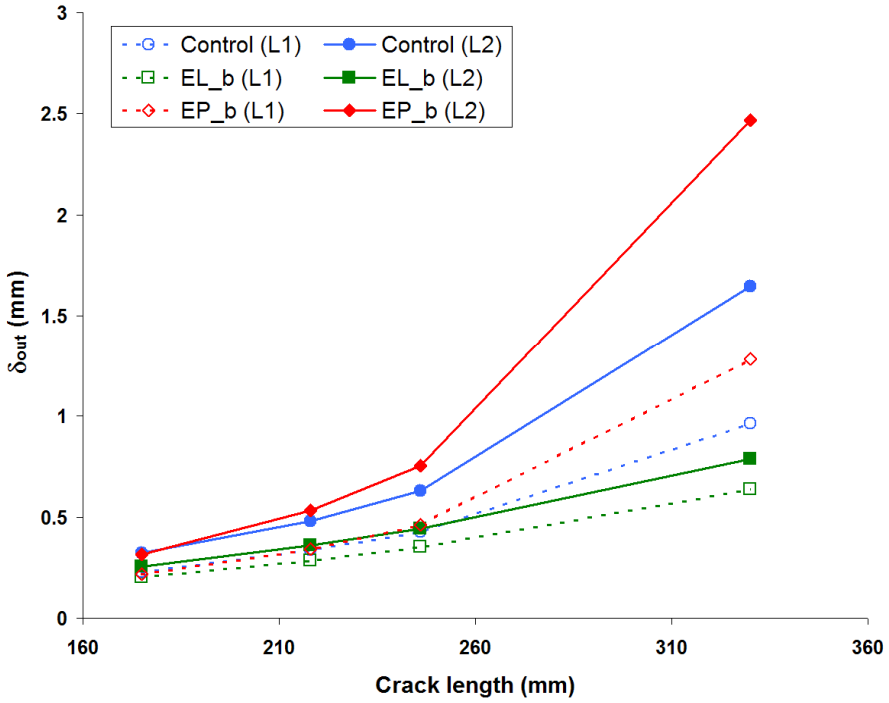

Figure 8.10b Equivalent crack opening parameter δ at the **outside surface** of the pipe. In the figure L1 indicates the results at load level 1 and L2 at load level 2.

8.5 Stress intensity factor

The stress intensity factor calculated in this section is based on the near-tip *J*-integral. Eq. (3.1) is used to obtain *K*. The standard *J*-integral, when evaluated close enough to the crack-tip will provide an accurate estimate of the *J*-integral calculated using the integral modified to account for residual stresses, as discussed in Section 3.1.

The *J*-integral along different paths is shown in Figure 8.11 for the case of a 160 mm long crack. The crack is simulated using the control method. Figure 8.11a demonstrates that the standard integral is, in general, path dependent. However, close enough to the crack tip, path independence is displayed as proposed in [4]. In this case, within 0.5 mm from the crack tip the *J*-integrals are almost path independent. Figure 8.11b shows a detailed view of the paths very close to the crack-tip. The *J*-integral is evaluated for three different positions along the crack front as defined in Figure 8.11.

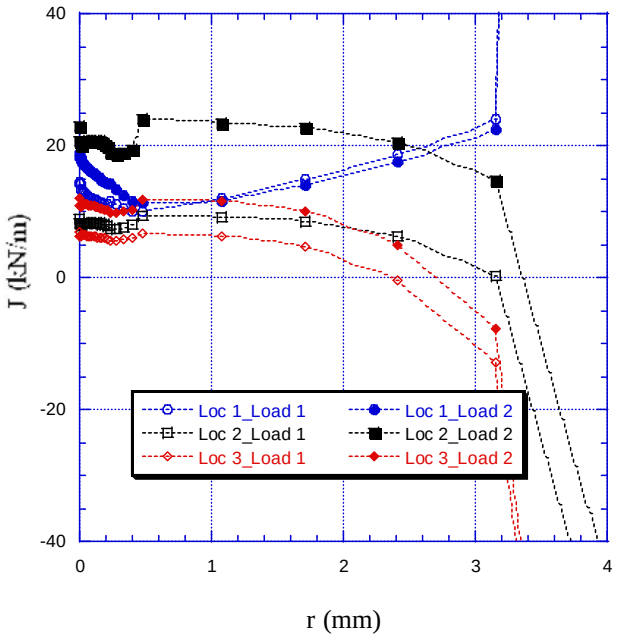

Figure 8.11a. *J*-integrals by control method for crack length 218 mm (including remote paths).

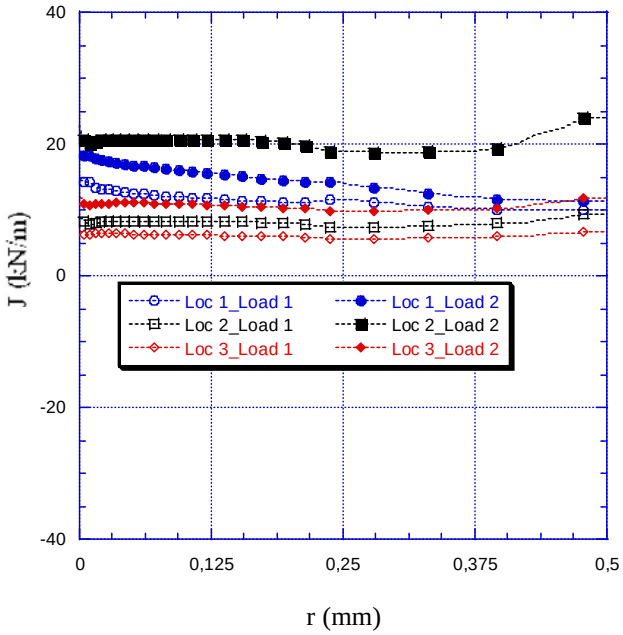

Figure 8.11b. *J*-integrals by control method for crack length 218 mm (25 near crack tip paths).

For this case it was chosen to determine *K* based on *J*-integrals calculated 0.06 mm from the crack-tip (path 10 from the tip).

The distributions of stress intensity factors along the crack front are shown in Figures 8.12-8.15. Results for three different methods are presented: control, elastic FEM and plastic FEM.

In this case the predicted stress intensity factors for the different methods typically have a sinusoidal shape similar in form but different in magnitude to that predicted by the 'residual stress only' case (EL (Resi. only)). The elastic and elastic-plastic FE methods both appear to be more sensitive to the application of loads than the control method since the peak to peak amplitude of these methods is always greater than the control method.

For *x/t* values between 0.25 and 1 the trend in the results is reasonably similar to those reported in case 1. The elastic FE and elastic-plastic FE methods give reasonably good agreement, especially for the shorter crack lengths. For *x/t* values between 0 and 0.25 and for lower *K*-values (load level L1, short cracks), the elastic FE and elastic-plastic FE predictions diverge. This deviation at the pipe inside is similar to that for the thin pipe from section 6.5.

It should also be pointed out that the maximum *K*-value does not always occur at the pipe inner or outer surface. In [14], stress intensity factor solutions at five locations along the crack front were provided. Estimates at these points could be added in ProSACC to provide a more accurate result.

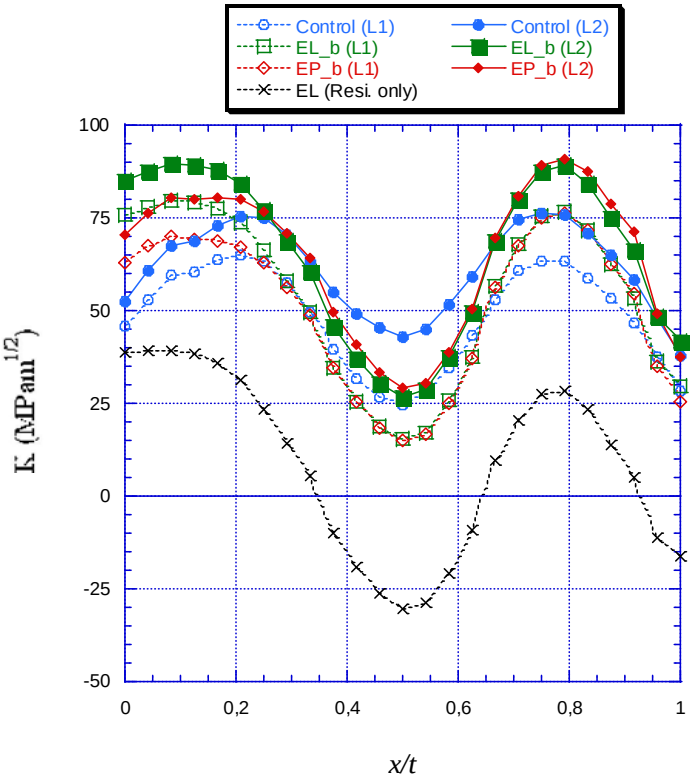

Figure 8.12 Stress intensity factors along the crack front for crack length 175 mm. In the figure, x = 0 at the pipe inner surface, L1 indicates the results at load level 1 and L2 at load level 2.

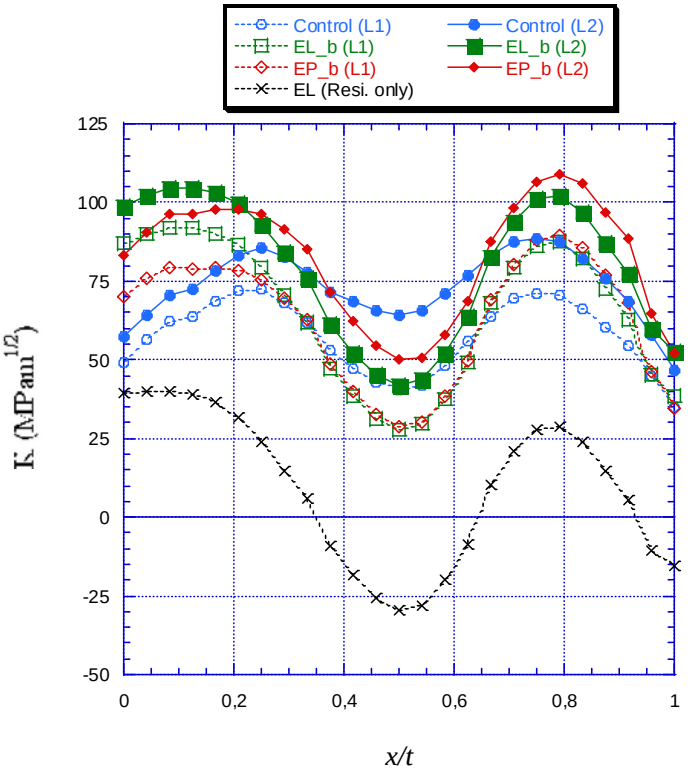

Figure 8.13 Stress intensity factors along the crack front for crack length 218 mm. In the figure, x = 0 at the pipe inner surface, L1 indicates the results at load level 1 and L2 at load level 2.

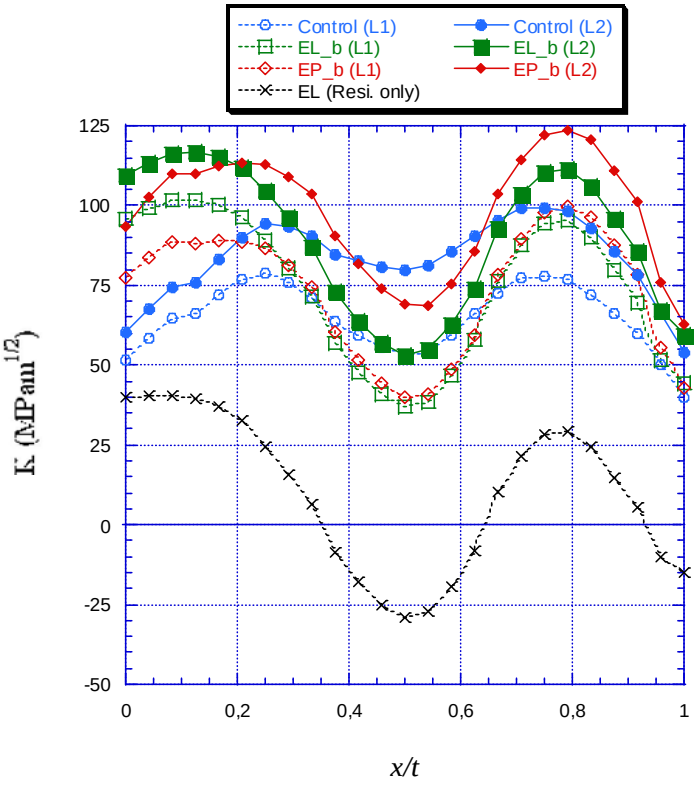

Figure 8.14 Stress intensity factors along the crack front for crack length 246 mm. In the figure, $x = 0$ at the pipe inner surface, L1 indicates the results at load level 1 and L2 at load level 2.

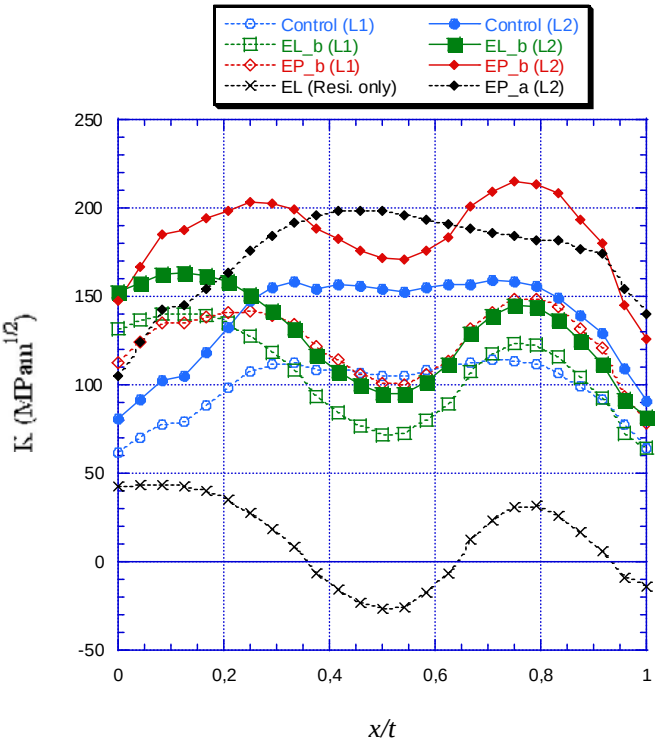

Figure 8.15 Stress intensity factors along the crack front for crack length 330 mm. In the figure, $x = 0$ at the pipe inner surface, L1 indicates the results at load level 1 and L2 at load level 2.

The results are also shown in Tables 8.2 and 8.3. Elastic *K* results from the ProSACC crack growth module are included for comparison.

For crack growth calculations it may be concluded that the ProSACC predictions overestimate *K* in comparison to the control results near the inner surface of the pipe.

Table 8.2 Stress intensity factors by different methods at load level 1.

Crack Length (mm)	Crack Location	Control (MPa√m)	$K_{Elastic}^{ProSACC}$ (MPa√m)	EL_b (MPa√m)	EP_b (MPa√m)
175	1	46.17	91.0	76.18	63.39
	2	24.56	-	14.92	14.52
	3	28.62	19.5	29.59	25.01
218	1	49.42	106.2	87.67	70.82
	2	40.28	-	27.39	28.49
	3	35.25	29.5	38.45	34.38
246	1	51.76	119.3	96.63	77.77
	2	52.87	-	36.72	39.67
	3	39.94	36.0	44.34	42.59
330	1	61.98	171.6	132.35	112.96
	2	105.04	-	72.12	100.63
	3	64.12	59.8	63.96	78.54

Table 8.3 Stress intensity factors by different methods at load level 2.

Crack Length (mm)	Crack Location	Control (MPa√m)	$K_{Elastic}^{ProSACC}$ (MPa√m)	EL_b (MPa√m)	EP_b (MPa√m)
175	1	53.18	102.1	85.35	71.17
	2	42.89	-	26.46	28.96
	3	38.03	32.6	41.56	37.20
218	1	57.26	120.7	99.34	83.52
	2	64.06	-	41.59	49.71
	3	46.72	44.5	52.16	51.70
246	1	60.46	136.3	110.21	94.17
	2	79.82	-	52.82	68.58
	3	54.11	52.1	59.12	62.55
330	1	80.52	198.2	153.06	147.98
	2	154.14	-	95.02	171.29
	3	90.80	79.3	81.86	125.61

Tables 8.4 and 8.5 show the contribution from the residual stress to *K* for the load cases chosen for analysis in this investigation. The elastic-plastic FE method was used for these calculations. The external loads applied are lower for the medium thickness pipe in case 2 than for the lower thickness pipe geometry in case 1.

Table 8.4 Comparison showing the contribution of the residual stress to *K* calculated using the elastic plastic FE model (load level 1).

Crack Length (mm)	Crack Location	Without residual stresses, (MPa√m)	With residual stresses, (MPa√m)
175	1	24.24	63.39
	2	45.22	14.52
	3	41.25	25.01
218	1	31.03	70.82
	2	58.38	28.49
	3	50.09	34.38
246	1	37.44	77.77
	2	68.92	39.67
	3	57.90	42.59
330	1	70.35	112.96
	2	127.63	100.63
	3	92.62	78.54

Table 8.5 Comparison showing the contribution of the residual stress to *K* calculated using the elastic plastic FE model (load level 2).

Crack Length (mm)	Crack Location	Without residual stresses, (MPa√m)	With residual stresses, (MPa√m)
175	1	32.02	71.17
	2	59.66	28.96
	3	53.44	37.20
218	1	43.73	83.52
	2	79.60	49.71
	3	67.41	51.70
246	1	53.84	94.17
	2	97.83	68.58
	3	77.86	62.55
330	1	105.37	147.98
	2	198.30	171.29
	3	139.69	125.61

8.6 Crack tip opening displacements

Crack tip opening displacements were calculated at the three locations indicated in Figure 8.11. The results are listed in Tables 8.6-8.7.

In comparison with the results by the control method, results by the elastic method (EL_b) are underestimated.

Table 8.6 Crack tip opening displacements estimated using different methods (load level 1).

Crack Length (mm)	Crack Location	Control (mm)	Elastic FEM EL_b (mm)	Elastic-plastic FEM EP_b (mm)
175	1	0.0094	0.0016	0.0033
	2	0.0033	0.0004	0.0093
	3	0.0041	0.0007	0.0063
218	1	0.0104	0.0018	0.0050
	2	0.0090	0.0007	0.0166
	3	0.0060	0.0009	0.0096
246	1	0.0112	0.0020	0.0070
	2	0.0154	0.0009	0.0247
	3	0.0076	0.0010	0.0129
330	1	0.0164	0.0028	0.0328
	2	0.0618	0.0017	0.0882
	3	0.0183	0.0015	0.0394

Table 8.7 Crack tip opening displacements estimated using different methods (load level 2).

Crack Length (mm)	Crack Location	Control (mm)	Elastic FEM EL_b (mm)	Elastic-plastic FEM EP_b (mm)
175	1	0.0137	0.0018	0.0054
	2	0.0100	0.0007	0.0172
	3	0.0067	0.0010	0.0110
218	1	0.0148	0.0021	0.0101
	2	0.0221	0.0010	0.0335
	3	0.0098	0.0012	0.0183
246	1	0.0164	0.0023	0.0162
	2	0.0350	0.0013	0.0518
	3	0.0129	0.0014	0.0260
330	1	0.0400	0.0032	0.3837
	2	0.1314	0.0022	0.1902
	3	0.0373	0.0019	0.1060

9 CASE FOUR - MEDIUM PIPE WITH A FULL CIRCUMFERENTIAL INTERNAL SURFACE CRACK

9.1 Finite element model

The pipe geometry considered in case four is the same as for case three with the difference that a full circumferential, internal surface crack is modeled, as opposed to a through-wall crack. The finite element mesh used for welding simulation is also the same, as shown in Figure 7.1. The finite element mesh for the fracture mechanics model is, however, different. A 2D, axisymmetric model was used and is illustrated in Figure 9.1. The notch radius is 0.001mm, allowing accurate prediction of near-tip-*J* and CTOD.

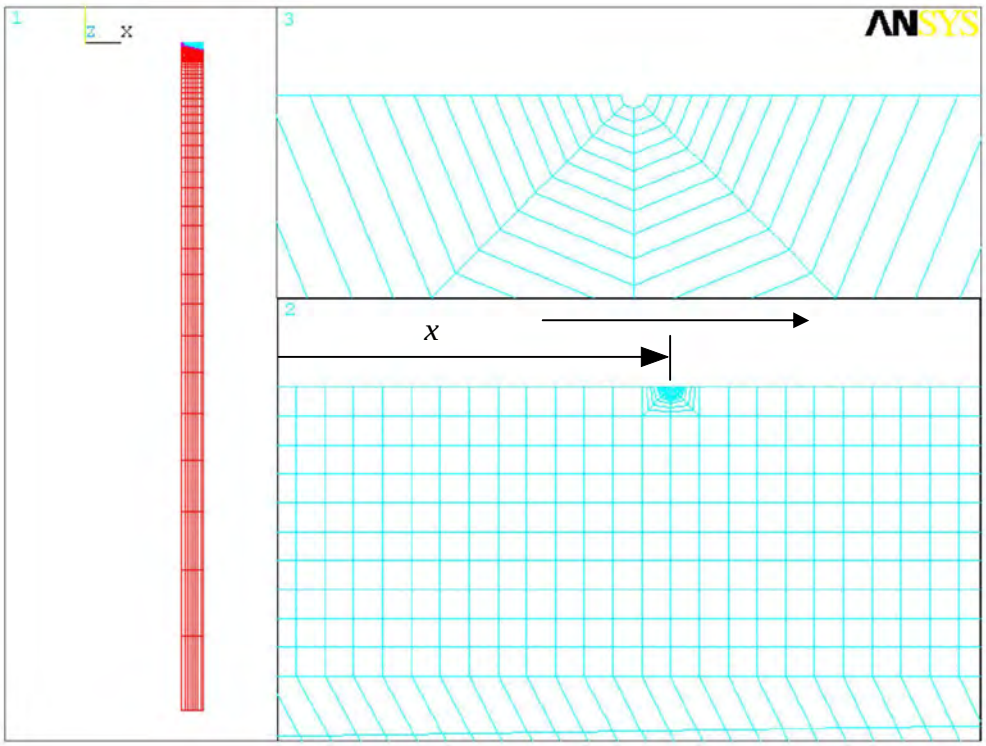

Figure 9.1 Finite element mesh with an internal surface crack. x = 0 at the inner surface of the pipe.

9.2 Crack profiles

Crack profiles through the thickness are shown in Figures 9.2 to 9.5 for the different evaluation methods. Each figure represents a different crack depth, ranging from a/t=0.2 to 0.8. Results are shown for the two load levels L1 and L2. In the figures, open symbols indicate results at load level 1 and the solid symbols at load level 2. Results due to residual stresses only, calculated by the elastic FE method, are also included.

Note that the crack opening displacement due to welding residual stress is most pronounced at small crack depths where it contributes more than 50% of the total COD for both the elastic and elastic-plastic FE methods. For large crack depths the effect is less pronounced. An important observation is that crack closure is predicted

at *a/t*=0.4. Inclusion of weld residual stresses is therefore very important in computation of COD for these cases.

It is observed that the crack opening displacement predicted by the elastic FE method and the elastic-plastic FE method are nearly identical when $a/t < 0.6$. This implies that the effect of plastic deformation in these cases is very limited.

In comparison to the control method, for the higher load level, both the elastic and elastic-plastic FE methods underestimate the crack opening displacement for *a/t* up to 0.6. For the lower load level there is no large difference between the predictions of the control method and the elastic-plastic FE methods.

For *a/t* equal to 0.8, at the higher load level L2, there is a significant contribution to the COD from plastic deformation, as predicted by both the control method and the elastic-plastic method for *a/t* up to 0.6.

Note that the surface COD due to residual stresses only decreases already after *a/t*=0.2, leading to the situation that it is more difficult to detect a large crack than a small one, especially for VT inspection methods. The scope of this study was not broad enough to obtain a full set of data necessary for conclusions regarding the VT method. Results for the control method for residual stresses only, and at room temperature, not at operating temperature, would be needed for more complete conclusions.

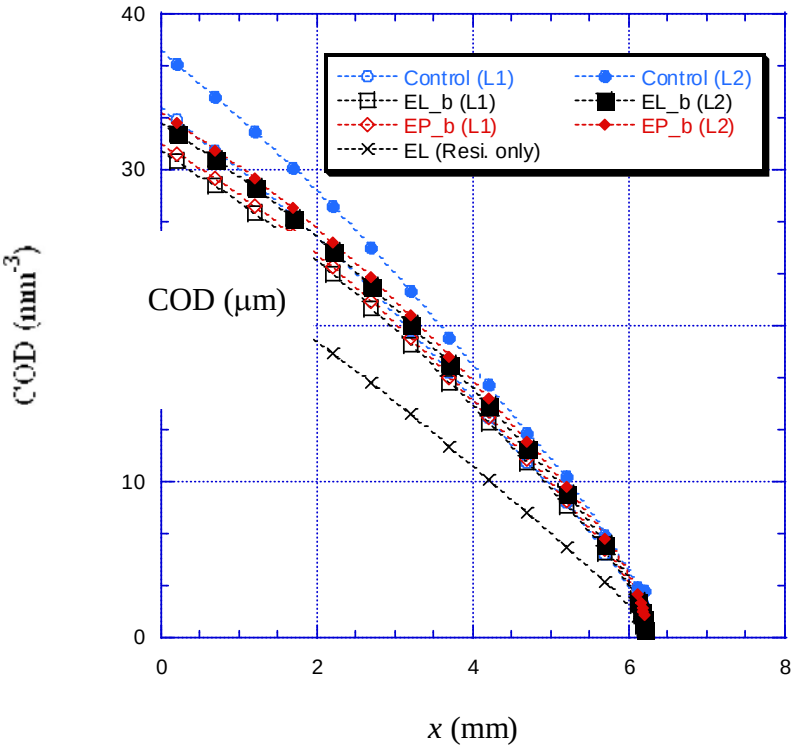

Figure 9.2 COD for *a/t* = 0.2. (*x* = 0 at the pipe inner surface).

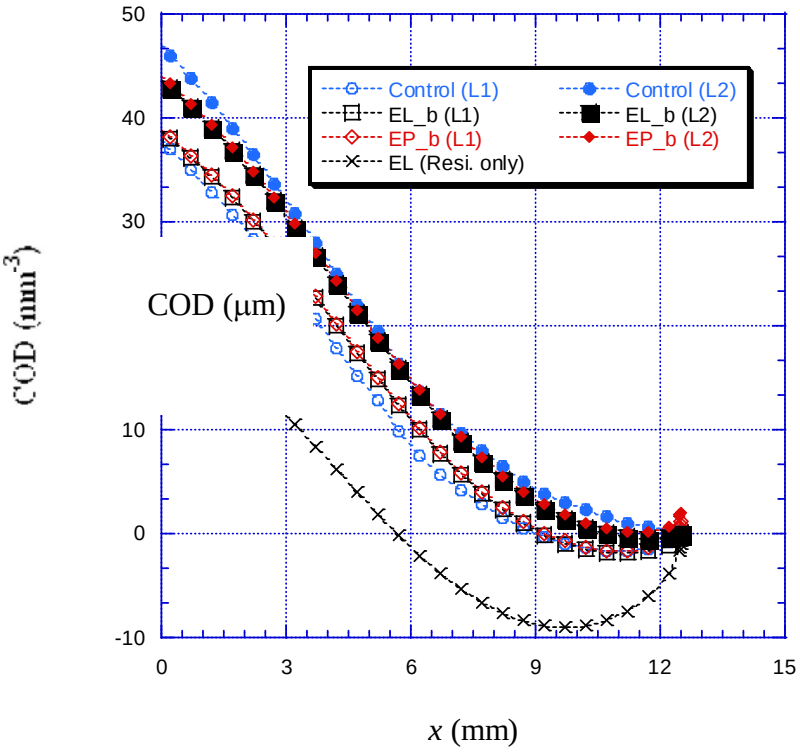

Figure 9.3 COD for *a*/*t* = 0.4.

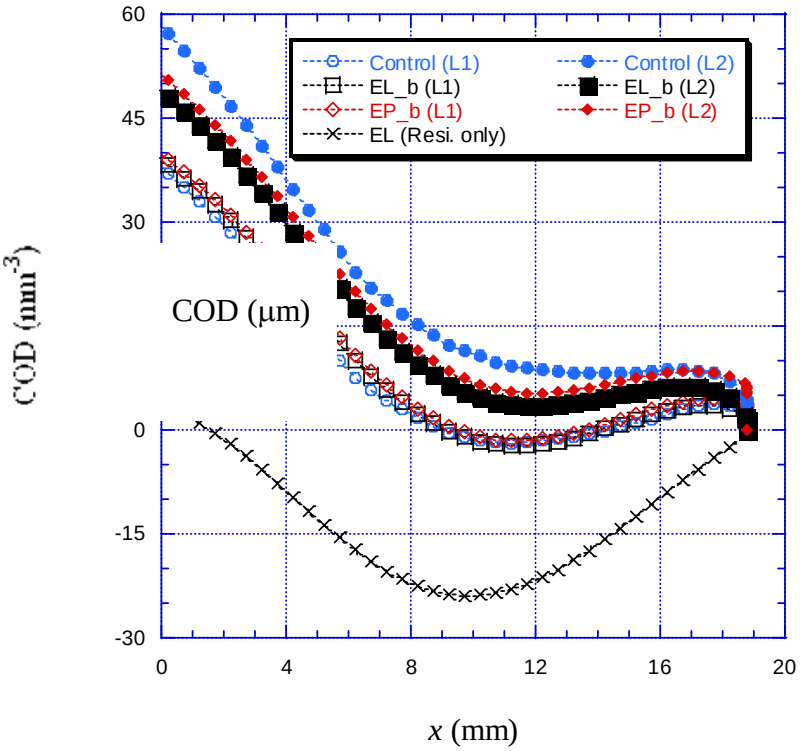

Figure 9.4 COD for *a*/*t* = 0.6.

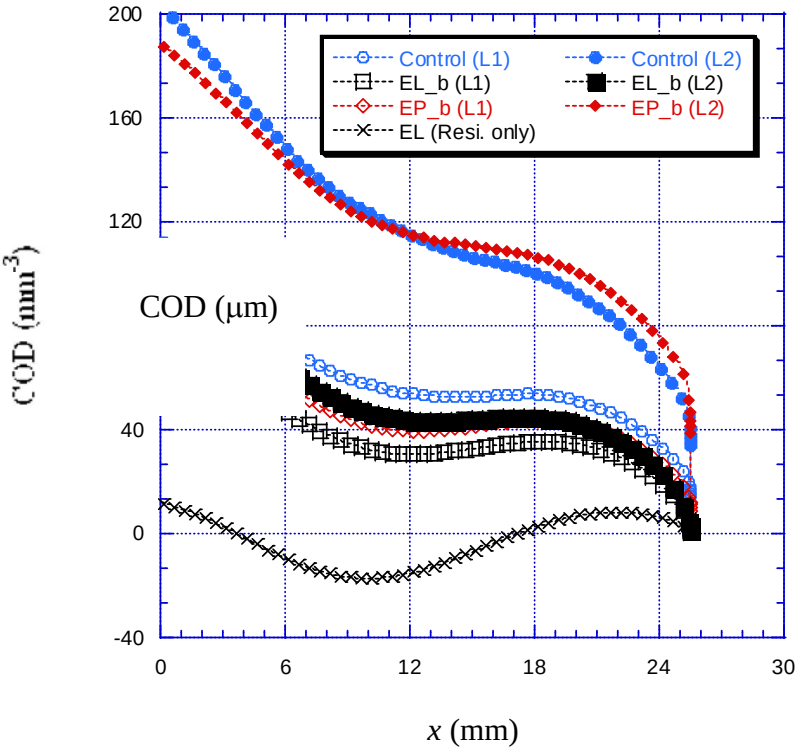

Figure 9.5 COD for a/t = 0.8.

9.3 Stress intensity factor

As before, the stress intensity factor calculated in this section is based on the near-tip J-integral. Eq. (2.1) is used to obtain K. The J-integrals for crack depth a/t = 0.6 are shown in Figure 9.6. The crack is simulated using the control method. It is shown that the J-integrals are path dependent about 0.1 mm away from crack tip. Within 0.1 mm from the crack tip, J-integrals are almost path independent. For this case it was chosen to determine K based on J-integrals at 0.1mm from the crack tip.

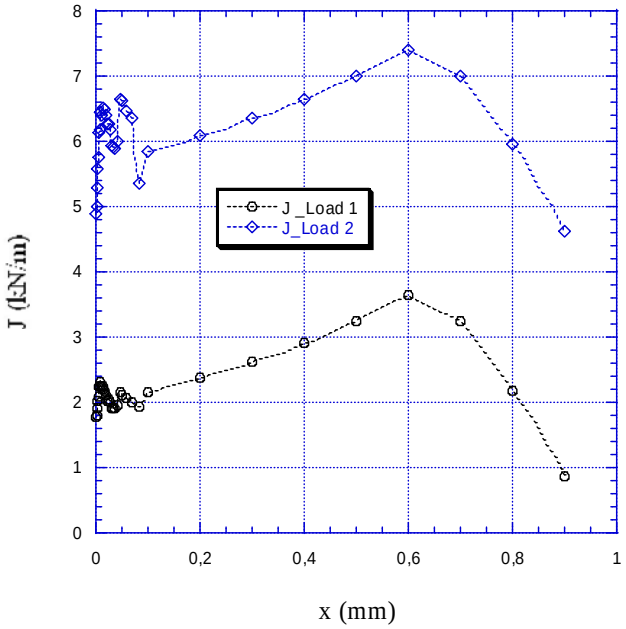

Figure 9.6a. *J*-integrals as function of distance *r* from the crack-tip for a crack simulated by the control method (crack depth *a/t* = 0.6).

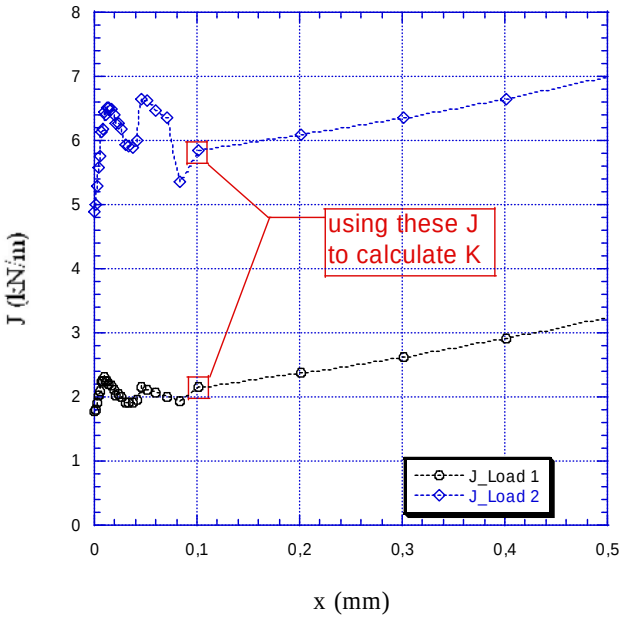

Figure 9.6b. *J*-integrals as function of distance *r* from the crack-tip for a crack simulated by the control method (crack depth *a/t* = 0.6). The 29 near-tip paths are shown.

Stress intensity factors for the different evaluation methods, including ProSACC, are shown in Table 9.1 and Figure 9.7. The results predicted by the elastic method agree well with the control method, except for the most shallow cracks and the high load level (L2) where EL_b overestimates *K*.

An important observation is that for a proposed mechanism of SCC, the crack would arrest at *a/t*=0.4. This is predicted by all methods. For the crack depths *a/t*=0.2 it is observed that the elastic *K*-values calculated by ProSACC are always greater than the control method.

Table 9.1 Case 4 - stress intensity factors estimated using the different evaluation methods.

Load Level	Crack Depth (a/t)	Control Method (MPa√m)	$K^{ProSACC}_{Elastic}$ (MPa√m)	EL_b (MPa√m)	EP_b (MPa√m)
L1	0.2	19.76	25.0	28.88	29.17
	0.4	0.00	-12.6	-8.55	0.00
	0.6	18.06	13.3	17.14	17.27
	0.8	63.15	~	62.12	68.06
L2	0.2	23.49	28.2	31.99	32.41
	0.4	0.00	-7.2	-3.16	0.00
	0.6	28.97	21.3	25.16	25.93
	0.8	87.00	~	74.32	114.28

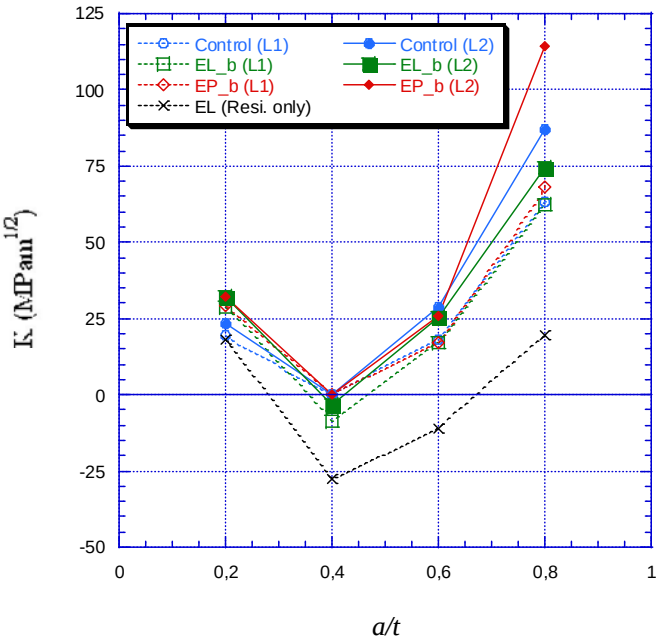

Figure 9.7 Stress intensity factors for internal surface crack.

9.4 Crack tip opening displacements

The results for CTOD are listed in Tables 9.2-9.3 for load level 1 and load level 2, respectively. In comparison with the results by the control method, results from the elastic FE method under and over estimate CTOD. Note that crack arrest would not be predicted at a/t=0.4 if using CTOD and EP_b, though it is predicted for the control method. Some variation in the results could be attributed to sensitivity to the near-tip mesh design.

Table 9.2 CTOD at load level 1.

Crack depth (a/t)	Control (mm)	Elastic FEM EL_b (mm)	Elastic-plastic FEM EP_b (mm)
0.2	0.0040	0.0008	0.0018
0.4	-0.0003	-0.0001	0.0024
0.6	0.0027	0.0004	0.0057
0.8	0.0280	0.0016	0.0172

Table 9.3 CTOD at load level 2.

Crack depth (a/t)	Control (mm)	Elastic FEM EL_b (mm)	Elastic-plastic FEM EP_b (mm)
0.2	0.0060	0.0009	0.0025
0.4	-0.0001	0.0000	0.0038
0.6	0.0070	0.0006	0.0091
0.8	0.0670	0.0019	0.0768

10 ALTERNATING FEM METHOD

In this section an alternating FEM method is evaluated for calculation of *K* and COD. One of the tasks in the project is to evaluate stress intensity factors and crack opening displacements for cracks subjected to a given residual stress field by using the alternating method [11-12]. As discussed in the background, one key aspect in treating residual stresses in fracture mechanics models is the consideration of displacement-controlled conditions. This is because a residual stress field must satisfy equilibrium conditions within a component of concern. For a growing crack, the residual stresses nearby re-distribute as stress-free surfaces are generated, while in load-controlled conditions, the far-field stresses can be assumed to be stationary.

One convenient method for computing stress intensity factors in a 3D geometry is the finite element alternating method. As illustrated in Figure 10.1, if stress intensity factors need to be calculated for a cracked body such as the T-fillet weld shown, a conventional finite element model is all that is needed without the need to model an actual crack. Therefore, the modeling efforts are significantly simplified.

The stress intensity factor calculation process for the alternating method using FEM and an infinite body solution can be described as follows:

1. For a given 3D cracked finite body (Figure 10.1b), the associated boundary traction conditions and crack face pressure are first obtained using a finite element model at the crack location, but without a crack being modeled.

2. The crack face pressures are then fitted into a polynomial function over the entire crack face so that the boundary tractions in the infinite body (Figure 10.1c) - but at the actual finite cracked body boundaries - can then be calculated using an analytical solution for an embedded elliptical crack in a 3D infinite body under given crack face pressure.

3. The analytically calculated traction conditions from Figure 10.1c at this stage are different from those given in Figure 10.1b. By defining the difference in tractions from the FE model and the analytical model and applying the residual tractions to the FE model, a new estimate of the corresponding crack face pressure can be obtained for feeding into the 3D analytical solution for calculating a new estimate of boundary tractions for the finite 3D body.

4. By alternating between the FE based traction solution and that from the analytical solution until the residual tractions between the two solutions become negligible, a converged solution is obtained.

5. The stress intensity factor can then be calculated by adding up the stress intensity factors calculated from all iterations.

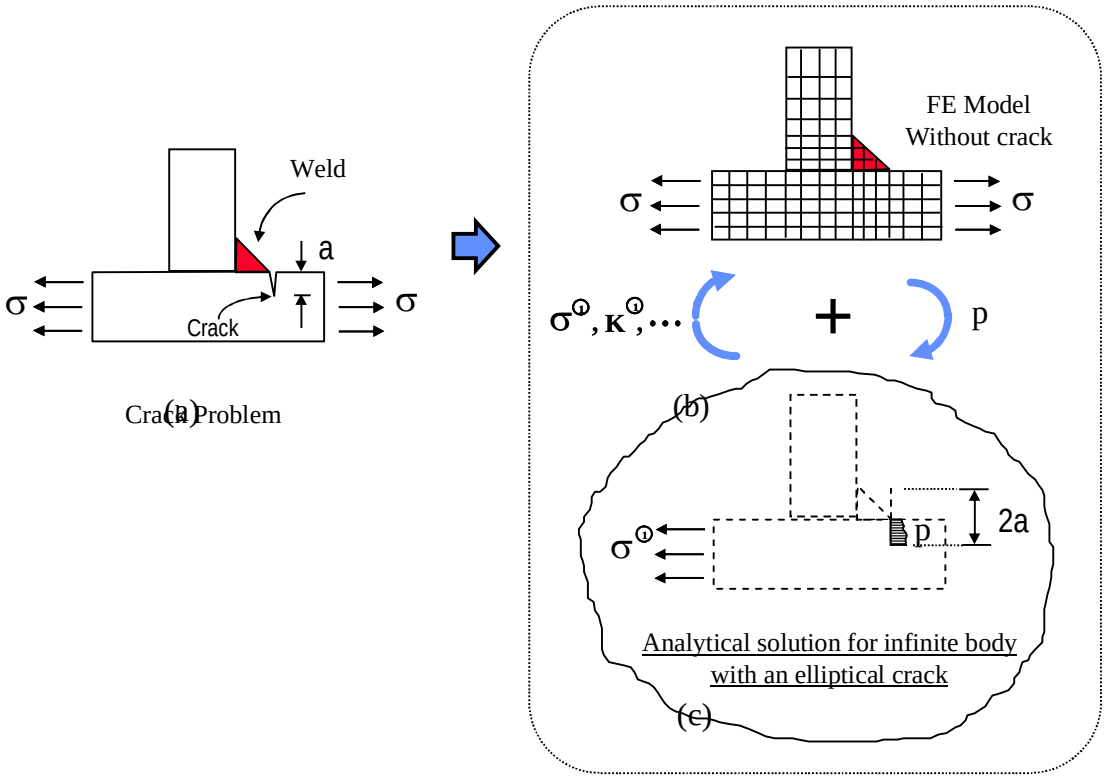

Figure 10.1 Illustration of finite element alternating method for stress intensity factor calculation using 3D solid model.

To deal with weld residual stress related stress intensity factor calculations, a mapping procedure is needed to map a given residual stress field to a 3D welded component so that a full-field residual stress field (e.g. any potential interaction effects between axial and hoop residual stresses in pipe girth welds) can be properly considered in stress intensity factor calculations.

10.1 Residual Stress Mapping, 3D Model and Crack Definition

Figures 6.3 and 6.4 summarize the residual stress distribution for a thin-wall pipe girth weld (*t* = 8.3 mm). The axial residual stress distribution in Figure 6.3 shows a strong through-wall bending action with tension at the inner and compression at the outer surfaces.

A representative 3D FE model for the same girth used for *K* calculations is illustrated in Figure 10.2. A circumferential surface crack to be considered is also given in the figure. The residual stress distributions in Figure 6.3 and 6.4 predicted using an axisymmetric model were mapped onto the 3D solid model in Figure 10.2. The resulting distributions in Figure 10.3 are consistent with those in Figure 6.3 and 5.4. Note that the mesh design in the 3D solid model in Figure 10.2 is intended to provide an adequate resolution regarding overall stress gradients for calculation of *K* solutions.

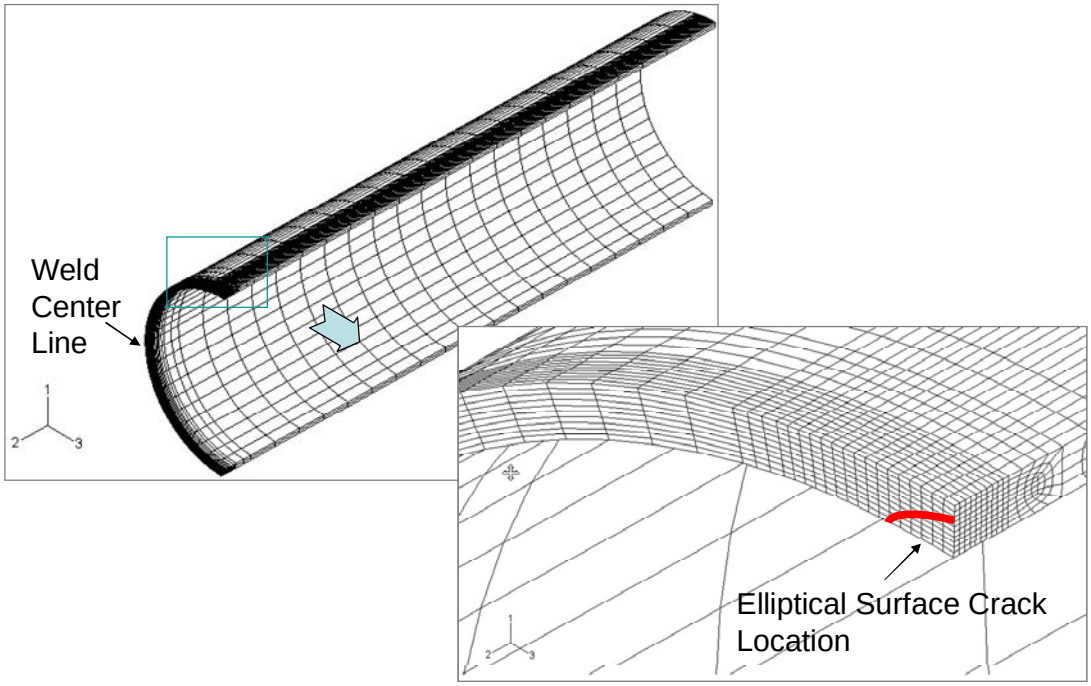

Figure 10.2. 3D finite element model for computing stress intensity factors using a finite element alternating method under displacement-controlled conditions.

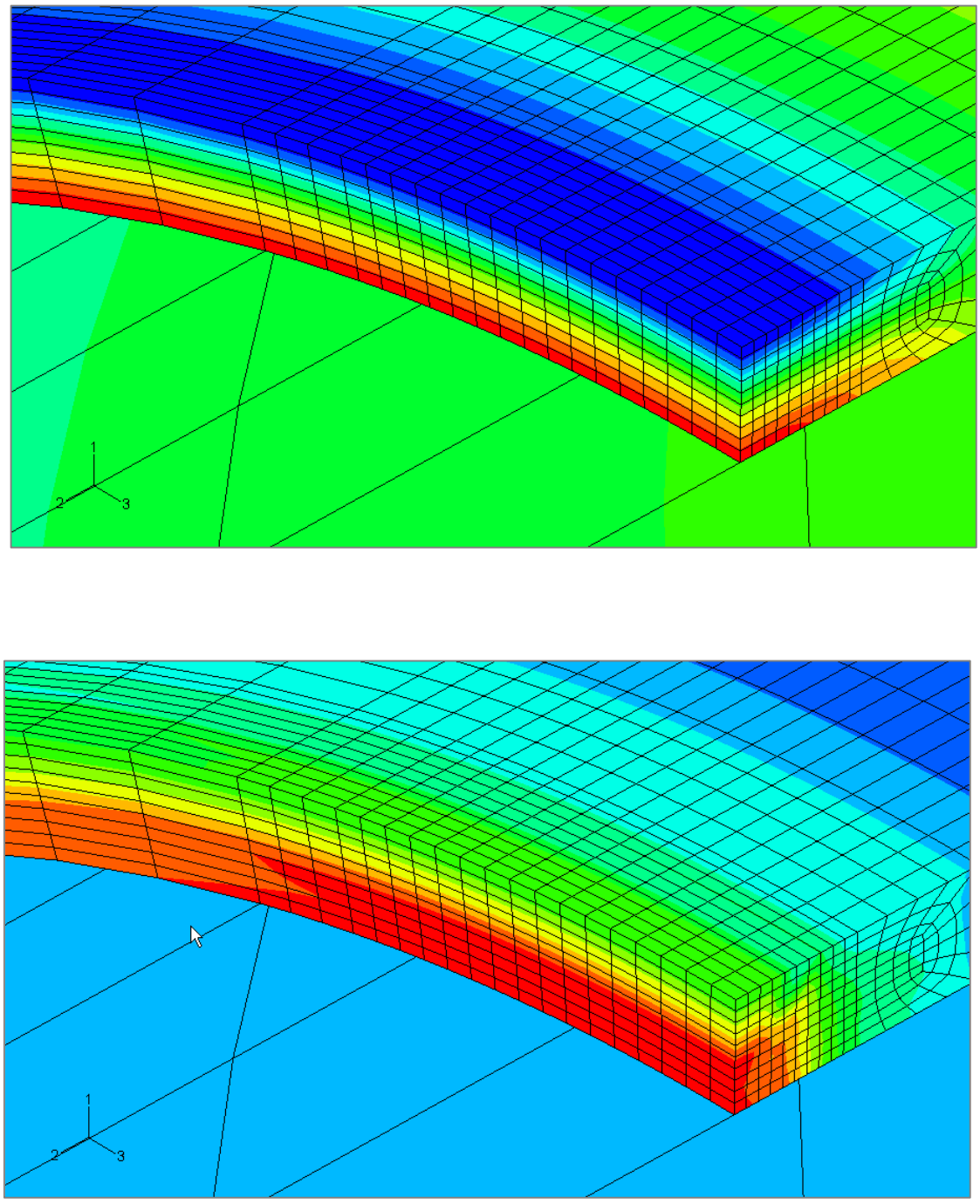

Figure 10.3 Residual stress distribution (axial and hoop direction) after mapping from the axisymmetric model to the 3D model.

10.2 Results for Surface Cracks

For the evaluation of K an elliptical crack was defined first for a crack length of 2c = 16 mm and a/t values between 0.2 and 0.8. The same procedure was then repeated for crack lengths of 24 and 32 mm, and the results are shown in Figures 10.4 to 10.6. Residual stresses only are considered.

When the surface crack is shallow, K reaches its largest value at the deepest position (or at an elliptical angle of 90°). However, as the crack depth increases, the maximum K values shift to the inner surfaces, as clearly indicated in Figures 10.4 to 10.6 for a/t = 0.6 and 0.8. The trend becomes less pronounced with the longer crack sizes. This behavior is directly related to the through wall axial residual stress distribution. The compressive axial residual stresses become increasingly dominant as the crack depth reaches beyond half thickness as shown in Figures 10.7a and b, where the results are replotted for fixed a/t ratios and varying crack lengths.

The above observations suggest that for stress corrosion cracking controlled by K, the crack growth would be inhibited in the depth direction and promoted in the circumferential direction at the inner surface.

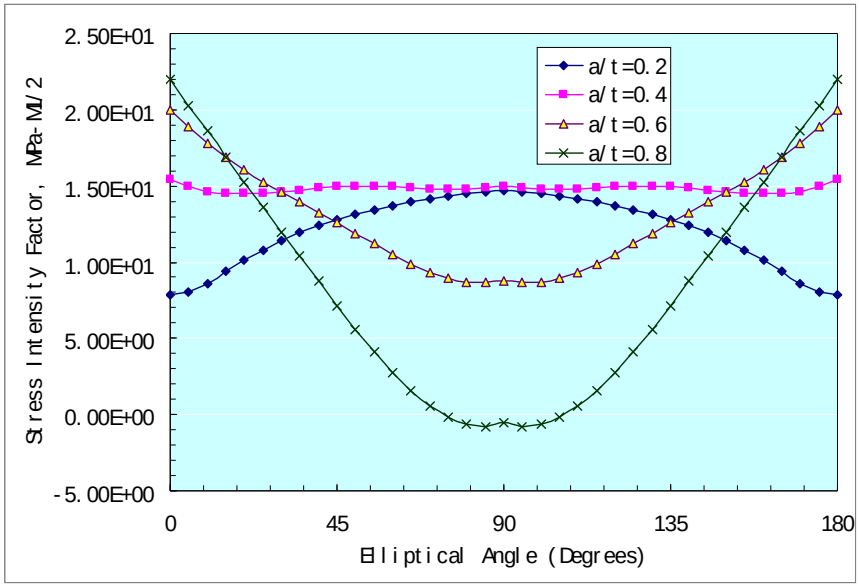

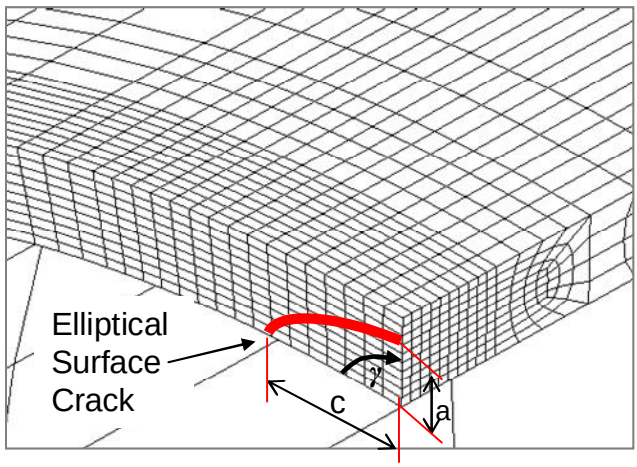

Inner Surface at Elliptical Angle γ = 0°,180°
Deepest Crack Point at Elliptical Angle γ = 90°

Figure 10.4 Stress intensity factor distribution as a function of relative crack depth a/t with 2c = 16 mm (t = 8.3 mm) . The elliptical angle and crack form parameters are defined in the sub figure.

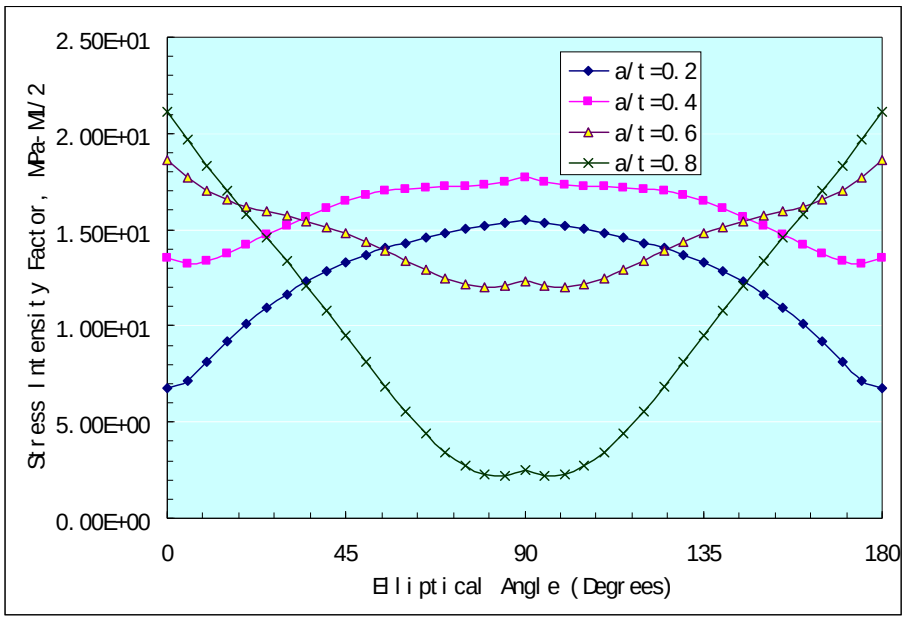

Figure 10.5 Stress intensity factor distribution as a function of relative crack depth (a/t) with 2c = 24 mm (t = 8.3 mm).

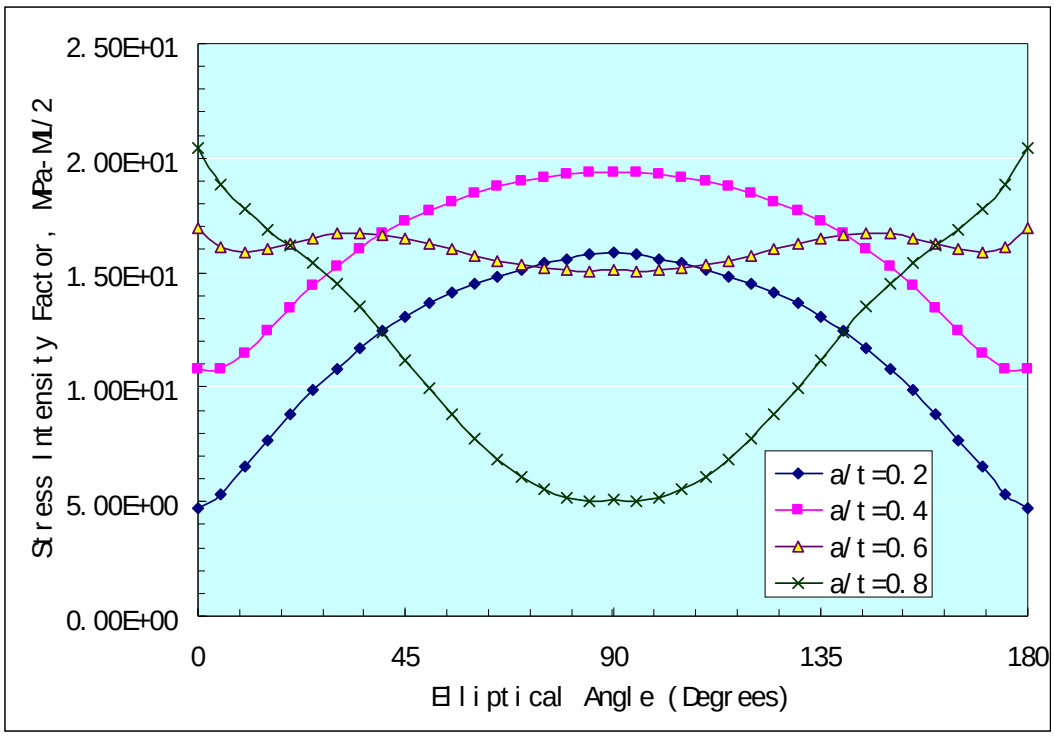

Figure 10.6 Stress intensity factor distribution as a function of relative crack depth (a/t) with 2c = 32 mm (t = 8.3 mm).

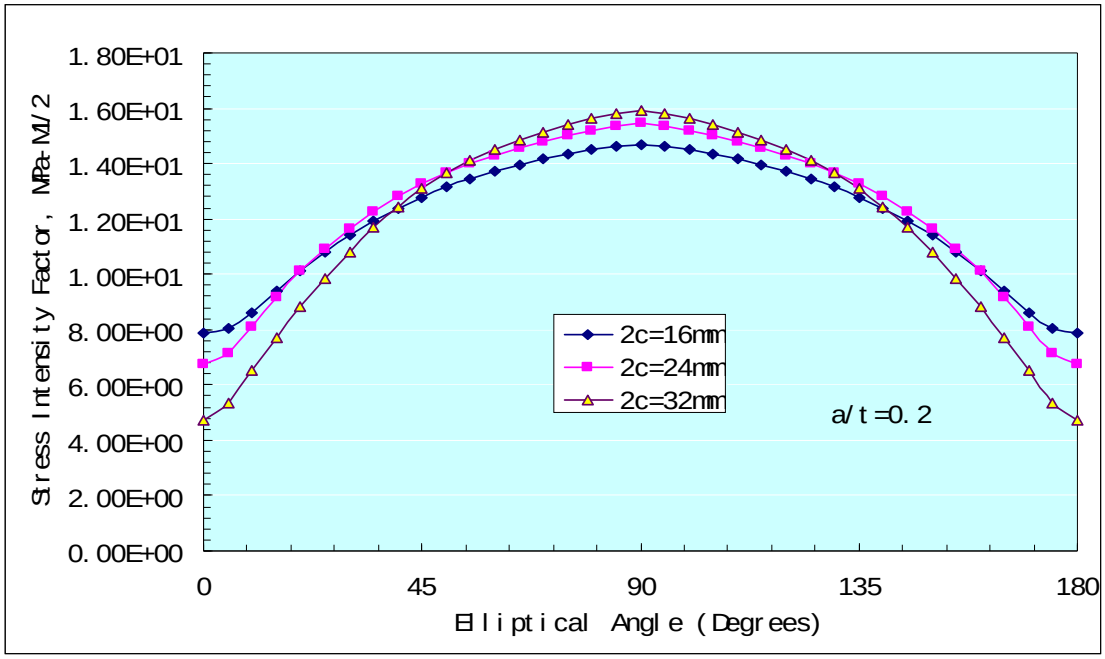

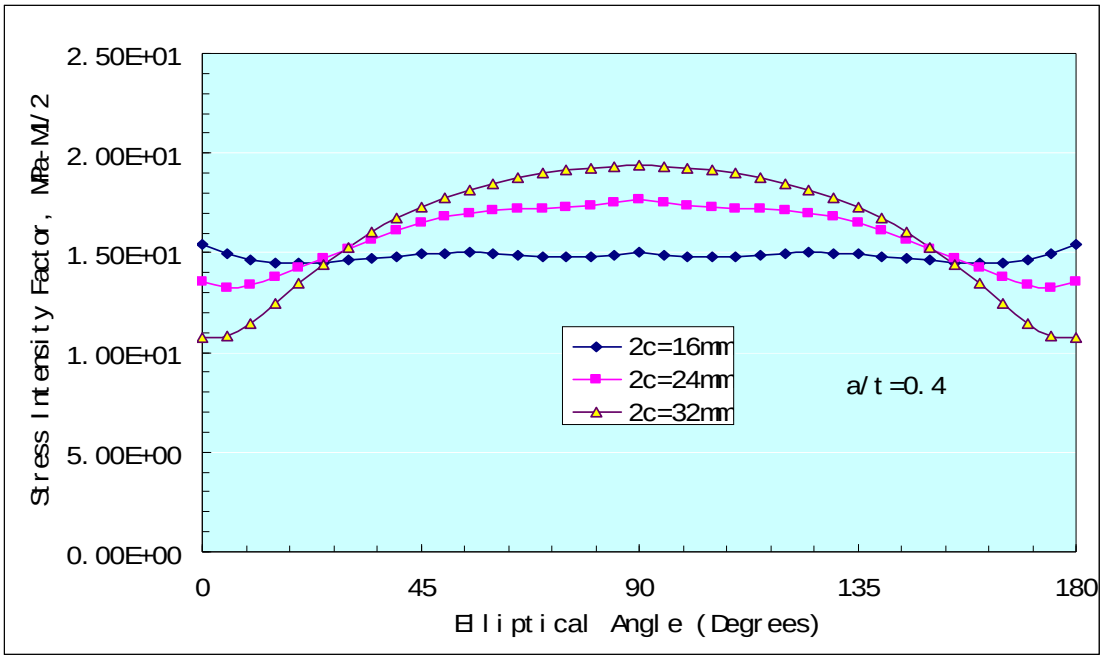

Figure 10.7a: Stress intensity factor distribution as a function of crack length (2c) with a constant depth (a/t) .

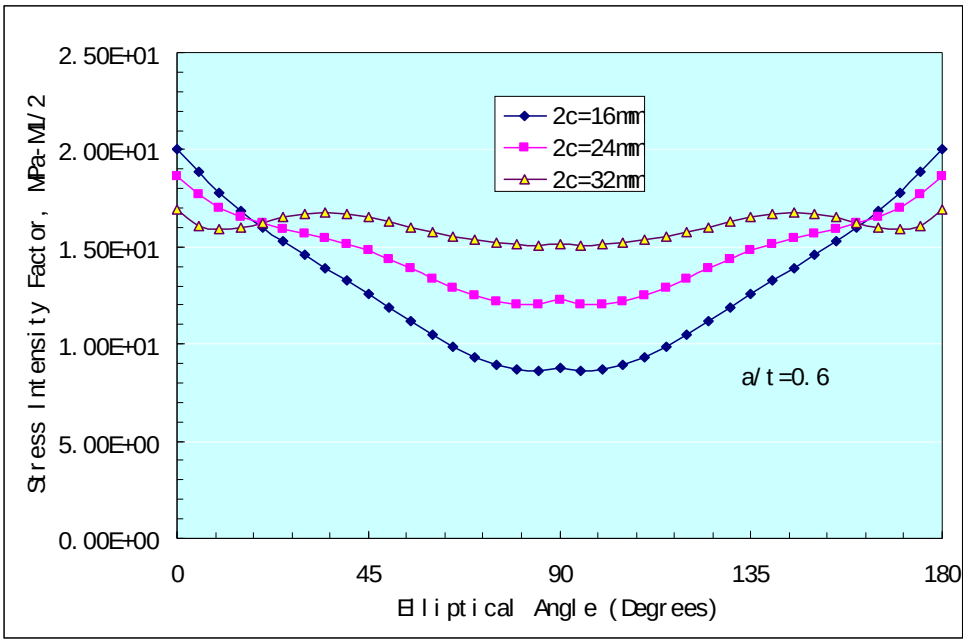

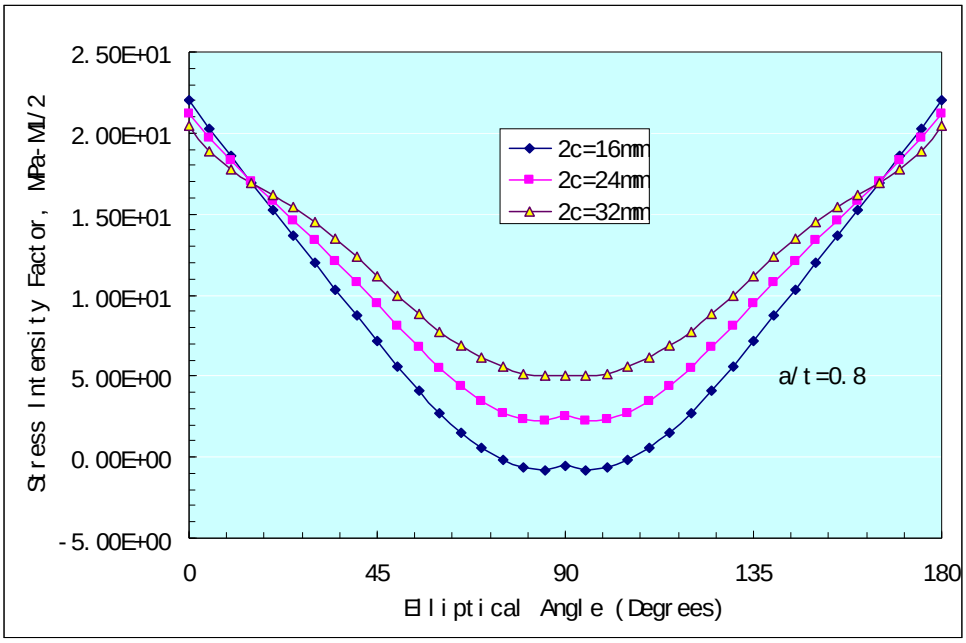

Figure 10.7b: Stress intensity factor distribution as a function of crack length (2c) with a constant depth (a/t) .

10.3 Results for Through-Wall Cracks

The through wall crack was defined as a full ellipse intersecting the pipe wall and was oriented in the circumferential direction (illustrated in Figure 10.8). Only residual stresses are considered. The actual crack front used in simulations is shown in Figure 10.9, and the points at which the stress intensity factor was estimated are shown in the figure subset. Note that the crack front becomes curved. Figure 10.9 also shows the variation of stress intensity factor along the crack front for crack sizes of 24 and 36 mm. The stress intensity factors are plotted from the outer to the inner surface. The two cases (2c = 24 mm and 36 mm) are not significantly different from each other, except for the case for 2c = 24 mm a slightly higher value of K is approached at the inner surface.

The corresponding crack opening displacements along both inner and outer surfaces for both cases are summarized in Figure 10.10. For 2c = 24 mm, the crack opening profiles approximately resemble an elliptical type of opening, as suggested by classical estimation scheme under remote bending. As the crack length increases, such as at 2c = 36, the outer crack surface starts to exhibit additional curvature, as shown in Figure 10.10.

To gain insight on the deformation behavior on the crack surface, two through-wall lines were chosen to examine crack opening displacement distributions. As shown in Figure 10.11, the crack opening displacements as a function of the through-thickness position is essentially linear, i.e., close to a pure rotation.

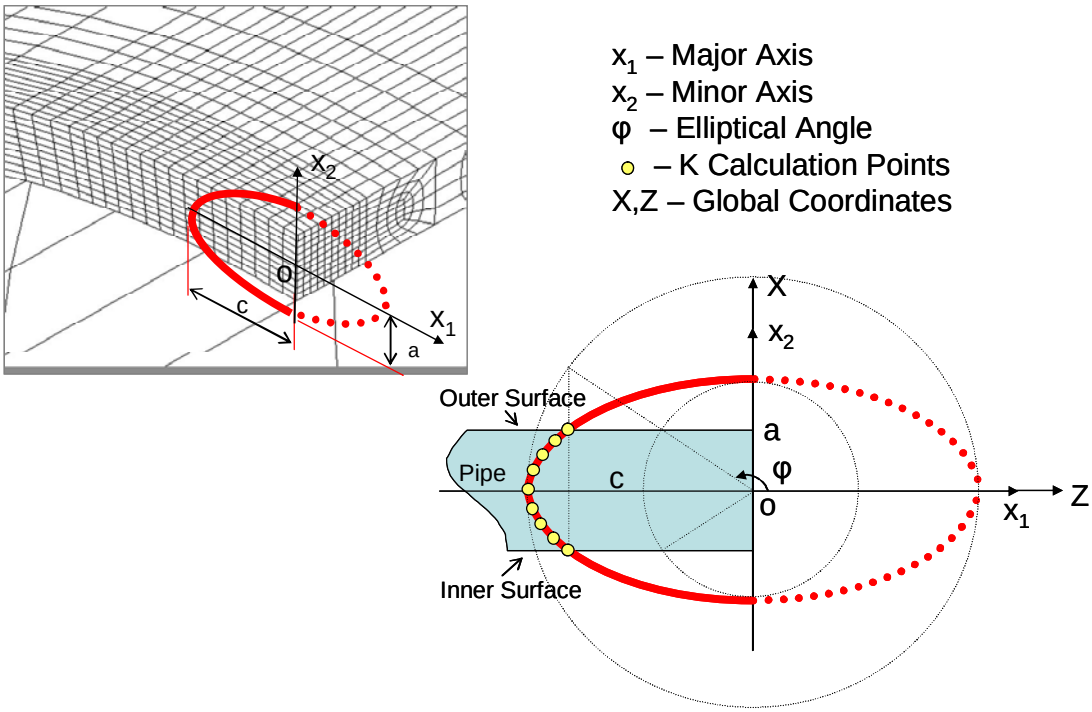

Figure 10.8: Through-wall elliptical crack definition in 3D FE alternating model.

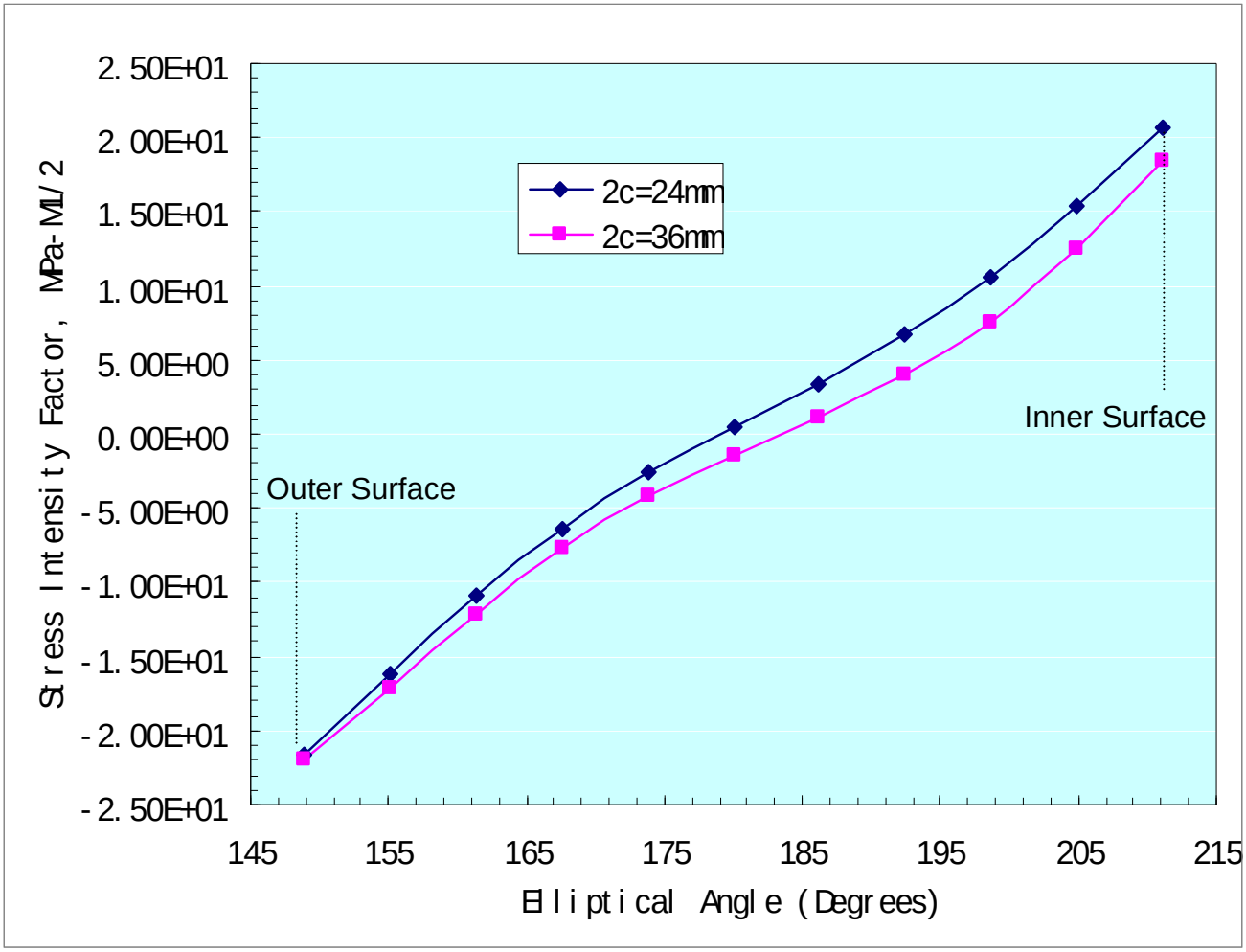

2c=24 mm & 36 mm
a=8 mm
$149^{o} \leq \varphi \leq 211^{o}$

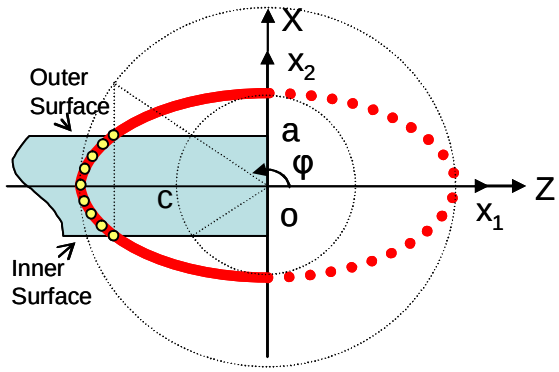

Figure 10.9 Stress intensity factor results for two through-wall elliptical cracks of 2c = 24 mm and 36 mm.

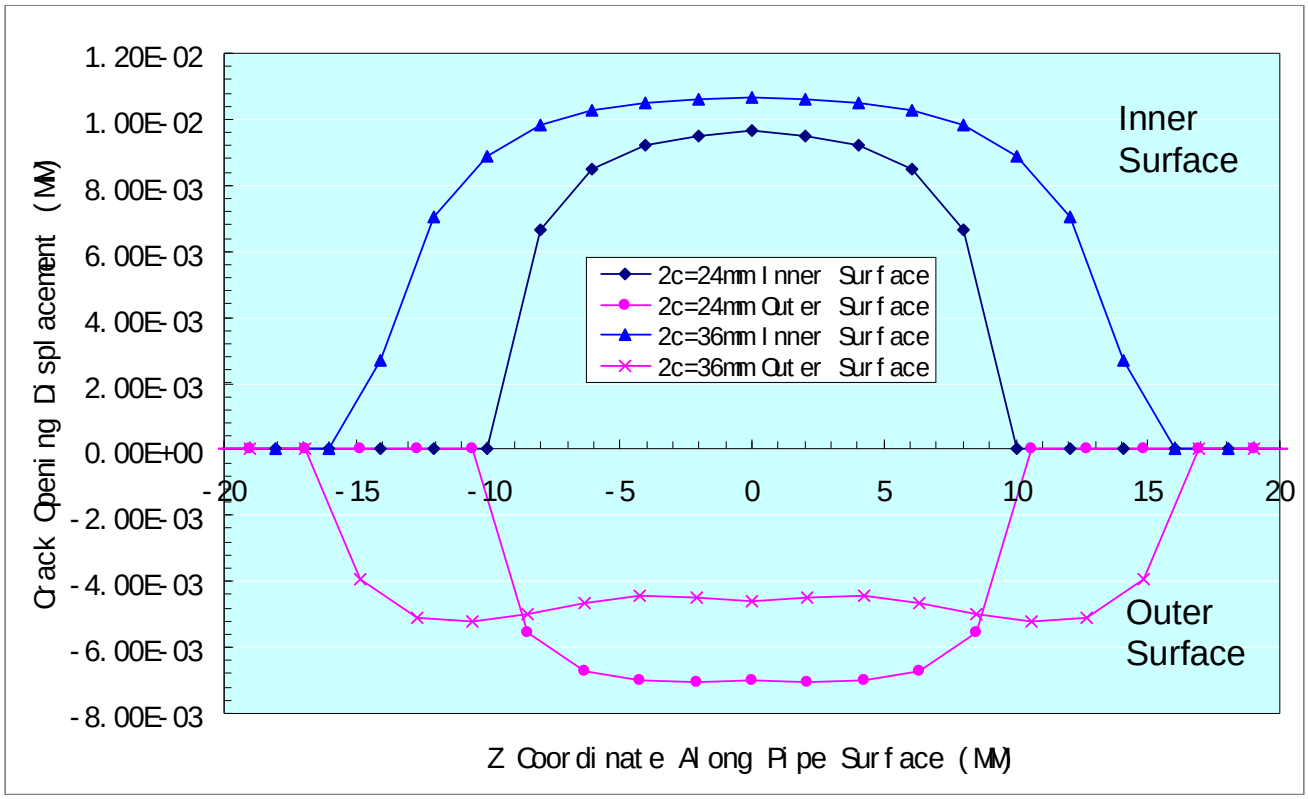

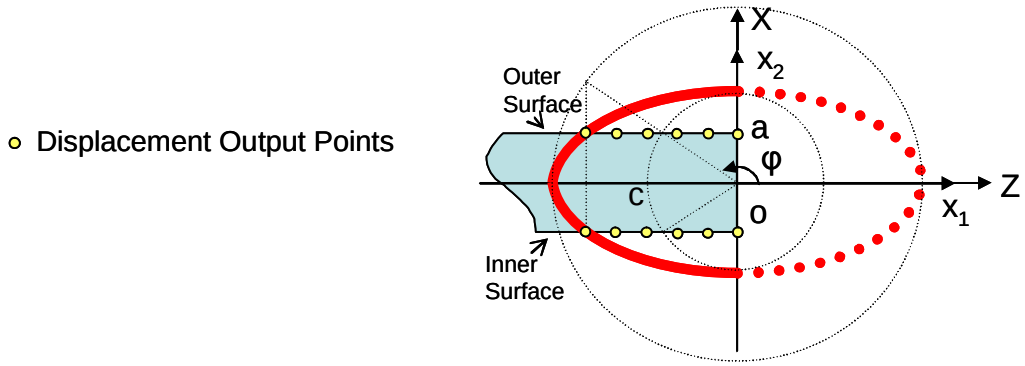

Figure 10.10 Crack opening displacement results for through-wall elliptical cracks of 2c = 24 mm and 36 mm.

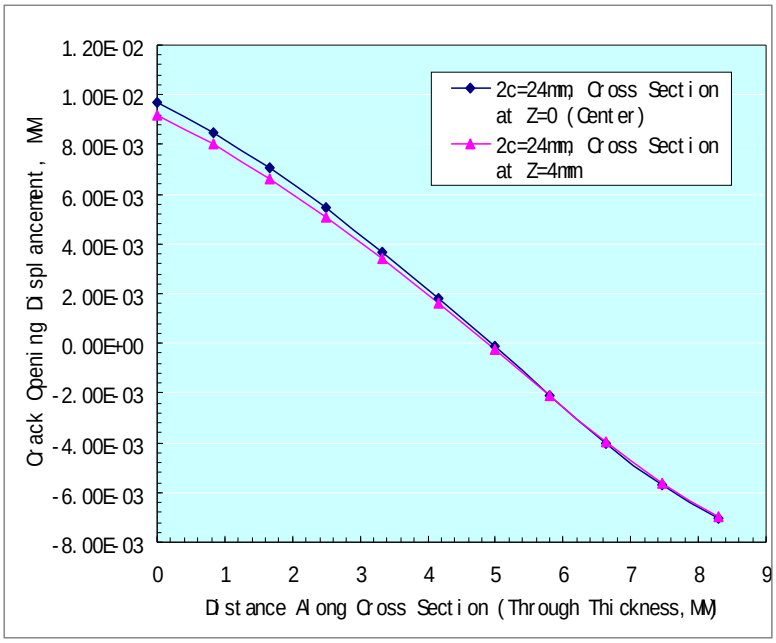

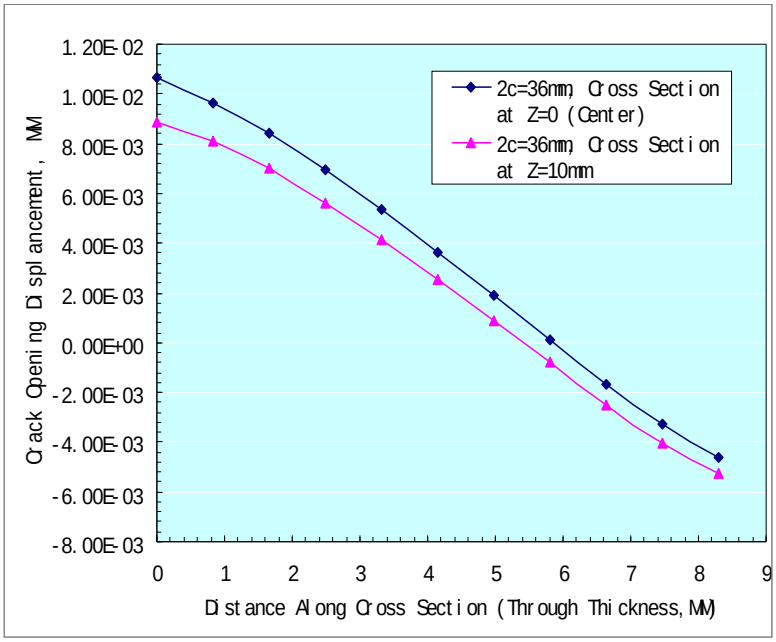

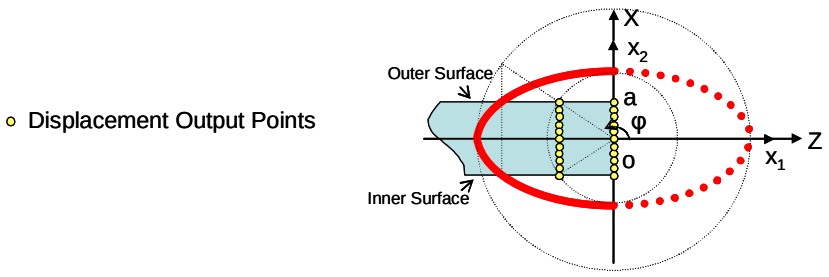

Figure 10.11 Crack opening displacement distributions across thickness – through-wall elliptical cracks.

10.4 Comparison to the crack face pressure method

In this section the results from the analyses by the present alternating method are compared with results from the crack face pressure method calculated by ProSACC.

Comparison to the results in Section 6.8 from the control method was not possible. With the current alternating method, the largest through-wall crack length with convergence is the 36 mm crack. It is possible to improve the convergence in the future by changing the iteration procedure. This is considered as a limitation of the alternating method.

In Table 10.1 stress intensity factors calculated for through wall cracks by the alternating method are compared to results from ProSACC (crack face pressure method). The values predicted by ProSACC are up to 95% higher. In ProSACC straight crack fronts are considered, while by the alternating method the crack front becomes approximated by a piece of an elliptical curve. This also contributes to the difference.

This deviation could possibly indicate that the CFP-method for through wall cracks is rough and it is possible that the inclusion of the out-of-plane stress might improve the agreement between the methods.

Table 10.1 Stress intensity factors *K* for through wall cracks estimated by alternating method and ProSACC.

Crack Length $2c$ (mm)	Position	Alternating method (MPa$\sqrt{m}$)	ProSACC, elastic (MPa$\sqrt{m}$)
24	Inner surface	20.7	30.7
	Outer surface	-21.6	-36.4
36	Inner surface	18.4	34.3
	Outer surface	-22.0	-41.8

Figure 10.12 shows the results for the surface cracks calculated by the alternating method (ALT) compared to results from the crack face pressure method calculated by ProSACC (CFP). Position A is the result at the deepest point of the crack front ($\gamma = 90°$), and position B is the result at the intersection to the inside surface ($\gamma = 0°$).

The same trends as a function of crack depth are predicted by both methods. This supports the use of the crack face pressure method for evaluation of *K* for surface cracks. Slightly higher *K*-values are predicted by the alternating method for the deepest point (position A), the values differ up to 15% for the longest crack. For the surface position B slightly higher values are predicted by ProSACC.

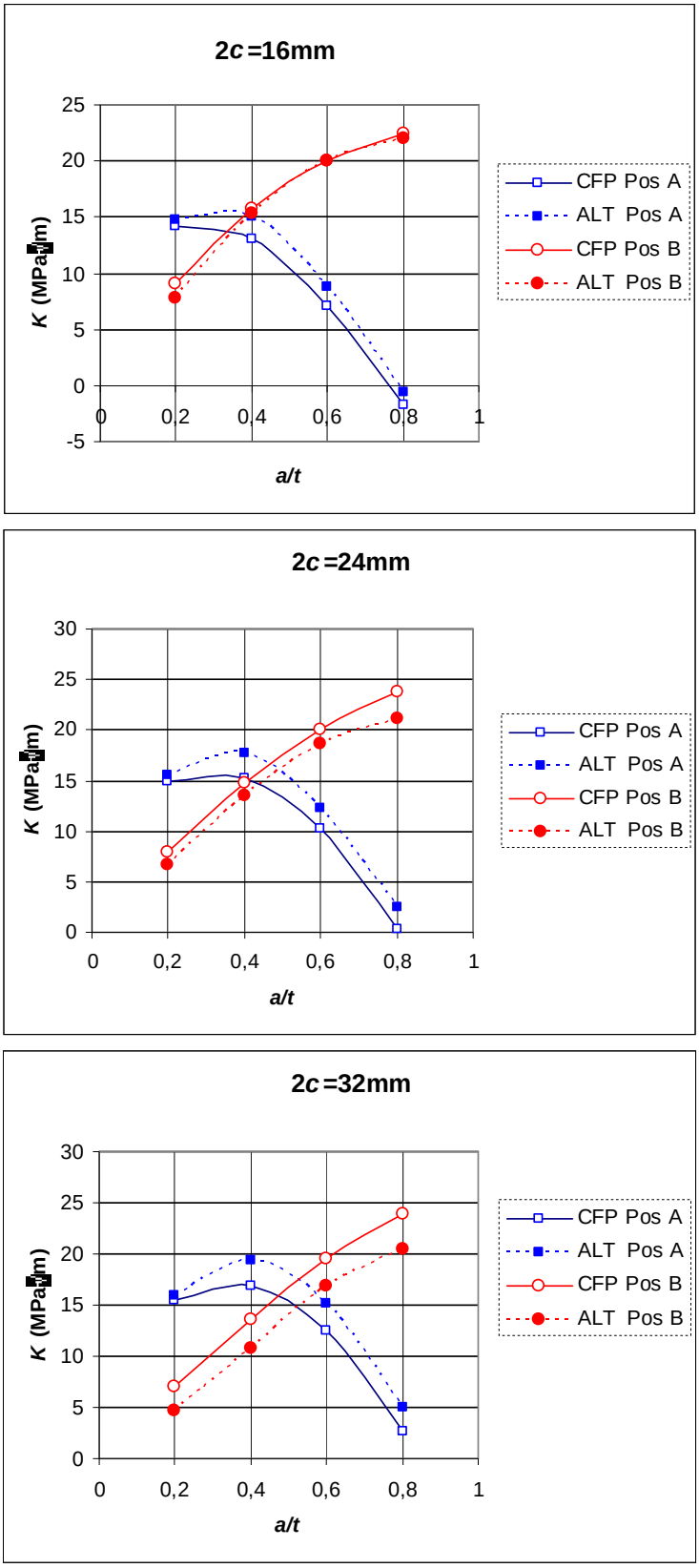

Figure 10.12 Comparison of *K* results for **surface cracks**. Results calculated by the alternating method (ALT) and by the crack face pressure method by elastic ProSACC (CFP). Pos A is the deepest point of the surface crack ($\gamma = 90°$), and Pos B is at surface ($\gamma = 0°$).

11 DISCUSSION

11.1 Crack opening displacements for leak before break assessments

The discussion in this section regards the predicted crack opening displacements for through wall cracks. The crack opening displacement COD is used to predict the crack opening area COA and leakage rates. An overestimate with respect to COD results in a larger predicted leak rate, which would be non-conservative with respect to the assessed probability of early detection of leakage.

For a thin walled pipe (t=8.3 mm) containing a through wall crack the COD at the outer-surface is limiting in terms of the leakage rate. The COD calculated by NURBIT is similar to the results by EP_b. For the crack lengths up to 185 mm, the crack opening area is overestimated by 7-26% for the lower load case L1 compared to the control method. Comparison to COD's calculated by the elastic FEM method indicates that plastic effects are substantial even for the moderate crack lengths and low load level.

For a medium thickness pipe (t=31.8 mm) containing a through wall crack the COD at the inner-surface is limiting in terms of the leakage rate. This is opposite to the thin-walled case, and can be attributed to the weld residual stress field. The elastic-plastic method consistently overestimates the COD by up to 15% compared to the control method. For a low load level and shorter cracks which is more relevant to lead before break situations, the COD is overestimated to a lesser degree – between 2 and 12% for crack lengths between 175 and 246 mm. This implies a small non conservatism with respect to LBB assessment with EP_B.

The elastic FE method underestimates the crack opening area, since plastic deformation is not accounted for.

11.2 Crack-tip parameters for crack growth assessments

The discussion in this section regards the predicted crack-tip parameters for through wall and surface cracks. The stress intensity factor K is used for prediction of crack growth rates. An underestimation of K results in a lower growth rate, which is non-conservative with respect to the predicted safe time period, for growth to the maximum acceptable crack size.

As discussed in section 3.1, the modified J-integral is expected to provide a valid measure of the mechanical state at the crack tip taking into account for weld residual stresses. Crack growth relations are usually based upon K and an equivalent stress intensity factor K may be calculated from the J-integral. An implementation of the modified J-integral accounting for residual stresses in 3D cases was not available, and instead near-tip estimates of the standard J-integral were used. It was judged that the standard J-integral evaluated close enough to the crack-tip was sufficient to demonstrate the key trends. The standard J-integral was evaluated between 0.01 and 0.1 mm from the crack tip. This may, however, introduce mesh sensitivity in the results, and use of the modified J-integral is recommended.

The results for surface cracks are most relevant for drawing conclusions about crack growth.

For a thin walled pipe containing an internal surface crack, K estimates from the elastic ProSACC method, the elastic FE method and the elastic-plastic FE method are very similar to the control method for crack sizes up to a/t=0.4. For deeper cracks, the crack face pressure method tends to underestimate K, the exception being the case EP_b and a/t=0.8.

For a medium thickness pipe containing an internal surface crack, crack arrest was predicted for a/t approximately equal to 0.4. This was predicted by all methods. For cracks up to a/t=0.2 (shallow cracks), K

was overestimated by all crack face pressure methods where there was a tensile residual stress near the inner wall. For the lower load level the elastic (and plastic) FE methods overestimated K by 46% for a/t=0.2.

When calculating inspection intervals, through wall cracks are not allowed for piping, but only for internal parts. It should be highlighted that the crack growth calculations made for stress corrosion cracking and fatigue cracking are almost always based upon a purely elastic estimation of K. This includes the growth analysis modules in ProSACC.

For the thin walled pipe, the shortest through wall crack and the lower load level (L1), the elastic ProSACC prediction overestimates K by 56% on the pipe inner surface. For the medium thickness pipe, the shortest through wall crack and the lower load level (L1), the elastic ProSACC prediction overestimates K by 65% on the pipe inner surface and underestimates it by 32% on the pipe outer surface. It is observed that where K is low the elastic ProSACC results can underestimate K at some positions along the crack front. However, the maximum value predicted by ProSACC is always overestimated. Note that the maximum value of K is not always obtained at the inner or outer surfaces for the control method and EP_b. This could have implications for predictions using ProSACC since only values at the surfaces are provided from ProSACC.

An investigation was also carried out concerning the alternating method. Only short cracks could be analysed. Estimates of K were compared with ProSACC results. For the through wall cracks, the ProSACC estimates were of a higher magnitude – they were more positive on the inner pipe surface and more negative on the outer pipe surface. For surface cracks the same trends are predicted by both methods. Slightly higher K-values are predicted by the alternating method for the deepest point and the values differ up to 15%. For the surface position slightly higher values are predicted by ProSACC.

11.3 COD for surface cracks and planning of visual inspection

The results for COD for surface cracks were calculated for normal operating conditions, however, some conclusions can be made with respect to VT inspection – which is conducted at room temperature after reactor shutdown. For the thin walled pipe, and for crack depths (a/t) up to 0.6, both the elastic and the elastic-plastic methods underestimate the COD. The results for the elastic and the elastic-plastic FE methods are essentially the same. It is concluded that the underestimation may be due to either the load controlled nature of these methods and/or the presence of high out-of-plane stresses that are not captured by these methods.

For the medium thickness pipe there is no large difference between the control method and the elastic/elastic-plastic FE methods. This may be because the out-of-plane stress is compressive for this pipe geometry when the crack is small.

Note also for the medium thickness pipe, where the axial weld residual stress profile is sinusoidal, the surface COD due to residual stresses only, decreases already after a/t=0.2, leading to the situation that it is more difficult to detect a deep crack than a shallow one. Further investigation is required to quantify this effect for more complicated residual stress fields. Results for the control method, for residual stresses only, would be needed for more complete conclusions.

12 CONCLUSION

This report investigates the treatment of weld residual stresses when performing fracture mechanical analysis of welded components. Weld residual stresses have a large influence on the behavior of cracks growing under normal operation loads and on the leakage-flow from a through-wall crack. Accurate estimates of crack characterizing parameters such as stress intensity factor *K* and the crack opening displacement COD are important for prediction of these events.

Engineering assessment methods that are commonly used account neither for the displacement controlled nature of weld residual stresses, nor for multi-axial residual stresses. Engineering methods commonly utilize a calculation procedure called the crack-face pressure method. The stress in an uncracked model is extracted along the plane were the crack is postulated. The stress normal to the crack plane is applied to the crack surface in a model where the crack exists, for calculation of *K* or COD. The crack-face pressure method involves an assumption of load-controlled conditions but is also used in situations where remote displacements are applied. These methods generally account neither for the displacement controlled nature of weld residual stresses nor for multi-axial residual stresses.

The objective of this work is to investigate if the approximation of the crack face pressure method provides reasonable and yet conservative results for weld residual stresses and normal operating conditions. Detailed simulations are made where a crack is created in full 3D weld residual stress fields by use of the node-relaxation technique. Crack-tip characterizing parameters and crack opening displacement determined from this control method model are compared with results obtained from different implementations of the crack face pressure method. Two pipe geometries with surface and through wall circumferential cracks are studied for normal operation cases where the weld residual stresses constitute a significant part of the loading.

For **through wall cracks** the crack opening area results are of interest for performing leak before break assessments. The main conclusion is that good agreement is obtained between the elastic-plastic FE method (crack face pressure method), NURBIT (crack face pressure method) and the control method for typical minimum detectable crack sizes and load levels commonly seen in Swedish nuclear reactors (load level 1). The maximum observed variation between the methods was 26%, where COD was overestimated.

For full circumferential **internal surface cracks** *K* estimates are of interest for crack growth predictions. The main conclusions are:

- For the 8 mm thick pipe there is generally good agreement between *K* predictions for the elastic ProSACC (crack face pressure) method and the control method for crack depths up to a/t=0.6.
- For the 32 mm thick pipe there is generally good agreement between *K* predictions for the elastic ProSACC method and the control method. The largest variation of 15% was for the higher load level and deepest crack (a/t=0.8).
- For the 32 mm thick pipe, where the axial weld residual stress profile is sinusoidal, the surface COD due to ‘residual stresses only’ decreases rapidly, leading to the situation that it is more difficult to detect a deep crack than a shallow one. This may have implications for VT testing.
- For the 32 mm thick pipe, all methods predict crack arrest. For shallow cracks, *K* was overestimated by all crack face pressure methods where there was a tensile residual stress near the inner wall.

13 FUTURE STUDIES

In the present study, a near-tip estimate of the *J*-integral was used. This was judged to provide an acceptable indication of the trends but for some cases it was necessary to take results very close to the crack tip and this may have induced a mesh dependency. Future investigations should use a modified *J*-integral because it is path independent in the presence of residual stress fields, prior plastic deformation and material unloading. Further development work is required for its implementation into 3D finite element models.

The present study has indicated key trends regarding crack face pressure methods for various pipe geometries. Nevertheless, it is not fully resolved in what situations displacement controlled modeling and when high out-of-plane stress contribute most to the deviation from the crack face pressure methods. A systematic study to clarify the separate contribution of each of these parameters is required. For example the reason for the large decrease in *K* in Figure 6.13 for the control method towards the pipe inner surface is not well understood.

Some observations were made regarding VT inspection. For medium thickness pipes, where the axial weld residual stress profile is sinusoidal, the surface COD due to residual stresses only, decreases rapidly, leading to the situation that it is more difficult to detect a large crack than a small one. Further investigations are required to quantify how this effect applies to more complicated residual stress fields. Results for the control method, and for residual stresses only at room temperature, would be needed for more complete conclusions.

Note that for through wall cracks in sinusoidal weld residual stress fields the maximum value of *K* is not always obtained at the inner or outer surfaces of the pipe when estimates are made using the control method, the elastic FE method and the elastic-plastic FE method. This could have implications for predictions using ProSACC since only values at the surfaces are provided from ProSACC. A future version of ProSACC could be updated to provide estimates of *K* at several positions through the thickness.

14 REFERENCES

[1] Zang, W., Gunnars, J., Dong, P. and Hong, J.K., *"Improvement and validation of weld residual stress modelling procedure"*, Inspecta Research Report No. 50002550-1, Rev 0, 2008.

[2] Dillström P. et al.,"ProSACC Handbook — A combined deterministic and probabilistic procedure for safety assessment of components with cracks", DNV RSE Report No 2004/01 Rev 4-1, Det Norske Veritas AB, DNV Technology Sweden, 2004.

[3] Moran, B and Shih, C.F., *"Crack tip and associated domain integrals from momentum and energy balance"*, Engineering Fracture Mechanics, Vol. 27, pp. 615-642, 1987.

[4] Lei, Y., O´Dowd, N.P. and Webster, G.A. *"Fracture mechanics analysis of a crack in a residual stress field*", Int J Fracture, Vol. 106, pp. 195-216, 2000.

[5] Lei, Y.,"*J-integral evaluation for cases involving non-proportional stressing*", Engineering Fracture Mechanics, Vol. 72, pp. 577-596, 2005.

[6] Mirzaee-Sisan, A. et al., "Interaction of residual stress with mechanical loading in an austenitic stainless steel", Fatigue Fract Engng Mater Struct, Vol. 31, pp. 223-233, 2007.

[7] von Unge, P., *"Calculation methods for cracks in residual stress fields"*, Inspecta Research Report No. 50008280, Rev 0, 2008.

[8] Anderson, T.L. "*Fracture mechanics, Fundamentals and applications*", Second edition, CRC Press, 1995.

[9] ProSACC version 1.0 Rev 5, 2008.

[10] Brickstad, B. and Zang, W. "NURBIT, NUclear RBI analysis Tool, A Software for Risk Management of Nuclear Components", DNV Technical Report 10334900-1, 2001.

[11] Wang, L. and Atluri, S.N., *"Recent advances in the alternating method for elastic and inelastic fracture analyses"*, Comput. Methods in Appl. Mech. Engrg., Vol 137, pp. 1-58, 1996.

[12] Han, Z. D. and Atluri, S. N., "SGBEM (for Cracked Local Subdomain) – FEM (for uncracked global Structure) Alternating Method for Analyzing 3D Surface Cracks and Their Fatigue-Growth", Computer Modeling in Engineering & Sciences CMES, Vol. 3, pp. 699-716, 2002.

[13] Zang, W. "*Influence of crack morphology on leakage before break margin*", Inspecta Technical Report No. 50004240, Rev 2, 2007.

[14] Zang, W, "Stress intensity factor solutions for axial and circumferential through wall cracks in cylinders", SINTAP/SAQ/02, 1997.

Strålsäkerhetsmyndigheten
Swedish Radiation Safety Authority

SE-171 16 Stockholm
Solna strandväg 96

Tel: +46 8 799 40 00
Fax: +46 8 799 40 10

E-mail: registrator@ssm.se
Web: stralsakerhetsmyndigheten.se